Template-Based Imaging Analysis of Arbitrary Nuclear Material Configurations Using Time and Directionally-Tagged Fast Neutrons

A Dissertation Presented for the
Doctor of Philosophy
Degree
The University of Tennessee, Knoxville

Kirsten Elise Peña
August 2015

Dedication

This work is dedicated to Oscar and June.

Acknowledgements

Thank you to my advising professor Dr. Jason Hayward and committee members, Dr. John Mihalczo, Dr. Howard Hall and Dr. Thomas Handler. Thank you to Dr. Seth McConchie for guidance and advice. A special thank you to my husband Jose for support and encouragement.

Abstract

Reduction of nuclear material worldwide requires that robust methods for template measurement systems be developed. For nuclear material in metal form, two scenarios where it is necessary to verify and account for the material include storage and treaty verification. In both of these scenarios, the nuclear material's high density, as well as possible heavy shielding or high radiation background, are obstacles to verifying the materials and configuration of an object with a high degree of confidence in a timely manner.

Addressing the need for confident verification, the template analysis method investigated in this work— the Kolmogorov-Smirnov (K-S) goodness-of-fit test—uses tagged neutron interrogation data to confirm whether or not measured objects match a template object. In tagged neutron interrogation, time and directionally tagged fast (14.1 MeV) neutrons are used to obtain the neutron attenuation and fissile nature of interrogated objects. Said method is evaluated using data acquired with Oak Ridge National Laboratory's Nuclear Materials Identification System (NMIS).

An evaluation of this template analysis method with existing NMIS measurement data indicates that it is invariant to the common measurement complications of shifting and magnification; yet, it is not completely robust to rotational offset of asymmetric objects. Additional testing also suggests that this method has the ability to confirm the fissile nature of materials present of order 1 min for annular uranium storage castings. Simulations of template analysis with a single DU annular casting indicate that it may be possible to detect the substitution of iron or tungsten, or an $^{1}/_{8}$ in. increase in the casting thickness, 92% of the time with a 4 min NMIS measurement, or without error by increasing to an 8 min measurement. Furthermore, a study of the effect of user-defined variables (giving control over the allowable error rate in matching objects to a template item) shows that the ability of the template analysis to correctly reject non-matching items is most strongly affected by the alpha value of the K-S test and the number of measurement subsamples, followed by the measurement time per subsample and the number of projections used in the measurement.

Table of Contents

Chapter 1 Introduction 1
1.1 Motivation 2
1.1.1 Arms Control and Treaty Verification. 2
1.1.2 Nuclear Materials Control and Accountability. 3
1.2 Confirming Nuclear Material Configurations 4
1.2.1 Visual Inspection. 4
1.2.2 Passive Measurements. 4
1.2.3 Active Measurements. 4
1.2.4 Ideal Template Construction. 5
1.3 Tagged Neutron Interrogation 5
1.4 Templates 8
1.4.1 Attribute confirmation. 8
1.4.2 Pattern Recognition. 9
1.4.3 Hypothesis Testing. 9
Chapter 2 Literature Review and Original Contributions 11
2.1 Measurements 11
2.1.1 Gamma Spectroscopy. 11
2.1.2 Imaging. 13
2.1.3 Fast Neutron. 13
2.1.4 Active Neutron Imaging. 15
2.2 Analysis 19
2.2.1 Pattern Recognition. 19
2.2.2 Hypothesis Testing. 22
2.2.3 Goodness-of-fit Tests. 22
2.3 Comparison Between Past Work and Presented Work 23
2.4 Original Contributions 24
Chapter 3 Method 26
3.1 Nuclear Materials Identification System 27
3.1.1 Physical Components. 27
3.1.2 Data Acquisition. 29
3.1.3 Data Organization. 30
3.2 Hypothesis Testing 33
3.2.1 Kolmogorov-Smirnov Test. 34
3.2.2 Components of Hypothesis Testing. 37
3.3 Template Analysis Testing 41
Chapter 4 Measurement Data Analysis 44
4.1 Existing Measurements and Datasets 45
4.1.1 Description of Existing Measurements. 45
4.1.2 Description of Datasets. 53

4.2 Simple Configuration 61
4.2.1 Electronic Variation. 61
4.2.2 Object Placement. 63
4.2.3 Fissile Detection. 69
4.3 Complex Configuration 72
4.3.1 Rotational Offset. 72

Chapter 5 Simulation Data Analysis 81
5.1 Simulation Description 82
5.1.1 Ray Trace Program. 82
5.1.2 Error Analysis. 87
5.1.3 Tested Configurations. 91
5.1.4 Analysis Testing Setup. 96
5.2 Simple Configuration 97
5.2.1 Material Substitution. 100
5.2.2 Changes in Object Dimensions. 102
5.3 Complex Configuration 104
5.3.1 Material Substitution. 106
5.3.2 Changes in Object Dimensions. 110

Chapter 6 Conclusions and Future Work 113

List of References 121

Vita 125

List of Tables

Table 1. Relationship between null hypothesis validity and test outcome 43
Table 2. Dimensions of Annular DU shields [29] 48
Table 3. Summary of existing measurement data used in template analysis testing 52
Table 4. Example portioning of IO datasets for creation of templates and test objects for algorithm testing. 57
Table 5. Results of template analysis for 2 min measurement of DU with steel shielding set as template and baseline correction applied. 68
Table 6. Results of template analysis testing the substitution of 93 wt.% ^{235}U casting with DU casting surrounded by various amounts of DU shielding, for a 1 min measurement. Alpha value of 0.05 used for all tests. 71
Table 7. Results of template analysis testing with IO 3 as template................................ 76
Table 8. Results of template analysis testing with IO 7 as template................................ 76
Table 9. Results of template analysis testing with IO 9 as template................................ 77
Table 10. Results of template analysis testing with IO 10 [H1] as template 77
Table 11. Results of template analysis testing with IO 10 [H2] as template 78
Table 12. Coefficient values for f(x)=A•exp(B•x)+C•exp(D•x) fit to attenuation error for measurement samples of 30, 60, 90 and 120 seconds.. 90
Table 13. Results of material change detection of simple configuration with template analysis using simulated attenuation profiles. 101
Table 14. Results of dimension change detection of simple configuration with template analysis using simulated attenuation profiles. 103
Table 15. Comparison of results of material change detection of simple configuration with template analysis using simulated attenuation profiles for templates with 4 subsamples and templates with 8 subsamples 105
Table 16. Results of material change detection of complex configuration with template analysis using simulated attenuation profiles and 8 min total measurement time. . 109
Table 17. Results of material change detection of complex configuration with template analysis using simulated attenuation profiles and 16 min total measurement time. 109
Table 18. Results of material change detection of complex configuration with template analysis using simulated attenuation profiles with 8 subsamples and 24, 32 or 80 min total measurement time. 109
Table 19. Results of dimension change detection of complex configuration with template analysis of simulated attenuation profiles for total measurement time of 4, 8, and 16 min. 110

List of Figures

Figure 1. Components of TRIS including sodium iodide gamma-ray spectrometer, commercial multichannel analyzer and trusted processor [16]................................ 12
Figure 2. Example of NMIS measurement; (top) Void and object profiles and (bottom) attenuation profile for one projection of a DU casting with steel shielding [11]. 16
Figure 3. Schematic (not to scale) of NMIS with induced fission radiation and transmission detectors. The DT generator is enlarged to show detail [25]............... 17
Figure 4. NMIS two-dimensional gamma attenuation image using a Cf-252 source. Color scale represents attenuation [24]. 18
Figure 5. NMIS components and orientation including D-T neutron generator, transmission detectors, and large plastic fission detectors [11]. 20
Figure 6. (left) Singogram and (right) tomograph of the same measured object, Inspection Object 3 from ORNL's INL measurement campaign data. The color scale on the right represents the relative attenuation. 32
Figure 7. Graphical representation of the Kolmogorov-Smirnov test [30]..................... 35
Figure 8. Graphical representation of classification threshold and misclassification with α-value of 0.05 39
Figure 9. Graphical representation of classification threshold and misclassification with α-value of 0.15 40
Figure 10. Comparison of configurations with a DU casting and varying shielding. 46
Figure 11. Annular DU shields [29] 48
Figure 12. IO 3's (left) transmission image and (right) photograph of the configuration [11]... 50
Figure 13. IO 7's (left) transmission image and (right) concept diagram of the material configuration near the vertical center [11]. 50
Figure 14. IO 9's (left) transmission image and (right) concept diagram of the material configuration near the vertical center [11]. 51
Figure 15. IO 10's (left) transmission image and (right) concept diagram of the material configuration near the vertical center [11]. 51
Figure 16. (a) Full measurement sinogram of the object seen at right in Figure 10. (b) Example template sinogram acquired from a. (c) Example true test object sinogram acquired from a. (d) Example false test object sinogram acquired from the full measurement of the left object seen in Figure 10. 54
Figure 17. Sinograms of (a) IO3, (b) IO7, (c) IO9, (d) IO10 [H1], and (e) IO10 [H2] 56
Figure 18. Example templates for (a) IO3, (b) IO7, (c) IO9, (d) IO10 [H1], (e) IO10 [H2] 59
Figure 19. Example test objects for (a) IO3, (b) IO7, (c) IO9, (d) IO10 [H1], (e) IO10 [H2] 60
Figure 20. (left) Transmitted neutrons and (right) attenuation as a function of detector position for four measurements of DU and steel [33]... 62

Figure 21. (left) Full and (right) close up views of uncorrected attenuation profiles for two 60 min measurements of DU and steel. Attenuation profiles have corrected detector positions. 65
Figure 22. (left) Full and (right) close up views of baseline corrected attenuation profiles for two 60 min measurements of DU and steel. Attenuation profiles have corrected detector positions. 65
Figure 23. Example uncorrected attenuation profiles for (left) four sample measurements of DU with steel shielding and (right) sample measurements of DU with steel shielding, DU with lead, poly and steel shielding and steel shielding without DU.. 66
Figure 24. (left) Attenuation as a function of detector position and (right) late singles as a function of alpha pixel for measurements of 93 wt.% ^{235}U with and without 1.5 in of DU shielding, and DU with and without 1.5 in of DU shielding........ 69
Figure 25. Top down view of object without rotational symmetry (right) at original position and (left) with 90°rotational offset........ 72
Figure 26. Diagram of test trial construction using an example consisting of 3 templates and 12 test objects to test a maximum rotational offset of 12°........ 74
Figure 27. ROC curves of template analysis results with IO 3 as template and IO 9 as false test object with varying alpha value........ 80
Figure 28. ROC curves of template analysis results with IO 7 as template and IO 9 as false test object with varying alpha value........ 80
Figure 29. Comparison of attenuation profiles from simulated DU casting with iron shield using ray trace program and MCNP6. 84
Figure 30. Comparison of attenuation profiles from measured casting of (a) aluminum, (b) DU, (c) iron, (d) lead, and (e) tungsten to those same casting simulated with the ray trace program. Attenuation is shown on the vertical axis with detector position on the horizontal axis........ 86
Figure 31. Average attenuation error as a function of attenuation at 1000 s for two measurements of DU and steel divided into measurement samples of various lengths........ 89
Figure 32. Average attenuation error as a function of attenuation from measurements of DU and steel fit with two exponential functions for (a) 30 s, (b) 60 s, (c) 90 s, and (d) 120 s measurement samples........ 90
Figure 33. Top down representation of simple configurations simulated for testing of altered dimension identification. The increase in casting thickness between the template and false test object 1 is $^1/_8$ in., or ¼ in for false test object 2........ 92
Figure 34. Attenuation profiles for simulated simple configuration of template DU casting, false test object 1 with $^1/_8$ in. increase in thickness and false test object 2 with ¼ in. increase (left) without error added and (right) with error equivalent to 30 s subsamples........ 93
Figure 35. Top down representation of complex configuration template simulated for template analysis testing. 94
Figure 36. Attenuation profiles of complex configuration with iron and tungsten castings substituted for DU for (a) full attenuation profile from ray trace program and details

of casting region of profile (b) without error added, (c) 30 s measurement error, and (d) 120 s measurement error. 95
Figure 37. True positive rate as a function of alpha value using (left) 4 subsamples and (right) 30 seconds per subsample for template analysis comparisons of simple configuration template and true test objects. 98
Figure 38. False negative rate as a function of alpha value using (left) 4 subsamples and (right) 30 seconds per subsample for template analysis comparisons of simple configuration template and tungsten false test object. 100
Figure 39. False negative rate as a function of alpha value using (left) 4 subsamples and (right) 30 seconds per subsample for template analysis comparisons of simple configuration template and false test object with $^1/_8$ in. increase in casting thickness. 103
Figure 40. True positive rate as a function of (left) number of projections using 8 subsamples with 30 seconds per subsample and (right) number of subsamples using 30 projections and an alpha of 0.25 for template analysis comparisons of simulated complex configuration template and true test objects... 107
Figure 41. True positive rate as a function of (left) number of projections using 4 subsamples with 60 seconds per subsample and (right) number of subsamples using 12 projections and an alpha of 0.20 for template analysis comparisons of simulated complex configuration template and tungsten false test objects............................ 107
Figure 42. False negative rate as a function of the change in the casting thickness of the simulated complex configuration. Each combination of measurement time per subsample, number of subsamples and number of projections produces a total measurement time of 8 min... 112
Figure 43. False negative rate as a function of the change in the casting thickness of the simulated complex configuration. Each combination of measurement time per subsample, number of subsamples and number of projections produces a total measurement time of 4 min... 112

Chapter 1

Introduction

The International Atomic Energy Agency (IAEA) categorizes nuclear material as source material or special fissionable material. Source material is defined as natural uranium, depleted uranium (DU) and thorium any the form of metal, alloy, chemical compound or concentrate whereas special fissionable material is defined as plutonium-239, uranium-233, and uranium enriched in the isotopes of 233 or 235 [1]. The high value of nuclear material from a consequence standpoint necessitates that the material be verified and accounted for. For nuclear material in metal form, two of these scenarios include storage and treaty verification. For both of these scenarios, it would be ideal to verify the content's materials and configuration with a high degree of confidence within a timely manner, in order to conserve resources and costs, and without opening the container, due the risk of revealing sensitive information.

One significant obstacle in verifying metallic nuclear material is the substance's high density and gamma attenuation. In the two scenarios being considered the nuclear material may also be heavily shielded, further decreasing the penetrability of gammas and x-rays. This makes measurements of gamma or x-rays in these situations either time consuming or inaccurate [2][3]. Using neutrons to interrogate the materials is a logical alternative given the increased penetrability compared to gammas or x-rays. When using neutrons to interrogate materials, the addition of fission neutrons from fissile materials present does pose a slight difficulty, however. In order to obtain clear configuration information, a way to distinguish the natural background radiation from the interrogating particles is needed. Thus, the method evaluated here uses time and directionally tagged fast neutrons, which not only have penetration needed to interrogate nuclear materials, providing material and geometrical information, but can also be distinguished from fission neutrons where fissile material is present, providing the fissile nature of interrogated materials. The template aspect of the evaluated method ensures reasonable measurement times in the likely scenario of needing to verify multiples of the same objects.

1.1 Motivation

Treaty verification as well as nuclear materials control and accountability are two potential applications for the presented method of verification since both are likely to have shielded metallic nuclear material that would need to be tested for both the materials present and their configurations.

1.1.1 Arms Control and Treaty Verification. The United States has signed several arms control treaties in the modern era including the Intermediate-Range Nuclear Forces (INF) Treaty, the Moscow Treaty (SORT), and START and New START treaties with the Russian Federation/Soviet Union. These treaties focus on the reduction of strategic offensive arms and the elimination of intermediate and shorter-range missiles (INF). Except for SORT, which provided no verification provisions, the aforementioned treaties contained verification means including data exchanges, on-site inspections, and national technical means (i.e., satellite observations). The only use of radiation detection equipment in the verification process is to ensure that declared non-nuclear objects are not emitting radiation [4]. These previous and current treaties contain no provisions for verifying nuclear materials.

Future arms control treaties have the possibility of looking much different in terms of verification than past treaties. As the number of warheads are reduced to a critical level, confirming the authenticity of warhead dismantlement and discouraging falsification of dismantlement will become paramount to treaty participants. Potential objectives of these future treaties could include tracing warheads post-deployment through dismantlement to long-term storage. Radiation measurements could be used to verify the presence of nuclear material or confirm dismantlement. Challenges for this verification scenario include evaluating a presented item while protecting the host country's classified information and allowing monitors, or those verifying dismantlement, to draw independent conclusions. Information barriers may have an important role in addressing this challenge.

1.1.2 Nuclear Materials Control and Accountability. Material control is the use of control and monitoring measures to prevent or detect the loss of material, while material accountability is the use of statistical and accounting measures to maintain knowledge of the quantities of nuclear materials present [5]. The current standard in nuclear materials control and accountability is gamma spectrometry [6]. Due to self-attenuation, this detection method is only able to detect gammas from a 3 mm thickness of surface material of enriched uranium, however, and does not provide any configuration information [7]. This decreases the potential accuracy of this method and makes it possible to spoof. An example of this is the Radiation Signature Testing Device designed by Blessinger where 50g of enriched uranium in an alloyed matrix on the surface of a sphere gives the same radiation signature as 2.5 kg of 90% enriched uranium when passively measured with gamma spectroscopy [8].

1.2 Confirming Nuclear Material Configurations

1.2.1 Visual Inspection. Visually inspecting nuclear material configurations is one method to confirm authenticity or accuracy. One advantage to visual inspection is that minimal information is divulged, essentially only the outside shape of the item is observable. The disadvantages to this method are that there is no confirmation of nuclear material and there is minimal monitor/inspector confidence.

1.2.2 Passive Measurements. Measurements of an object's natural radiation signature can be used in some cases to confirm characteristics or authenticity. Advantages of using passive measurements include the confirmation of nuclear material as well as possible isotope, enrichment, and fissile mass determination. Disadvantages to passive measurements are the possible difficulties introduced by shielding materials and the increased ability to spoof compared with active measurements.

1.2.3 Active Measurements. Making measurements while objects are interrogated by radiation constitutes an active measurement. Some advantages to active measurements are that the measurement may be performed through moderate shielding; they are more difficult to spoof; there is the possibility of confirming the fissionable nature of nuclear material, as well as the possible determination of enrichment, mass, etc. Disadvantages include that the data obtained is more likely to contain sensitive information, it is more difficult to obtain isotopics, and there are increased administrative and logistical concerns with active sources. For example, increased dose fields from active sources cause a need for additional radiation safety measures such as shielding and distance. Given the advantages and disadvantages of each type of confirmation method, an ideal technique for confirming nuclear materials can be developed for the desired scenarios.

1.2.4 Ideal Template Construction. Templates in a verification scenario for hypothesis-testing-type confirmation need to foremost be robust and fast. Templates need to provide enough information to accurately confirm a match without taking an inordinate amount of time. They need to be able to measure high-density metallic objects and unseen objects. Unseen objects may be shifted or rotated within a container. Likewise, only a single measurement should be needed due to both time constraints and host-monitor agreements. Templates should also be able to detect changes in material or configuration, as well as fissile nature for this type of template application.

1.3 Tagged Neutron Interrogation

Tagged neutron interrogation has been demonstrated to provide varied and valuable information from an interrogated object [9]. The possible modalities include transmission imaging, induced fission, elastic scattering and non-elastic scattering. Additionally, the high penetration capability of fast neutrons is indispensable for the high-density metallic objects being measured. A tagged neutron interrogation system also provides sensitivity to changes in object configuration, as well as the potential ability to identify changes in object material and fissile nature.

Neutrons, like photons, are uncharged, allowing them to travel appreciable distances in matter without interacting. While the interaction of neutrons with electrons is negligible, neutrons can collide with atomic nuclei, leading to either scatter or absorption. Fast neutrons on the MeV and sub-MeV energy scales tend to interact mostly through elastic scattering [10]. As with photons, a narrow beam of monoenergetic neutrons is attenuated exponentially by matter. This behavior is expressed mathematically for thin objects in terms of the ratio of transmitted particles, I, to incident particles, I_0, as

$$\frac{I}{I_0} = \exp(-\mu x) \qquad (1)$$

where μ is the attenuation coefficient and x is the thickness of the object's material. For incident neutrons, $\mu = N\sigma$, where N is the nucleic density (nuclei per cm^3) and σ is the total cross-section (1 barn = 10^{-24} cm^2). Since the cross-section of most materials is strongly dependent on the energy of the incident neutron, the attenuation, μx, depends upon the materials present and the paths that particles traverse through the configuration.

Although neutrons and photons are each exponentially attenuated in matter, the imaging capabilities associated with each differ. Due to neutron scattering kinetics, neutrons are strongly attenuated by low Z materials and penetrate well through high Z materials. In contrast to neutrons, photons interact with the electron cloud of an atom, leading photons to be strongly attenuated by high Z materials but to penetrate well through low Z materials.

In a transmission imaging measurement, the object to be imaged is placed between the particle source and a set of detectors. For each detector, the number of particles passing through the object and detected on the opposite side, as well as the number of incident particles, is recorded. By taking the negative natural log of the ratio of these two numbers, the effective attenuation, μx, of the neutrons traveling through the object to that detector create an attenuation pixel. As such, the attenuation is given as

$$\text{Attenuation} = -\ln\left(\frac{I(\text{detector pixel})}{I_0(\text{detector pixel})}\right) \tag{2}$$

Analogous to the image pixels of a digital picture, when the attenuations of each detector pixel are combined an attenuation image of the object is formed. Likewise, more pixels lead to higher image resolution.

The number of detector pixels in the attenuation image is not the only factor contributing to image quality, however. Neutron sources which are useful for neutron transmission imaging generally emit neutrons on the MeV energy scale and have intensities on the order of 10^6 to 10^8 neutrons per second into 4π [11]. The tendency for these sources to emit neutrons in all directions can affect the quality of the transmission image. For example, neutrons can scatter from one source-to-detector path to another, leading to neutrons being detected in detector pixels other than the one in the original path of the incident neutron and, thereby, causing the number of transmitted neutrons along many paths to be misrepresented. As the attenuation of the object increases, the probability of this misrepresentation increases. This results in an inaccurate association of attenuation values in the attenuation image, but knowledge of the time and direction of each emitted neutron reduces this effect [12], as described next.

While the options for transmission images include counting all of the neutrons detected, counting only those neutrons tagged in time, or counting only those neutrons tagged in time and direction, the highest quality images with the best resolution are obtained by counting only those neutrons tagged in time and direction. In the simplest material configurations, all three options can produce similar attenuation images, but significantly different images can result when the object contains a material such as iron with a higher probability of neutron scatter in the forward direction.

1.4 Templates

1.4.1 Attribute confirmation. Template testing can have several different meanings, even within the context of treaty verification. Template testing is sometimes seen in terms of attribute confirmation. In this context, the template contains certain specific information, or attributes, about a reference item which may include mass, enrichment, material arrangement, etc. The template, in this case, is not necessarily a measurement, but more of a checklist of requirements for an unknown object to be confirmed as matching a declared object. For instance, the measurement may need to confirm if the mass of Pu is greater than 8 kg or if the uranium enrichment is above 20% (IAEA safeguards glossary 2002). While attribute confirmation does provide the highest degree of confidence to inspectors, it also deals with sensitive information and often requires a significant amount of time.

1.4.2 Pattern Recognition. Pattern recognition is when data is taken in and an action is taken based on the “category” of the pattern [13]. In other words, it is assigning a category or label to some information based on its features or attributes. In terms of template matching, pattern recognition is used to assign an unknown object into one of several categories. For example, representative objects from three different classes, A, B and C, would be measured to provide a template for each class of object. An unknown object would then be measured and pattern recognition used to provide which class of object, either A, B or C, the unknown object most closely matched. Its important to note that this approach does not actually confirm that the unknown object is actually in classes A, B or C, just which class most closely matched the unknown object. For example, it could be that the unknown object is from class D, but pattern recognition will still return either A, B or C since these are the only references available. This type of template testing would be ideal in a storage situation where objects needed to be categorized into one of several classes.

1.4.3 Hypothesis Testing. Although often confused with pattern recognition, hypothesis testing answers a fundamentally different question. Pattern recognition may ask, “To which class does the object belong? A, B or C?” On the other hand, hypothesis testing asks, for example, “Is the object from class D?” From a statistics perspective, hypothesis testing is where some collected data is used to decide whether or not to reject some assumption or null hypothesis in favor of an alternative hypothesis. This null hypothesis could be, for example, that a variable is equal to some value or, alternatively, that two distributions are the same, while the alternative hypothesis is that the variables or distributions are not the same. The hypothesis is then tested, and, if the probability of obtaining the data, assuming the null hypothesis is true, falls below a certain "significance" threshold, or alpha value, then the null hypothesis is rejected in favor of the alternative hypothesis [13]. In other words, hypothesis testing is where "… we make an assumption, and if we observe a very unlikely outcome, we decide that the assumption was false, realizing that there is a small risk that we are wrong" [14].

Template testing via hypothesis testing has benefit in either a treaty verification scenario or a material control and accountability scenario because it takes much less time than a full attribute determination. For example, in the situation where there are many objects to be confirmed that should all be the same, it would take much less time, while still maintaining accuracy, to confirm only one object through attribute testing and then to simply confirm that the other objects match the first object through hypothesis testing, compared to the case of using attribute testing on each object. Likewise, if an object, which was already confirmed through attribute testing, needed to be quickly verified as remaining unchanged because inspectors were unable to stay continually with the object, then simply confirming via hypothesis testing that the object was the same as previously measured would be the easiest approach.

Chapter 2

Literature Review and Original Contributions

Template matching and tagged neutron interrogation have been used in several different applications for treaty verification and nuclear materials control and accountability purposes. Both the measurement and analysis aspects of these previous methods were of interest in the development of the presented method and are detailed in the following sections.

2.1 Measurements

2.1.1 Gamma Spectroscopy. The Trusted Radiation Identification System (TRIS), developed in 2001, employs a template method as part of possible treaty verification. This system uses a sodium iodide detector to measure the passive gamma spectra from an object and uses these spectra as basis for template analysis, thereby allowing for the secure confirmation of certain Treaty Accountable Items (TAIs) [15]. There are two measurements made: a foreground spectrum of the object and a background spectrum without the object present. These are used to produce a net spectrum, where the background is subtracted from the foreground spectrum. The spectrum is then binned into a fixed, 17-channel group structure that is used for the template matching analysis. Figure 1 shows the components of TRIS.

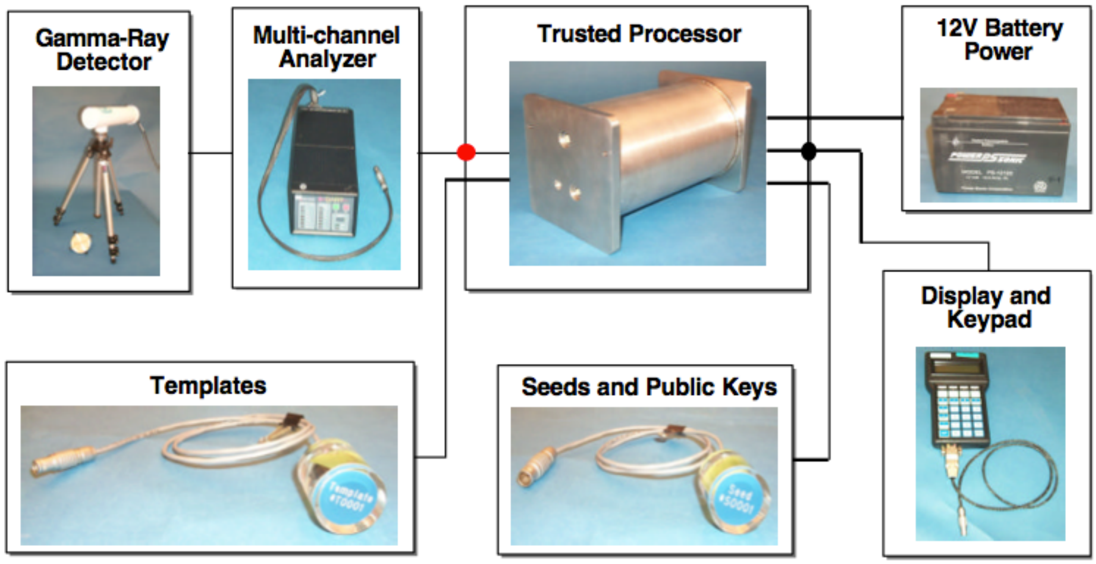

Figure 1. Components of TRIS including sodium iodide gamma-ray spectrometer, commercial multichannel analyzer and trusted processor [16].

2.1.2 Imaging. Jarman et al. proposed using the passive gamma spectra from SNM to image objects, along with other methods of confirming attributes, for a treaty verification scenario. In their 2011 annual report, they described a simulation of two Pu spheres which where distinguishable from natural background after processing the images with a spectral dissimilarity ratio algorithm [17]. The important potential benefit of this technique is that the background does not have to be measured separately. The report did not, however, provide information as to whether this technique had been simulated with shielded configurations, enriched uranium objects, or in the presence of high count rate background. This technique is likely to have difficulties with these situations, which may decrease the observed image contrast between the nuclear material and background.

In addition to the utilization of the passive gamma spectra from nuclear material, Jarman et al. also looked at using active interrogation of nuclear material by x-rays to provide images for attribute extraction [18]. Specifically, they used K-edges in the mass attenuation coefficients from materials to confirm declared material configurations, the absence of nuclear materials and Pu mass estimates. They report, however, that material confusion is possible with this technique, namely between high-Z materials, Pu and U. The authors proposed that future work should use ORNL neutron imaging systems such as NMIS [18].

2.1.3 Fast Neutron. In a 2012 INMM paper, Chichester, Johnson and Seabury propose that the spontaneous fission spectrum of Pu within an object can be used to actively interrogate its surrounding materials, taking advantage of the fast neutron resonances of common materials such as Be-9, C-12, N-14, and O-16. In reported experiments, a neutron generator or Cf source was substituted for the Pu [19]. One drawback to the widespread use of this technique for nuclear material in general is that it would not work for objects that contain enriched uranium instead of Pu since the spontaneous fission rate would be too low. Ten kilograms of enriched uranium metal produces <100 n/s, while 100g of Pu metal produces 10,000-40,000 n/s [20].

In 1997, Valentine et al. reported using the nuclear weapons identification system (NWIS) in a template-based confirmation measurement of nuclear weapons components in storage at Y-12 [21]. The NWIS used a time-tagged Cf-252 source along with one or two liquid or plastic detectors and a signal processor to record signatures of an interrogated object, including auto and cross correlations, multiplicities, auto and cross spectra, coherences, ratios of spectral densities, and source-correlated count rates. Further information on the signatures recorded with NWIS can be found in reference 22. Since the Cf-252 source was enclosed in an ionization chamber [23], the time occurrence of fission and, thus, the emission time of the interrogating neutrons and gamma rays was known. Using this information and time-of-flight calculations, they were able to distinguish the direct radiation due to Cf-252 fission from the late fission neutrons of the interrogated object and background radiation. Additionally, gammas and neutrons could be distinguished using either pulse shape discrimination with the liquid detectors or time-of-flight with the plastic detectors, given enough source-to-detector distance.

For this template-based measurement reported by Valentine et al., a reference object was measured multiple times in several different shipping containers and in different locations within each container to account for statistical variations, variations associated with object locations within the container, and variations from source-detector locations. Cross power spectral density, which is the fast Fourier transform of the time distribution of events in a detector after Cf fission, was used as the signature of comparison between the reference object and the unknown objects. As long as the signature of the unknown object was within a set amount of variation about the signature of the reference, which was determined by the multiple measurements of the reference object and several measurements of the same object, then the unknown object was confirmed as matching the reference. While performing multiple measurements of a reference object in varying positions is completely acceptable in a storage situation, it may not be possible in a treaty verification scenario, depending on host-monitor agreements. This would lead to a need for an alternative method of determining the allowable variation in the reference signature for this method's possible use in a treaty verification scenario.

2.1.4 Active Neutron Imaging. The Nuclear Materials Identification System (NMIS) is a continuation of NWIS but includes imaging capabilities, as the one or two detectors of NWIS are replaced with 32- 1x1x6 in. plastic scintillators in an arc array opposite the source in NMIS [24]. See Chapter 3 for additional information. The data from this array is used to produce a one dimensional attenuation image of the inspected object placed between the source and detector, as well as providing all of the aforementioned signatures possible with the NWIS system. An example attenuation profile obtained with this system is shown in Figure 2. In addition to the Cf-252 source, a deuterium-tritium (D-T) neutron generator, with a $d + t \rightarrow \alpha + n$ reaction that produces neutrons opposite an

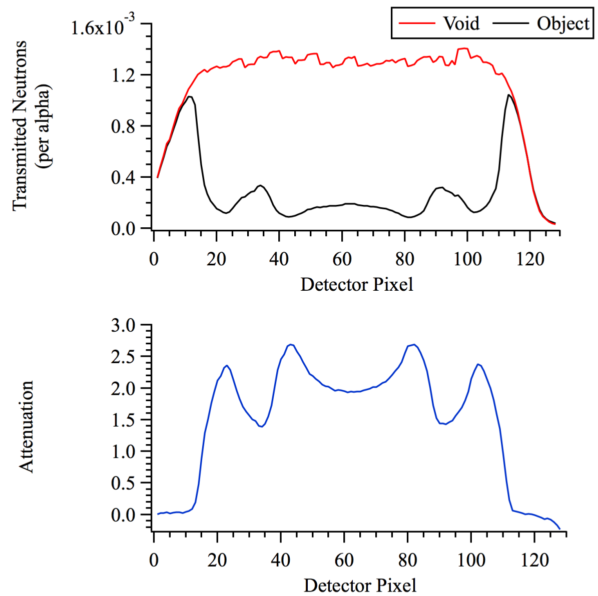

Figure 2. Example of NMIS measurement; (top) Void and object profiles and (bottom) attenuation profile for one projection of a DU casting with steel shielding [11].

alpha particle, is also utilized. With a 16 pixel YAP(Ce) detector or a 15 pixel semiconductor in the generator to detect the alpha particle from the D-T reaction, the 14 MeV neutrons interrogating the object are both time and directionally tagged. A diagram of the NMIS components is shown in Figure 3.

NMIS was utilized in 2007 by Mullens et al. to measure a shipping container with unknown contents [24]. A Cf-252 source was selected as the source, producing both neutron and gamma radiographs of the shipping contents. These two dimensional images were constructed by moving the detector arm and source vertically and recording the particles transmitted through the object at multiple heights. The detector arm is also moved incrementally to increase pixels and image resolution. The images produced in these

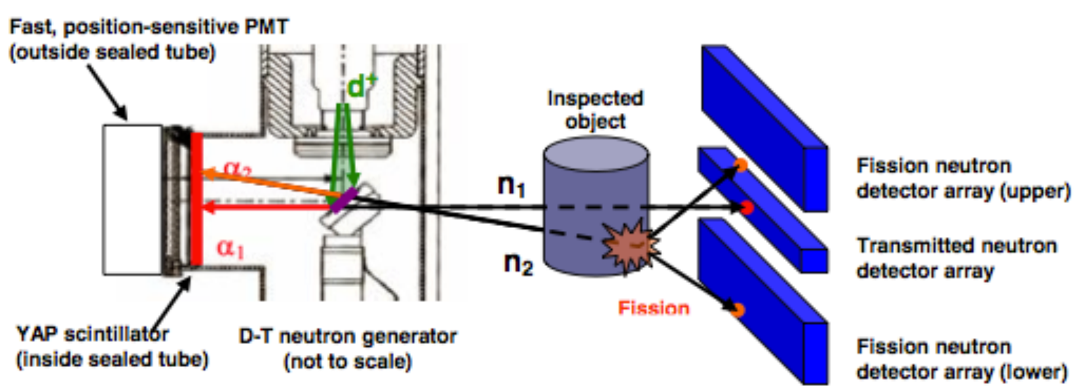

Figure 3. Schematic (not to scale) of NMIS with induced fission radiation and transmission detectors. The DT generator is enlarged to show detail [25].

measurements (e.g., see Figure 4) demonstrated that low- and high-Z materials as well as low-density hydrogenous materials are visually distinguishable small, thin-walled containers with NMIS.

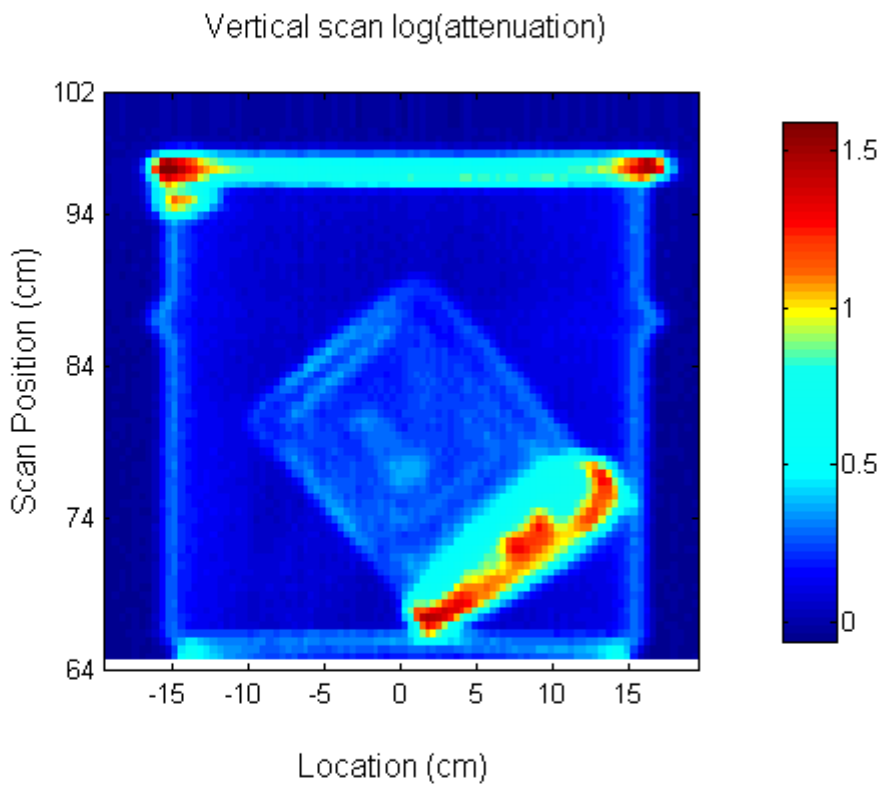

Figure 4. NMIS two-dimensional gamma attenuation image using a Cf-252 source. Color scale represents attenuation [24].

In 2010, NMIS was used to measure unknown objects at Idaho National Lab's (INL) Zero Power Physics Reactor (ZPPR) facility; in this case a tagged D-T generator was utilized as the source [25]. Plutonium, natural uranium and enriched uranium were contained within the unknown measured objects that were arranged into 10 different inspection object (IO) configurations. IO 3, 7, 9 and 10 were measured with NMIS. Fission mapping, which is the spatial distributions of the events or two coincident events in the detectors, was accomplished in this measurement by using eight – 25x25x8 cm scintillation detectors arranged around the inspection object in a large fission detector array. This arrangement is shown in Figure 5. Late singles and doubles in these detectors along with the information from the alpha detector indicating the direction of the neutron that induced fission were used in reconstructing the location of the fission reaction.

Additionally, tomographs were constructed of the INL inspection objects. This was accomplished by rotating the objects radially and taking standard transmission measurements at 6° or 12° intervals, then reconstructing the images to provide a top-down view of the object. The results of tomographic reconstruction showed that it was possible to detect small aluminum parts within the fissile metal plates, even when the parts were in close proximity to the plates, as well as to map fissions to regions within the object. The presence of some materials such as poly, however, did lead to blurring in the fission map image due to scattering of neutrons within the low-Z material. The reported findings indicated that this issue could be mitigated by also using the transmission images to determine high-Z metallic regions of fissile material.

2.2 Analysis

2.2.1 Pattern Recognition. Previous pattern classification with a template approach to treaty verification includes Jarman et al. who reported in 2011 using a type of distance

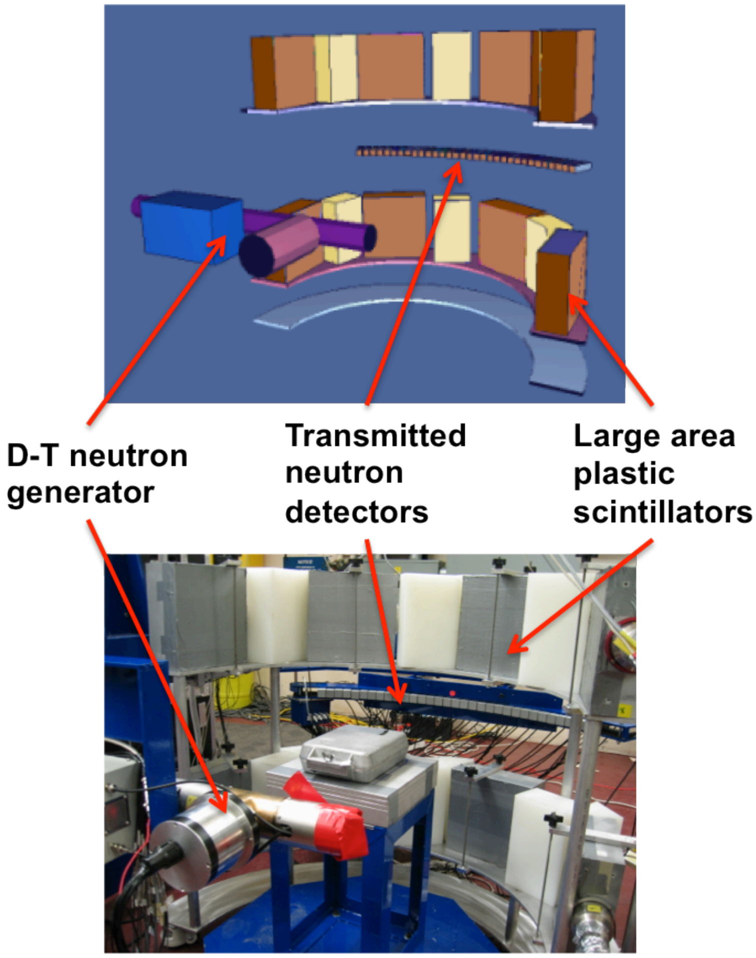

Figure 5. NMIS components and orientation including D-T neutron generator, transmission detectors, and large plastic fission detectors [11].

metric similar to a Mahalanobis distance, or a measure of the distance between a point and a distribution, to determine a match between two objects.

In 2011, Grogan reported on using pattern recognition analysis on images produced with NMIS fast neutron measurements [26]. A fully assembled object consisting of an annular DU casting shielded by poly and then steel was measured. A 'library' of parts was measured individually, all having dimensions identical to one of the parts in the fully assembled object but with a variety of different materials. The fractional error was calculated for three attributes – inner diameter, outer diameter, and attenuation coefficient – of these library parts and then summed them in quadrature to compute the total fractional error. The material from the library with the lowest total fractional error was chosen as a match. There are two drawbacks as implemented: (1) a material is chosen from the library regardless of how large the total fractional error is (i.e., if the material does not exist in the library one will still be chosen as a match), and (2) at the time the testing was being performed, the number of parts in the fully assembled object had to be manually entered by the operator.

Grogan also reported using a maximum likelihood expectation maximization (MLEM) algorithm to reconstruct the measured images of individual parts and then summed the parts measurements to produce every possible composite object from the available materials measured [26]. Methods of matching the correct composite object to the fully assembled object included visual identification or use of the minimum sum of squared errors (SSE), where images were compared pixel-by-pixel. This latter method, like the alternative analysis, is more of an attributes approach with pattern classification, since specific materials are identified along with their precise dimensions and configuration. This method could be converted to a hypothesis testing template-matching approach, but reconstructing full tomographs for each object would require a considerable amount of computational time.

2.2.2 Hypothesis Testing. Mullens, Valentine and Mihalczo used hypothesis testing for the template matching of weapons components with NWIS [27]. There the Mahalanobis distance was used with the cross power spectral density by subtracting the reference signature value from the unknown signature value and dividing by the standard deviation of the reference signature values. Then the mean and standard deviation of the distance function is calculated, which would have expected values of 0 and 1, respectively if the unknown signature were a match. The standard deviation was then used as the variable for hypothesis testing with the null hypothesis being H_0: $\sigma^2=1$. A chi-square distribution is used to test the null hypothesis using the number of measurements minus one as the degrees of freedom and returning a significance level between 0 and 100%. The significance level is provided to give an indication of the distance between the unknown and reference, but the null hypothesis is rejected at the 5% significance level, or alpha of 0.05.

2.2.3 Goodness-of-fit Tests. Goodness-of-fit tests, which are a type of hypothesis testing, are also used in template matching. Two examples of goodness-of-fit tests are the chi-square and the Kolmogorov-Smirnov (K-S) test. The Chi-square test works well with larger data sets but requires a reference “function.” The K-S test is non-parametric, can be used with smaller data sets and does not require a reference function. It can also be used to compare two samples.

TRIS is one example where hypothesis testing, although not formally utilized, is employed for template matching. More specifically, a chi-square goodness-of-fit test is used to determine the differences in spectral shapes and intensities of foreground, background and template spectra. The sum of variances resulting from the statistical uncertainty of these three spectra is used to form a variance array. Additional uncertainties are also added to the array to account for differences between items associated with typical isotopic variations. If the computed reduced chi-square is below 4, then the template is confirmed as matching; otherwise, it is rejected. The authors [15] did not address the error rates expected for a threshold of 4.

2.3 Comparison Between Past Work and Presented Work

TRIS [15] and the methods proposed by Jarman et al. [17][18] rely on either passive gamma detection or active x-ray interrogation. In comparison to these methods, the benefit of using neutrons as the interrogating particle is their increased penetrability, especially where high-density metallic objects are present, thereby avoiding the issues of surface effects. As discussed, Chichester et al. [19] proposed using the spontaneous neutron spectrum from Pu for template purposes but the evaluated method's use of an active neutron source would allow for the measurement of enriched uranium as well as Pu. Valentine et al. [21] and Mullens, Valentine and Mihalczo [27] used a template-based approach in 1997 that most closely resembles the methods described in this work. Their approach was not able to use the imaging capabilities of NMIS, however, since they had not yet been developed. This meant that the template had to be measured multiple times in order to account for unknown variations within the container, such as shifting off center. Since this work relies on the imaging abilities of NMIS, it may be possible to correct measurement data for variations like shifting, and only one template measurement will be necessary, which would most likely be a full attribute-type measurement. Grogan et al. [26] also utilized the fast neutron imaging capabilities of NMIS, but that work used a pattern recognition approach best suited for an attribute type measurement. By using a hypothesis testing approach, the method described in this work looks to provide a fast and accurate template matching analysis that allows users to control desired error rates for the tests performed.

2.4 Original Contributions

The method evaluated investigates the use of fast neutrons (14 MeV) from a tagged neutron interrogation system capable of penetrating high-density metallic objects for treaty inspections or nuclear materials control and accountability. In this tagged neutron interrogation method, measurements with time and directionally tagged neutrons are expected to accurately characterize fissile material assemblies, even in the presence of high background [28]. The ability to measure and perform analysis without opening the object's outer container is required in order to maintain secrecy, reduce required security, and minimize measurement time. The presented work investigates for the first time the

- Use of a template-based approach in inspections that employs tagged neutron interrogation in order to decrease the time required to verify the presence of a particular object (e.g., a particular uranium assembly) when multiple objects may be present
- Development of image-based analysis of tagged neutron interrogation datasets which can provide confirmation of matching materials, quantities, and configurations without the need for multiple measurements of the template object
- Creation of hypothesis testing algorithms that estimate expected error rates and allow for adjustment of expected error rates based on the user's needs

Chapter 3

Method

The template matching analysis evaluated in this work is based on the measurements performed by the Nuclear Materials Identification System, or NMIS. Although this measurement system has undergone significant evolution since its original implementation, the basic components of its current state include a neutron generator situated on one side of the interrogated object with an array of 32 transmission, or imaging, detectors on the opposite side of the object. This allows for the detection of neutrons travelling through the object and, thus, the calculation of how many neutrons are scattered or absorbed by an object as a function of location, leading to a transmission image of the object. The system also contains eight large plastic detectors for the detection of fission neutrons and an acquisition system for recording and correlating events on the nanosecond time scale.

The template matching analysis utilizes hypothesis testing, or, more specifically, the Kolmogorov-Smirnov (K-S) test, which allows for the comparison of two samples to determine if they are from the same underlying distribution. These tests either confirm or reject a null hypothesis based on the alpha, or threshold, value chosen. Other than the data itself, the alpha value has the greatest impact on the error rates of the test, i.e., whether the null hypothesis was correctly confirmed or rejected.

Using each of the performed K-S tests as a trial for a specific combination of sample factors, error rates can be determined for a statistically significant number of trials, giving way to deductions that can be drawn from the tested samples. This method of using NMIS measurements coupled with the hypothesis testing of the K-S test to provide the basis of the template matching analysis allows for the high volume trials and results presented in the following chapters.

3.1 Nuclear Materials Identification System

The Nuclear Materials Identification System (NMIS) is a measurement system developed by the Oak Ridge National Laboratory that interrogates objects with time and directionally tagged fast neutrons. The measurement system, along with data acquisition and specially designed software, enables imaging of unseen objects as well as providing an abundance of additional information including auto and cross correlations, multiplicities, auto and cross spectra, coherences, ratios of spectral densities, and source-correlated count rates.

3.1.1 Physical Components. The main physical components of NMIS consist of a neutron generator, transmission detectors, fission detectors and an object turntable. In addition to the main components, there is a support structure and motors designed to permit the movement of both the measurement system and measured object during the measurement. Together these components provide for improved image quality and measurement data.

The neutron generator used by the system is a Thermo Scientific API-120 that operates by accelerating deuterium onto a tritium target, creating the fusion reaction

$$^2_1H + \, ^3_1H \rightarrow \, ^4_2\alpha + \, ^1_0n$$

The product neutron has a kinetic energy of 14.1 MeV, and the alpha particle and neutron are emitted in nearly opposite directions from the reaction site. The approximately 180° difference in direction is crucial in determining the direction of the emitted neutron. A thin cerium-doped Yttrium Aluminum Perovskite (YAP(Ce)) crystal, a fast inorganic scintillator, is mechanically coupled inside of the generator and positioned opposite the tritium target. The YAP(Ce) crystal produces light when an alpha particle is detected that is transmitted through the generator's fiber-optic faceplate to an optically coupled Hamamatsu H9500 photomultiplier tube (PMT). The PMT is position sensitive, and one of its 16 pixel rows is used to determine the location of each alpha particle detection and thus the direction of each tagged outgoing neutron. The angular and timing resolution of emitted neutrons are approximately 5° and 1 ns and the maximum output of the generator is 4×10^7 n/s.

Located on the opposite side of the interrogation object from the generator is an arced array of 32 Scionix EJ-200 1×1×4-in. plastic scintillators. These are the transmission detectors used to detect the transmitted 14 MeV neutrons needed for constructing the object image. These detectors are in the same horizontal plane as the generator and are typically positioned between 110 and 115 cm from the tritium target.

The neutron generator and transmission detectors have the ability to move in tandem vertically to image an object at different heights, producing horizontal image slices for each height. The transmission detector array also moves radially along its arc to increase the number of image pixels for better image resolution. Additionally, a turntable is available to rotate an object so that attenuation projections may be obtained from different angles. This allows for the image reconstruction of objects that are not radially symmetric.

Eight Scionix EJ-200 10×10×4-in. plastic scintillators are employed in the measurement system for the detection of late-arriving fission chain neutrons. These neutrons arrive approximately 30 to 90 ns after an alpha event and can easily be distinguished from direct source neutrons by using time-of-flight. The fission detectors are arranged in two rows along an arc 19 in. from the center of the object. The front face of each detector has a ¼ in. thick layer of Pb to decrease the number of low energy gammas that reach the detector. The fission detectors provide the data necessary for gaining information about the fissile material in objects and, when coupled with the transmission data, can be used for mapping the location of the fissile material within an imaged object. For additional information on the details of NMIS see reference 29.

3.1.2 Data Acquisition. The detection events that occur in the alpha detector, transmission detectors, and fission detectors are recorded with two custom made boards and acquisition software called Data Acquisition and User Interface (DAUI). Each event's time stamp is recorded for each detector signal, and this information is used to correlate events between detectors. Using the correlation of events between detectors permits the selection of only the events that are useful to the measurement.

One such useful event is the detection of transmitted neutrons since these events are the neutrons that were not scattered or absorbed in the object's material and comprise one half of the attenuation equation (Eq. 1). Neutrons are time-tagged by the detection of an alpha event and, since they are monoenergetic at 14.1 MeV, will travel at approximately 5.2 cm/ns. By using time-of-flight and an equidistant source-to-detector distance of 110 cm, direct neutrons should arrive at the transmission detectors at around 21 ns after the detection of the alpha. This information allows for the correlation of alpha events with transmission detector events that occur within a certain time window, removing random background events and late fission neutrons that reach the detectors.

Another way correlation is useful in isolating direct neutrons is by utilizing the fast neutron's directional information. Just as the neutrons are time-tagged with the detection of an alpha, they are also directionally tagged since the alpha detector is pixelated horizontally. For instance, the alphas detected in the first pixel of the alpha detector may be correlated with neutrons detected in transmission detectors 1-8 since the chance of detecting a direct neutron in transmission detectors outside of this range is very small. By correlating the alpha pixels with their corresponding transmission detectors, scattered neutrons and random events arriving within the correct time frame can also be removed from the dataset used to form the radiograph.

3.1.3 Data Organization. Once the direct neutrons that pass through an object are isolated for use in the radiograph, the DAUI uses a preloaded void measurement to complete the required dataset given by the attenuation equation (Eq. 1). A void measurement is where direct neutrons are recorded without an object in place. In addition to providing the attenuation, dividing the object measurement by the void measurement has the added benefit of reducing the effect of small variations that may occur from detector to detector since the value used is a ratio rather than straight counts.

The array of 32 transmission detectors can also be moved incrementally to sample the space between detectors, allowing edge features to be better sampled. The detectors are translated horizontally some fraction of the width of the detector, and, when the data from the completed measurement is organized, all of the subsample data for a detector are placed together forming additional image pixels for each detector. For example, if the measurement is set to acquire four subsamples, then the detector array is moved ¼ of the width of a detector for each new subsample; detector 1 provides pixels 1-4 of the image, detector 2 provides pixels 5-8, etc., up to detector 32 with pixels 125-128.

The turntable can also rotate the object so that the attenuation at different positions can be obtained. The attenuation profile measured at each rotational position is called a projection. Each projection provides a one-dimensional attenuation snapshot of the object at that rotational location. There are two ways to view multiple projections in a two-dimensional plot. The first way is called a sinogram and it is the simpler method computationally to construct but more difficult for the casual viewer to interpret. In this method, the projections are essentially stacked on top of one another such that the pixel number is along the horizontal axis and the projection number is along the vertical axis. The attenuation value of each plot pixel is depicted in the color scale as seen in the left side of Figure 6. Although it can be difficult for the viewer to conceptualize, the sinogram actually contains all of the information about an object's composition and arrangement.

The second method for viewing measured data from multiple projections in a two-dimensional plot is called a tomograph. A tomograph represents a top-down view of a

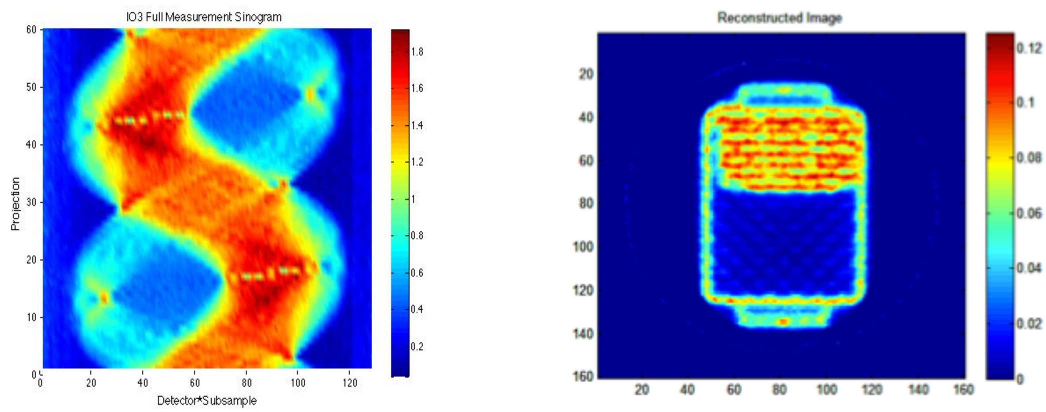

Figure 6. (left) Singogram and (right) tomograph of the same measured object, Inspection Object 3 from ORNL's INL measurement campaign data. The color scale on the right represents the relative attenuation.

horizontal slice of an object. This attenuation image is reconstructed from the multiple projections using an image reconstruction algorithm, such as a filtered back projection or a maximum likelihood estimation method. In this plot, the horizontal and vertical axes represent the physical, two-dimensional space and the color scale again corresponds to the relative attenuation, as seen in the image on the right side of Figure 6. The tomograph's obvious advantage is its ease of interpretation to the viewer; however, its disadvantages include significantly increased computational time and the possibly sensitive nature of highly detailed images. Since sinograms contain the same information and accomplish the same goals as tomographs but require less time than a full image reconstruction, sinograms were used instead of tomographs for the template matching analysis in this work.

3.2 Hypothesis Testing

As described in Chapter 1, hypothesis testing is where sampled data is used to decide whether or not to reject some assumption or null hypothesis in favor of an alternative hypothesis. Hypothesis testing-based template matching fits well in this work since the objective is to determine if two objects match given some allowable error rate. The error rate here is actually two fold in origin, including type I error, where a matching object is incorrectly rejected as such, and type II error, where a nonmatching object is incorrectly accepted as matching.

Two important factors to consider when optimizing the performance of hypothesis tests are the type of testing algorithm employed and the alpha value, or threshold, to use for the test. Ideally, knowing some information about the data to be tested helps in deciding the best testing algorithm fit. For instance, some test algorithms are designed to work with certain underlying distributions, like a Gaussian distribution, while other non-parametric tests can be used even if the underlying distribution is unknown. The alpha value determines what threshold should be employed for accepting or rejecting the null hypothesis and corresponds directly to the maximum allowable type I error rate.

3.2.1 Kolmogorov-Smirnov Test. Several objectives were considered when looking at potential hypothesis testing algorithms for the template matching analysis. First, the test needed to be non-parametric since the underlying distribution was unknown and therefore, cannot be expected to follow a standard statistical distribution. Second, the test would most likely need to come from the class of hypothesis tests known as goodness-of-fit tests. These tests essentially compare how well two distributions fit one another with the null hypothesis being that they are from the same distribution. Also, since one of the aims of the template matching analysis is to provide a method that can be used with reasonably short measurement times, an algorithm that would work well with small data samples would be necessary.

Given these criteria, two goodness-of-fit tests were considered as the testing algorithm for the template matching analysis: the Chi-squared goodness-of-fit test and the Kolmogorov-Smirnov, or K-S, test. Although both are non-parametric, the K-S test turned out to be the better fit for two reasons. The first reason is that the Chi-squared goodness-of-fit test is a one-sample test where a sample distribution is compared to a known function. It is possible that with a sufficiently long measurement time the template measurement would have enough precision to serve as the known function but it would be preferable to have a test that did not require a known function. On the other hand, the K-S test has the ability to compare two samples to determine if they both come from the same underlying distribution, which permits the use of a shorter template measurement if needed. The second reason is that the K-S test performs better than the Chi-squared test with small sample sizes and does not require grouping of the data as the Chi-squared test does [30][31]. The K-S test's performance with small sample sizes is a significant advantage due to the possibility of reduced image pixels in the effort to minimize measurement times.

The two-sample K-S test works by comparing the differences between the cumulative distribution functions (CDFs) of two distributions, and, if the absolute value of the largest difference between the two CDFs is greater than some critical value, then the null hypothesis – that the two distributions are the same – is rejected. A graphical representation of this can be seen in Figure 7.

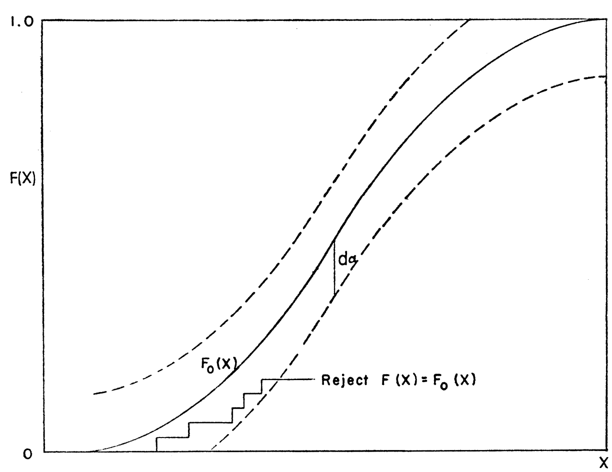

Figure 7. Graphical representation of the Kolmogorov-Smirnov test [30].

In a traditional statistical application, the two distribution samples in the K-S test would be defined as

$$F_N(x) = \frac{k}{N} \tag{3}$$

and

$$G_M(x) = \frac{k}{M} \tag{4}$$

where k is the number of data samples less than or equal to x. For the purpose of this template matching analysis, however, $F_N(x)$ and $G_M(x)$ are defined as the sum of attenuation coefficients in the attenuation projection profile up to x image pixels. The distance metric, d, is defined as

$$d = \max\left|F_N(x) - G_M(x)\right| \tag{5}$$

The d metric is then compared to a critical value, c. If $c>d$, then the greatest distance between the two empirical distributions is smaller than the critical value, and the distributions would be confirmed as matching (null hypothesis accepted); if $c<d$, then the differences between the two distributions is greater than the critical value and the two distributions would be rejected as matching (null hypotheses rejected). Normally, the value of c depends on the number of data points in the distribution sample and a specified alpha value, α. The quantity α is also referred to as the significance level, representing the probability of rejecting the null hypothesis in error. For instance with $\alpha = 0.05$, one would expect up to 5% of tests to reject two distribution samples as matching, even when

they are the same, simply by the chance of the differences between the two distributions being larger than the critical value. For the purpose of this template matching analysis however, the alpha value is used as a classification threshold, which is adjusted to achieve optimal classification.

3.2.2 Components of Hypothesis Testing. In hypothesis testing, an assumption is made that some statement, or null hypothesis H_0, is true. That null hypothesis is then tested to determine whether that assumption is in fact a good one or whether an alternative hypothesis H_A is more likely. The purpose of hypothesis testing is not to definitively prove the null hypothesis or the alternative hypothesis however. It simply provides the most likely hypothesis given the data with some level of confidence or error.

In order to determine that error, a test statistic T is defined as being some function of the data used to test the null hypothesis H_0. For the purpose of this work, the template and measured distributions and possible outcomes of hypothesis testing are as follows:

$$\vartheta = measurement\ of\ 'test'\ object$$

$$\vartheta_0 = measurement\ of\ template\ object$$

$$H_0 : \vartheta = \vartheta_0 \ \ versus\ \ H_A : \vartheta \neq \vartheta_0$$

The significance level α and the critical region C, where $C = (-\infty, -c] \cup [c, \infty)$ are determined such that $P(T \in C) = \alpha$, under the assumption that H_0 is true. If $T \in C$, we reject H_0 in favor of H_A. For instance in the case of the K-S test $T=D$, or the sum of the distance between the two distributions. If $|T|$ is larger than some critical value c, then the null hypothesis should be rejected. The value of c is determined based on what level of risk is acceptable for rejecting a null hypothesis which is actual true. That level of risk is represented by the significance level α, and commonly used values of α are 0.05, 0.01, and 0.001 or 5%, 1% and 0.1%, respectively. This value corresponds to the probability that the test statistic T will fall into the critical region C, thus causing the null hypothesis to be rejected, even though the null hypothesis is in fact true. This type of error is referred to as a false positive, or type I error. The other type of error is type II error, or false negative. A false negative occurs when the null hypothesis is false and should be rejected but the test fails to reject it, thus affirming the null hypothesis as true when it is not.

Minimizing these two types of error leads to a bit of a balancing act when choosing an α value for the test because in choosing a low value for α the probability of a type I error is low but the probability of a type II error increases as the α value decreases. Type II error is also difficult to calculate since it means that H_A, the alternative hypothesis, is actually true. Furthermore, H_A could be (∞-1) different sets since it can be anything but H_0, or, in this case, any object except for the template. Therefore, the probability of rejecting H_0 depends on "how false" it is, or here, how dissimilar the measured test object is from the template object.

As a simple example, imagine that single data sample is drawn from an unknown distribution and used to test the null hypothesis that the single sample was drawn from Sample Distribution 1, with the alternative hypothesis that it was drawn from Sample Distribution 2. This example is illustrated via two normalized distributions in Figure 8. Let's say that a selected alpha value of 0.05 produces a unitless threshold value of 2. In this example, if the data sample is below 2, then the null hypothesis is accepted, and, if it

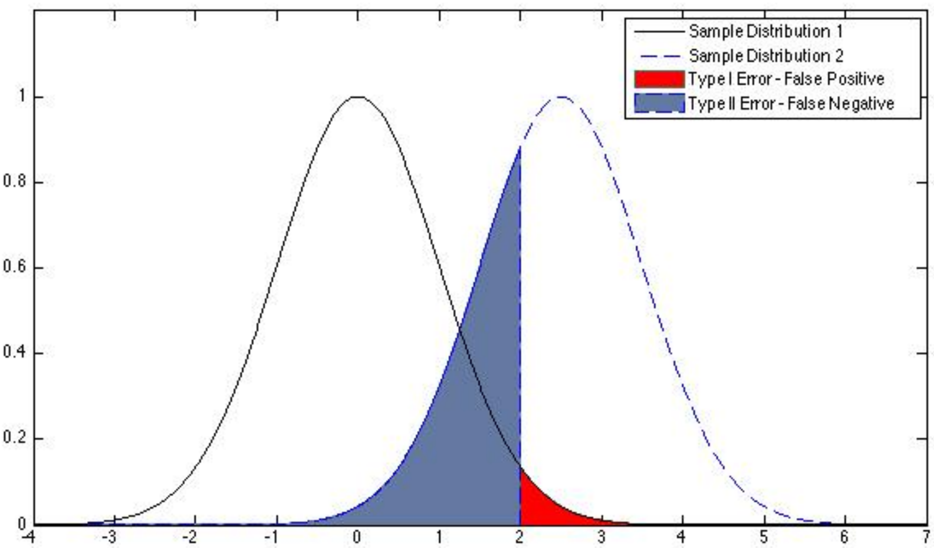

Figure 8. Graphical representation of classification threshold and misclassification with α-value of 0.05

is above 2, it is rejected. The red shaded area of Sample Distribution 1 represents the type I error. If the sampled data is actually from Sample Distribution 1, there is a 5% chance that it will fall in this region, and the null hypothesis will incorrectly be rejected. The gray shaded area (the portion falling below 2) of Sample Distribution 2 represents the type II error. Here a data sample that is actually from Sample Distribution 2 falls below the threshold, so the null hypothesis would incorrectly be accepted.

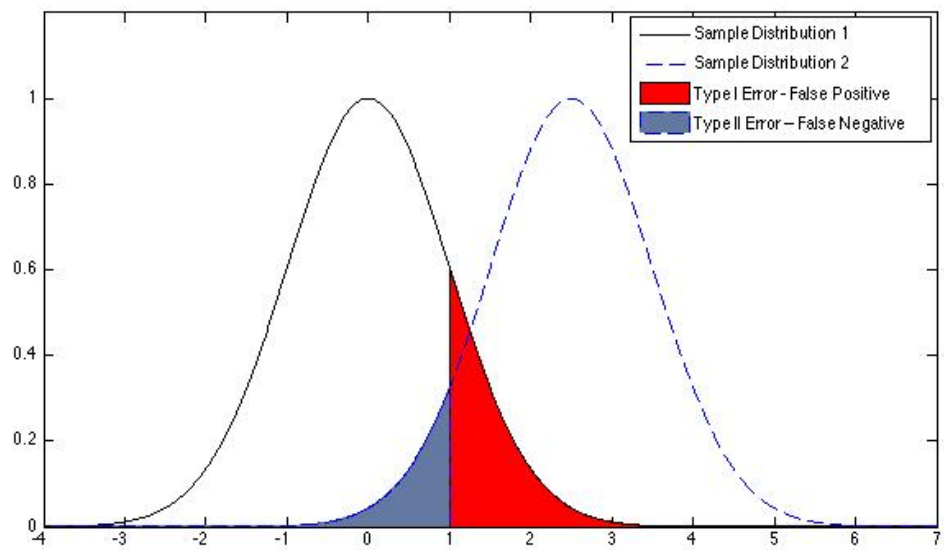

Figure 9. Graphical representation of classification threshold and misclassification with α-value of 0.15

This example can also be used to show how the alpha value affects error rates by changing the alpha value from 0.05 to 0.15. As seen in Figure 9, the threshold for accepting or rejecting the null hypothesis is now 1, and the red shaded area represents a 15% chance of rejecting a null hypothesis that is true. As the alpha value and the type I error increases, the type II error decreases, however. In this example, since the two distributions overlap, there will always be either type I or type II error, regardless of alpha value. Thus, perfect classification is not possible and the alpha value must be set in a way that best fits the situation. The alpha value might be set at 0.05 if it is more important to minimize the type I error than the type II error, for example.

3.3 Template Analysis Testing

The application of the presented method in a measurement environment is fairly straightforward. The first object is measured to make a template, which consists of multiple projections of the attenuation profile joined to form a sinogram. Each additional object is then measured, and its sinogram is compared to the template to confirm that they are the same. To confirm the objects as matching, each projection of the test object sinogram is tested against the corresponding projection in the template using the K-S test set with the null hypothesis that the two match. If any of the test object's projections are rejected as matching the template's corresponding projections then the object is also rejected as matching the template.

Although the method as a whole is simple, there are several user-defined variables that will strongly affect the test accuracy and measurement duration. These variables include the alpha value, the number of projections in the test object sinograms, the number of subsamples in each projection, and the measurement time of each subsample. In order to study the effects of these variables, as well as study the method's performance with changes in material, object dimensions, and object location, a framework for testing the template analysis was developed.

The framework of the template analysis testing was designed to focus on the performance of the template analysis to one specific change in the object, such as a change in material, and then look at the effects of the user-defined variables, such as alpha value. First, a sinogram, measured or simulated, was obtained and designated as the template. Then sinograms of the same object as the template, but slightly different due to statistical uncertainty, were designated as true test objects. An object with the alteration to be studied, such as with a different material but same dimensions, was then selected and its sinograms designated as false test objects.

The comparison of the template to one test object was considered a single trial and, since each of the test objects were slightly different due to statistical uncertainty, multiple trials of each combination of template/test object and user-defined variables were conducted to improve the accuracy of the error rates reported. Each unique combination of template/test object and user-defined variables was considered a set. Each set had hundreds to thousands of trials and each combination of template/test object had multiple sets, depending on how many different user-defined variables were studied. In some cases, hundreds of different combinations of user-defined variables were studied.

Error rates were used as the metric of performance for the template analysis. True positive rates, corresponding to 1 - type I error rate, or false negative rates, corresponding to the type II error rate, were reported for each set depending on whether the test object was a true test object (matching the template) or a false test object (different from the template). Table 1 shows the relationship the null hypothesis and test outcome. For instance, if a template was compared to 100 true test object sinograms and 1 out of 100 trials were rejected the null hypothesis, then the true positive rate was reported as 0.99. Conversely, if a template was compared to 100 false test object sinograms and 5 out of 100 trials were accepted the null hypothesis, then the false negative rate was reported at 0.05.

Table 1. Relationship between null hypothesis validity and test outcome

	Null Hypothesis (H_0) is True	***Null Hypothesis (H_0) is False***
Accept Null Hypothesis	True Positive (1-α)	Type II Error False Negative
Reject Null Hypothesis	Type I Error False Positive (α)	True Negative

Chapter 4

Measurement Data Analysis

The template analysis testing benefited greatly from the availability of existing NMIS measurements made by others [25][29]. This measurement data allowed for testing the method's performance with various materials and configurations as well as for studying the effects of user-defined variables on measurements performed in the field. Additionally, measurement data provided the unique opportunity to study the uncertainty that comes with performing measurements that cannot be duplicated in simulated data. One such uncertainty is the electronic variation or fluctuation that may occur in measurement equipment from day to day. Existing measurement data was also used to study how the method performs (1) when the imaged object is not correctly centered causing the image to be shifted or magnified, and (2) when the test object sinogram is started from a projection different from the template, leading to a rotational offset between the template and test object sinogram. The ability to determine when fissile material present in a template is replaced with non-fissile material of the same dimensions and attenuation was also explored using NMIS measurement data.

Although it is not possible to determine the performance of the method under all conditions or using every possible material and configuration, the measurement examples investigated in this chapter provide a basis of understanding that can be applied to future measurement situations. Measurement data studied during the template analysis testing includes both simple and complex object configurations that contain a variety of common materials likely to be encountered when using this method. Together these examples serve to provide a clearer picture of what can be expected with the application of this method during a measurement campaign.

4.1 Existing Measurements and Datasets

Several measurements useful to the template analysis testing were selected from existing NMIS measurements. The objects imaged in these measurements general fell into two types: cylindrically symmetric configurations and non-symmetric configurations. The cylindrically symmetric configurations were termed simple configurations since they could be completely imaged with a single projection given their symmetry, i.e. all of the image projections would essentially appear the same since the object is being rotated about its center axis. Conversely, the cylindrically non-symmetric configurations were termed complex configurations since they require multiple attenuation projections to be imaged and each projection provides unique information about the imaged object as it rotates.

4.1.1 Description of Existing Measurements. The first measurement, a cylindrically symmetric configuration, is a DU casting and steel ring assembly shown on the left side of Figure 10. The DU casting has a 3.5 in. inner diameter, 5.0 in. outer diameter, and 6 in. height. The steel ring is 1 in. thick, and the gap between the casting and ring is also 1 in. The distance from the source to detector array was 110 cm and the plane of the neutron generator and detector array was about 3 in. from the bottom of the casting. Four

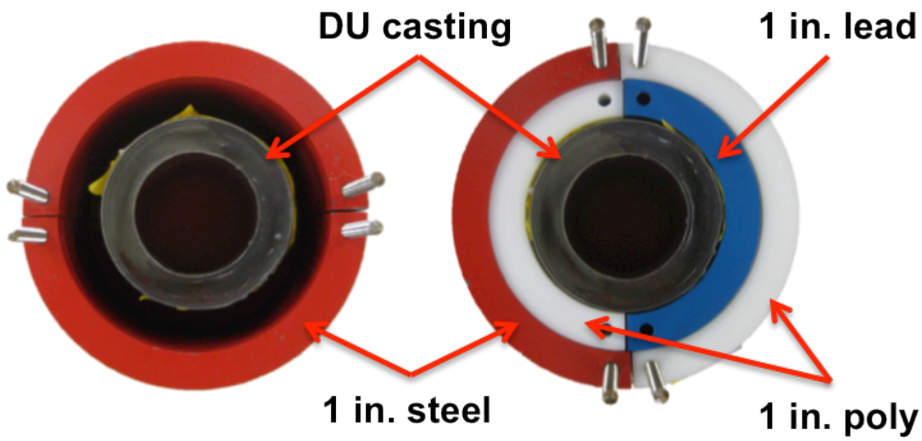

Figure 10. Comparison of configurations with a DU casting and varying shielding.

subsamples were taken for a total measurement time of one hour. Imaging measurements were performed with and without the DU casting.

For these simple configurations, there are multiple measurements on different days spanning one year. Having measurements of the same object imaged at different times was key to the study of systematic effects like detector response drift and changes in the location of the object in relation to the measurement system. Additionally, measurements were performed at heights of 30 cm, 64 cm, and 73 cm relative to the floor and with different source-to-assembly center distances of 34 cm and 42.5 cm. The time-of-arrival of each alpha and detector event was saved to permit analysis of shorter measurement times.

Another simple configuration was used in the template analysis testing of late fission neutrons to determine if the substitution of fissile material could be detected. These measurements used the DU casting described above as well as a 93.186 wt. % ^{235}U casting with the same dimensions, 3.5 in. inner diameter, 5.0 in. outer diameter, and 6 in. height [29]. In addition to measuring the castings alone, measurements were also taken of the castings surrounded by up to three layers of annular DU shields. A picture of the DU shields used can be seen in Figure 11. The DU shields had a height of 7 in. and dimensions described in Table 2. The source to transmission detector distance was 110 cm and the distance from the source to the center of castings was approximately 28 cm.

The first measurement of a complex, or non-symmetric, configuration is related to the simple configurations described above and consists of a DU casting and varying

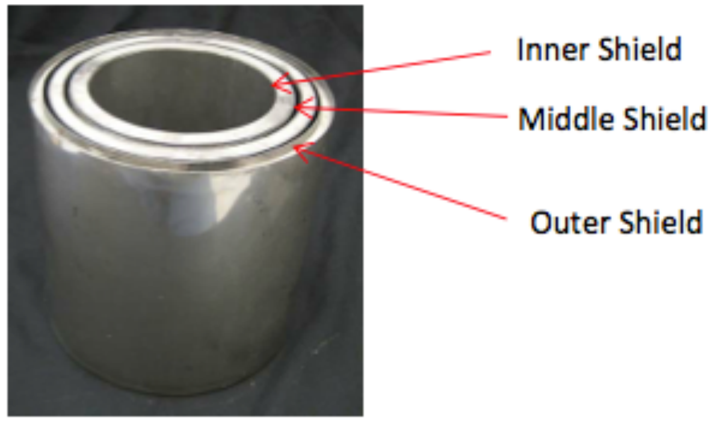

Figure 11. Annular DU shields [29]

Table 2. Dimensions of Annular DU shields [29]

	Inner Diameter (in.)	Outer Diameter (in.)	Thickness (in.)
Inner Shield	5.300	6.234	0.467
Middle Shield	6.642	7.394	0.377
Outer Shield	7.790	8.394	0.303

shielding materials. This configuration is shown on the right side of Figure 10. In this more complicated assembly, the casting was surrounded by 2 in. of shielding containing steel, lead, and polyethylene. The distance from the source to the front of the detector array and from the source to the center of the casting were 110 cm and ~37 cm, respectively. The height to the center of the DU casting was 64 cm relative to the floor. Since the materials in this assembly are not cylindrically symmetric, 60 projections were measured with four subsamples for 51.2 seconds at each projection. The total measurement time was about 3.4 hours.

Another group of complex configuration measurements were available from the 2010 INL Active Measurement Campaign. Each configuration is referred to as an inspection object (IO) and was presented either in the standard aluminum Zero Power Physics Reactor (ZPPR) clamshell or a cubical aluminum box with 8×8×8-in. inner dimensions and 3/8 in. thick walls [32]. Four of the ten IOs were measured: IO 3, IO 7, IO 9, and IO 10. The distance from the source to the transmission detector array was 115 cm and the distance from the source to center of each IO was approximately 40 cm. IO 3 is a collection of plutonium-aluminum (PuAl) plates with dimensions 2×2×1/8-in. filling half of a clamshell. IO 7 is a solid rectangular cuboid of enriched uranium surrounded by DU. IO 9 is a rectangular cuboid of PuAl surrounded by enriched uranium with a void in the center. IO 10 is a rectangular cuboid of PuAl surrounded by DU, which is surrounded by high-density polyethylene. A tomograph reconstruction of each IO transmission measurement and a photograph or concept diagram for each corresponding IO is shown in Figures 12-15.

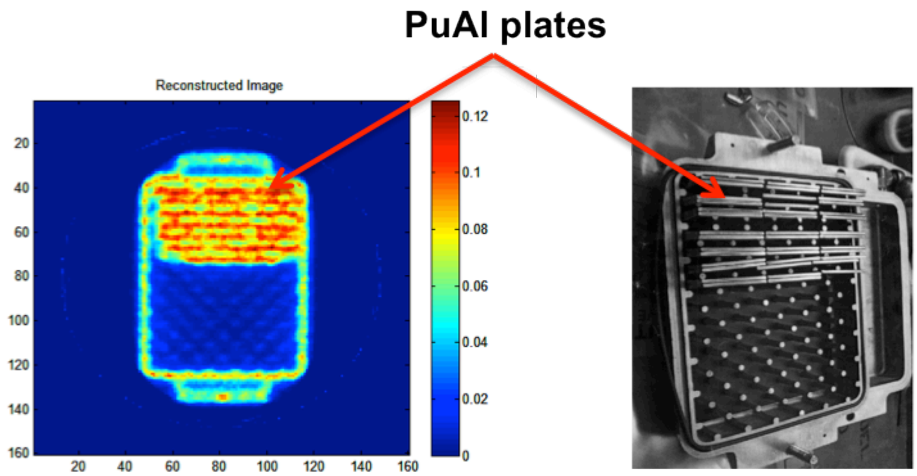

Figure 12. IO 3's (left) transmission image and (right) photograph of the configuration [11].

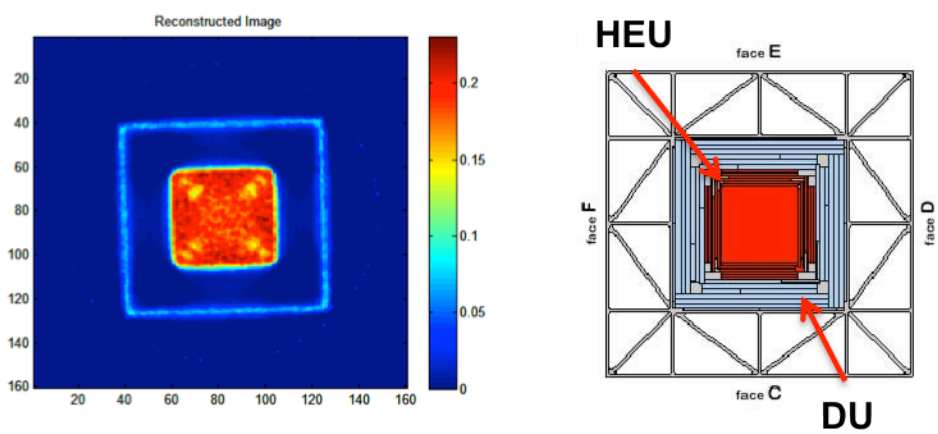

Figure 13. IO 7's (left) transmission image and (right) concept diagram of the material configuration near the vertical center [11].

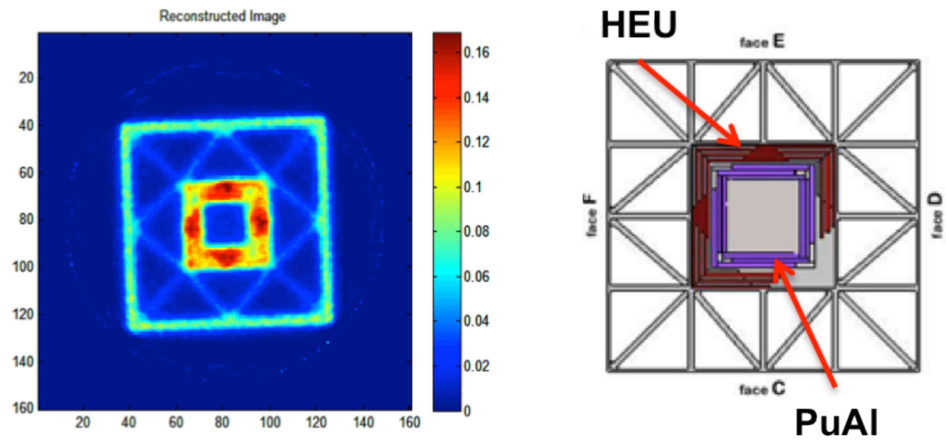

Figure 14. IO 9's (left) transmission image and (right) concept diagram of the material configuration near the vertical center [11].

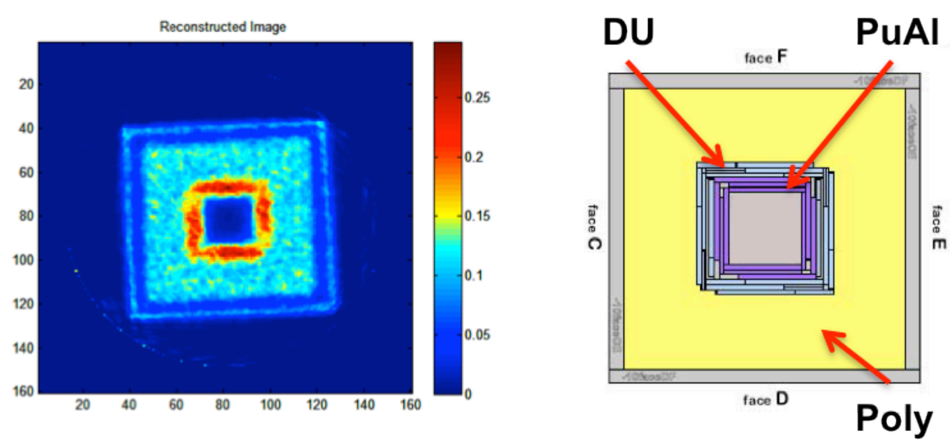

Figure 15. IO 10's (left) transmission image and (right) concept diagram of the material configuration near the vertical center [11].

For most of the measurement sets collected to generate multiple projections, the plane of the neutron generator and detector array was set to the middle of the material configuration inside the clamshell or aluminum box, which corresponded to about 70 cm, 74 cm, 72 cm, or 70 cm relative to the floor for IO 3, IO 7, IO 9, or IO 10, respectively. An extra height was measured for IO 10 near the top of its material configuration for comparison. For IO 3, IO 7, and IO 9, 60 projections were measured with four subsamples, each of duration 25.6 s for each projection such that the total measurement time was 1.7 hours. For both of the heights of IO 10 where data was recorded, 30 projections were measured with four subsamples, each measured for 25.6 s for each projection so that the total measurement time was also 1.7 hours. The details of all measurements are summarized in Table 3. These imaging results were first presented in Reference 25, which was reviewed in Chapter 2.

Table 3. Summary of existing measurement data used in template analysis testing

	Measurement	Source-to-center distance(s)	Source-to-detector distance(s)	Number of projections	Subsamples per projection	Time measured/ projection (total)
1.	DU + 1 in. steel	34 cm, 37 cm	110 cm, 115 cm	1	4	15 min (1 hour)
2.	Meas. (1) without DU	37 cm	110 cm	1	4	15 min (1 hour)
3.	DU + DU shields	28 cm	110 cm	1	4	7.5 min (30 min)
4.	^{235}U + DU shields	28 cm	110 cm	1	4	7.5 min (30 min)
5.	DU + steel + poly + lead	37 cm	110 cm	60	4	0.9 min (3.4 hours)
6.	IO 3	40 cm	115 cm	60	4	0.4 min (1.7 hours)
7.	IO 7	40 cm	115 cm	60	4	0.4 min (1.7 hours)
8.	IO 9	40 cm	115 cm	60	4	0.4 min (1.7 hours)
9.	IO 10	40 cm	115 cm	30	4	0.4 min (1.7 hours)

4.1.2 Description of Datasets. For the purpose of template analysis testing, the measurements described above were subdivided into smaller segments to increase the number of measurement samples available for testing and to provide datasets corresponding to shorter measurement duration times. Measurements 1-5 in Table 3 were acquired in list mode where every detector interaction is recorded with its corresponding time stamp. This mode of data acquisition is useful for subsequent analysis of the measurement data and in this case, the data file was split into sections corresponding to the desired measurement time for analysis.

For example, the simple configuration measurements of DU and steel, measurements 1 and 2 in Table 3, were subdivided into 30 s measurement samples per subsample for a total measurement time of 2 min. This division of the full measurement produced 30 – 2 min measurement samples for each of the simple configuration measurements. Increasing the number of measurement samples by decreasing the length of the measurement time allowed for 900 unique tests to be run between the two objects in the template analysis testing. The measurements of DU and ^{235}U castings with DU shields as well as the measurements of the DU casting with steel, poly, and lead were also subdivided into smaller measurement samples in this same way.

In addition to subdividing the fifth measurement from Table 3 consisting of DU, steel, poly and lead by decreasing the measurement time per subsample, this measurement was also subdivided by decreasing the number of projections in sinograms used for testing. Sinograms in Figure 16 show the full measurement of the DU, steel, poly and lead configuration as well as an example template and test object created from the

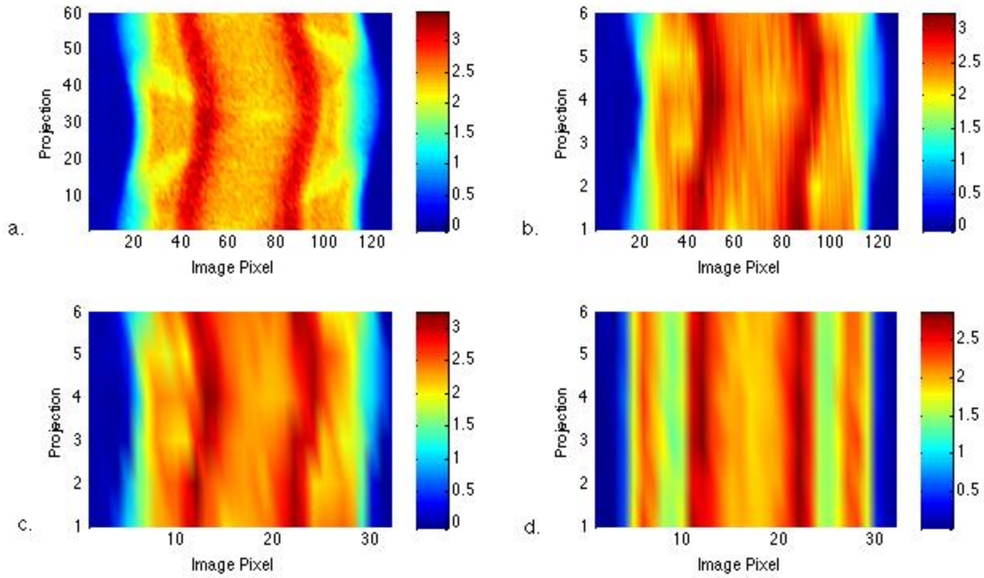

Figure 16. (a) Full measurement sinogram of the object seen at right in Figure 10. (b) Example template sinogram acquired from a. (c) Example true test object sinogram acquired from a. (d) Example false test object sinogram acquired from the full measurement of the left object seen in Figure 10.

full measurement for testing. The full measurement of 60 projections was subdivided into 10 template measurements each consisting of 6 projections and 4 subsamples for a total 128 image pixels. The full measurement was again subdivided into 80 test objects each consisting of 6 projections and 1 subsample for a total of 32 image pixels. The templates drawn from the full measurement represent what would be a 20.4 min measurement and the test objects represent a 1.5 min measurement. The simple configuration measurement of DU with steel shielding was used as a false test object in order to test the type II error, or false negative rate, when compared to the template of DU shielded by steel, poly, and lead. To construct the false test object sinograms, six of the divided measurement samples of the DU and steel measurement described above were merged to form a single sinogram. An example of this false test object sinogram is shown in Figure 16. Thus, the DU and steel false test object sinograms represented datasets of 6 projections and 1 subsample, matching the true test object datasets and corresponding to a 3 min measurement. This subdividing of the original measurements allowed for testing the template analysis 800 times with true test object sinograms and 64 times with false test object sinograms.

The 2010 INL measurements, measurements 6-9 in Table 3, comprise the remaining complex configurations using for template analysis testing. Sinograms constructed from the full fast neutron transmission measurement for each of the inspection objects (IOs) measured can be seen in Figure 17. The measurement time for each subsample of the IOs was only 25.6 s so measurement data was not divided as in previous datasets. An example of how the datasets were created is seen in Table 4. Like

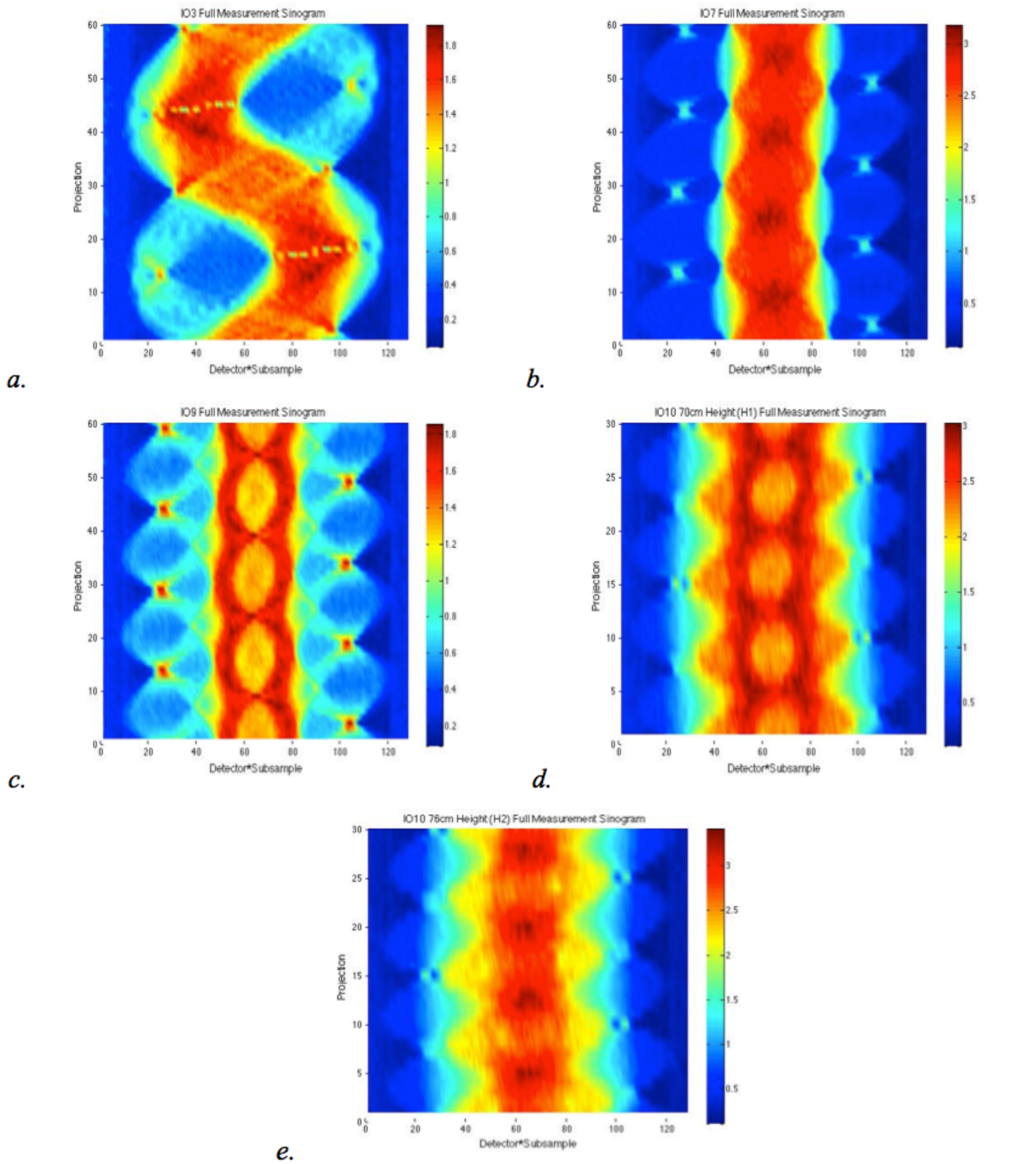

Figure 17. Sinograms of (a) IO3, (b) IO7, (c) IO9, (d) IO10 [H1], and (e) IO10 [H2]

Table 4. Example portioning of IO datasets for creation of templates and test objects for algorithm testing.

Example Portioning of Full Measurement for Templates & Test Objects							
Full Measurement	**Projection1**	**Projection2**	**Projection 3**	**Projection4**	**Projection5**	**…**	**Projection 60**
	Subsample 1	Subsample 1	Subsample 1	Subsample 1	Subsample 1	…	Subsample 1
	Subsample 2	Subsample 2	Subsample 2	Subsample 2	Subsample 2	…	Subsample 2
	Subsample 3	Subsample 3	Subsample 3	Subsample 3	Subsample 3	…	Subsample 3
	Subsample 4	Subsample 4	Subsample 4	Subsample 4	Subsample 4	…	Subsample 4
Templates							
Template 1	**Projection 1**		**Projection 11**		**Projection 21**	**…**	**Projection 51**
	Subsample 1		Subsample 1		Subsample 1	…	Subsample 1
	Subsample 2		Subsample 2		Subsample 2	…	Subsample 2
	Subsample 3		Subsample 3		Subsample 3	…	Subsample 3
	Subsample 4		Subsample 4		Subsample 4	…	Subsample 4
…							
Template 2		**Projection 10**		**Projection 20**		**…**	**Projection 60**
		Subsample 1		Subsample 1		…	Subsample 1
		Subsample 2		Subsample 2		…	Subsample 2
		Subsample 3		Subsample 3		…	Subsample 3
		Subsample 4		Subsample 4		…	Subsample 4
Test Objects							
Test Object 1	**Projection 1**		**Projection 11**		**Projection 21**	**…**	**Projection 51**
	Subsample 1		Subsample 1		Subsample 1	…	Subsample 1
Test Object 2	**Projection 1**		**Projection 11**		**Projection 21**	**…**	**Projection 51**
	Subsample 2		Subsample 2		Subsample 2	…	Subsample 2
Test Object 3	**Projection 1**		**Projection 11**		**Projection 21**	**…**	**Projection 51**
	Subsample 3		Subsample 3		Subsample 3	…	Subsample 3
Test Object 4	**Projection 1**		**Projection 11**		**Projection 21**	**…**	**Projection 51**
	Subsample 4		Subsample 4		Subsample 4	…	Subsample 4
Test Object 5		**Projection 2**		**Projection 12**		**…**	**Projection 52**
		Subsample 1		Subsample 1		…	Subsample 1
Test Object 6		**Projection 2**		**Projection 12**		**…**	**Projection 52**
		Subsample 2		Subsample 2		…	Subsample 2
…							
Test Object 39	**Projection 10**		**Projection 20**		**Projection 30**	**…**	**Projection 60**
	Subsample 3		Subsample 3		Subsample 3	…	Subsample 3
Test Object 40	**Projection 10**		**Projection 20**		**Projection 30**	**…**	**Projection 60**
	Subsample 4		Subsample 4		Subsample 4	…	Subsample 4

the DU, steel, poly and lead measurement above, the template sinograms created from the full IO measurements consisted of 6 equally spaced projections and 4 subsamples while the test object sinograms consisted of 6 equally spaced projections and 1 subsample. In the example shown in Table 4, the full measurement consists of 60 projections with 4 subsamples for each projection so this is split into 10 templates with 6 projections for each template separated by 60 degrees and 4 subsamples for each projection. The same full measurement is also split into 40 test objects with 6 projections for each template separated by 60 degrees and 1 subsample for each projection.

For testing with the IOs, templates consisted of 6 projections at 60-degree separations. Each projection had 4 subsamples measured for 25.6 s per subsample. An example template sinogram for each of the IOs is shown in Figure 18. These example template sinograms correspond to a measurement time of 10 minutes. Using 6 projections for the template means that multiple templates can be sampled from each full measurement and used to increase the number of test trials run in the testing stage. For IO 3, IO 7 and IO 9, ten separate templates were portioned out of the full measurement with a 6-degree rotational offset between each template sinogram, and from each height of IO 10, five template sinograms were obtained with a 12-degree rotational offset.

Example test object sinograms created from the full measurements of each IO are shown in Figure 19. Each test object sinogram can be used as either as a true test object sinogram or a false test object sinogram depending on which template it was being compared. Test object sinograms consisted of 6 projections at 60-degree separations and 1 subsample for a measurement time of 25.6 s per projection. This corresponds to a

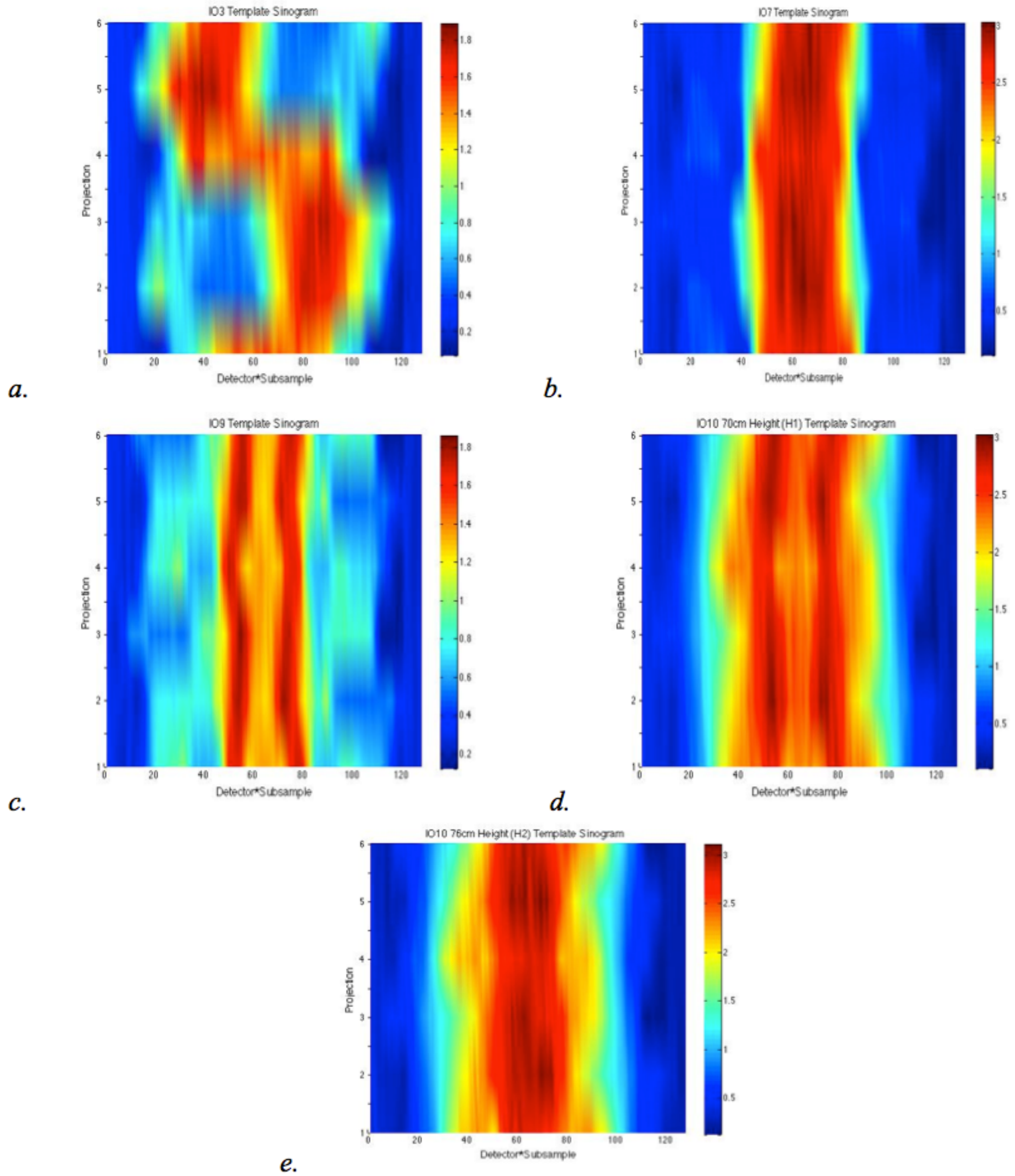

Figure 18. Example templates for (a) IO3, (b) IO7, (c) IO9, (d) IO10 [H1], (e) IO10 [H2]

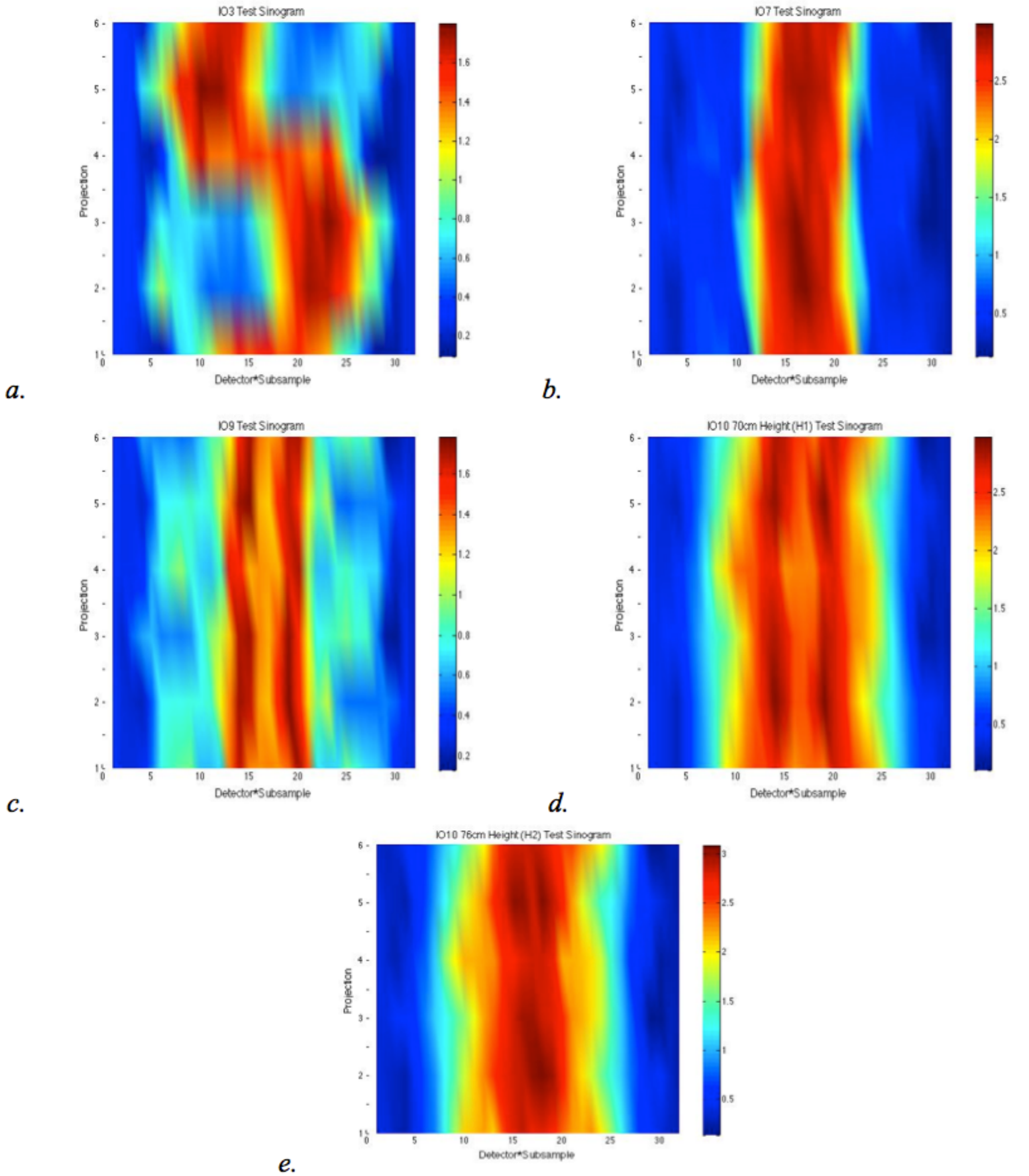

Figure 19. Example test objects for (a) IO3, (b) IO7, (c) IO9, (d) IO10 [H1], (e) IO10 [H2]

measurement time of 2.5 minutes for each test object. Having the larger number of test objects for testing will increase the confidence of testing of accuracy. For IO 3, IO 7 and IO 9, 40 test objects portioned from each full measurement and from each height of IO 10, 20 test object sinograms were constructed for a total of 160 test object sinograms.

4.2 Simple Configuration

4.2.1 Electronic Variation. Electronic variation is a systematic error that affects measurement data but that is difficult to replicate in simulations. Electronic variation may occur due to the normal fluctuations of electronic equipment or detector response drift, adding to the uncertainty beyond the standard statistical uncertainty of radiation measurements in general. The concern with this systematic effect was the possibility that it could result in enough variation added to the measurement that matching objects measured with a considerable amount of time separating the measurements, e.g., on different days, could be rejected as matching. In order to look at this effect and determine if the template analysis would be affected by the variation it caused in the measurement, four measurements using the same setup taken on four different days over a nine-month time span were utilized. These measurements of DU surrounded by steel shielding are summarized in the first row of Table 3, labeled as measurement 1.

The systematic error associated with electronic differences in each measurement is demonstrated by the distribution of total transmitted neutrons on the left side of Figure 20. Since the object was positioned slightly differently in each measurement, a translational offset correction was applied to view the effects due to electronic variation

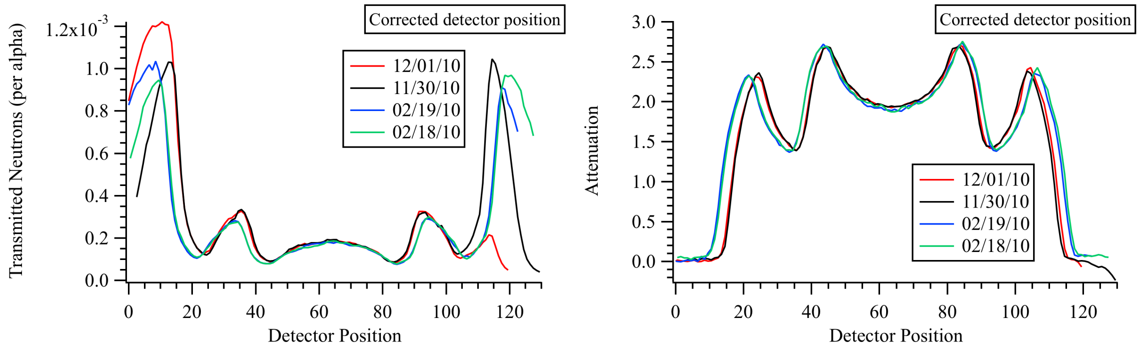

Figure 20. (left) Transmitted neutrons and (right) attenuation as a function of detector position for four measurements of DU and steel [33].

alone. While the transmitted neutron distributions look similar through the center detector positions where the object is located, the differences in the outside detector positions are significant. The K-S test rejected the different measurements of DU and steel as matching when using these transmitted counts, in fact, even when using the full measurement time of 60 min, which essentially removes statistical error as a factor in the template analysis. In these tests, an alpha value of 0.05 was used, and the measurement conducted on 02/18/10 was used as the template while the remaining three measurements were treated as test objects.

The plot on the right side of Figure 20 shows the attenuation profile of the four DU and steel measurements and demonstrates that the majority of variations shown in the outer detector positions are removed when constructing the attenuation plots, although some differences in magnification, which is covered in the following section, is still present. The removal of variation in the attenuation profiles is due to the attenuation being calculated from the ratio of transmitted counts with and without the object present, thus cancelling electronic differences that are present in both measurements. Since the void measurement, performed without the object present, and the measurement of the object are performed on the same day, most of the electronic variation, such as detector gain differences, will be present in both measurements and, therefore, removed in the attenuation determination.

4.2.2 Object Placement. Although electronic variation is removed with the calculation of attenuation, some variation between the measurements is still present in the attenuation profiles. Assuming uniformity in all settings and equipment, one would expect to see the outside detectors, which are out of view of the object, to receive approximately the same number of counts in both the void and object measurements, leading to an attenuation of zero in these areas. Some measurements, however, have a slightly non-zero baseline, as seen, for example, in Figure 21. Small angle scatters of interrogating neutrons on the outer edge of the measured object, which are detected in the outside detectors, cause the non-zero baseline. By detecting the small angle scatters, the outside detectors will record more counts in the measurement of the object than in the void measurement. This leads to the ratio of counts being greater than one and the attenuation value in these detector positions to be non-zero even though they are outside of the view of the object [34]. The different measurements of DU and steel here have dissimilar baselines due to slightly different source-to-object distances in the measurements. Although the effect is small in the attenuation profile, causing an offset of only about 1-2% of the object's maximum attenuation, the effect is large in the template analysis, leading to the rejection of matching objects.

For the measurements of DU and steel, the K-S test rejects the attenuation profiles of two of the three measurements as matching the template measurement performed on 02/18/10 without the baseline correction. With the baseline correction, all three measurements are confirmed as matching the template. The baseline correction consists of averaging the attenuations for the first five image pixels, or detector positions, where the object is not in view and subtracting the value from the entire attenuation profile to correct the offset as seen in the example shown in Figure 22.

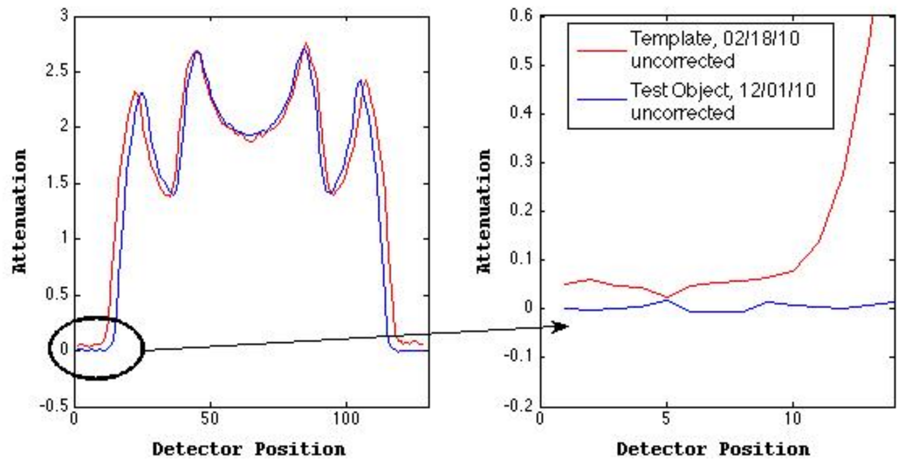

Figure 21. (left) Full and (right) close up views of uncorrected attenuation profiles for two 60 min measurements of DU and steel. Attenuation profiles have corrected detector positions.

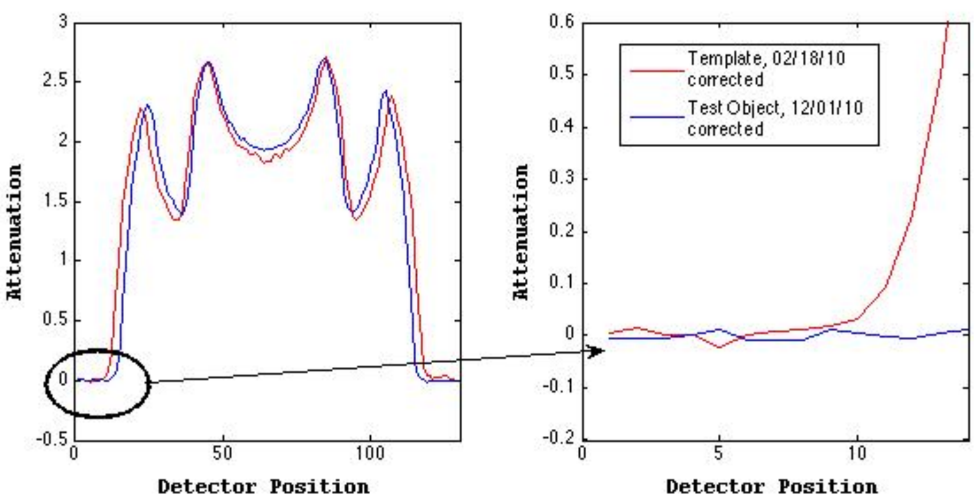

Figure 22. (left) Full and (right) close up views of baseline corrected attenuation profiles for two 60 min measurements of DU and steel. Attenuation profiles have corrected detector positions.

Magnification or shifting of an attenuation profile occurs when a measured object is translated from the position of the object in the original measurement. In other words, if a measured test object were not in the exact location that the template object was located at when it was measured, then the attenuation profiles of the two objects would have the shape and amplitude but would be translated with respect to the transmission detector positions. An example of this effect can be seen on the left side of Figure 23. This effect can occur with any type of object, whether rotationally symmetric or not.

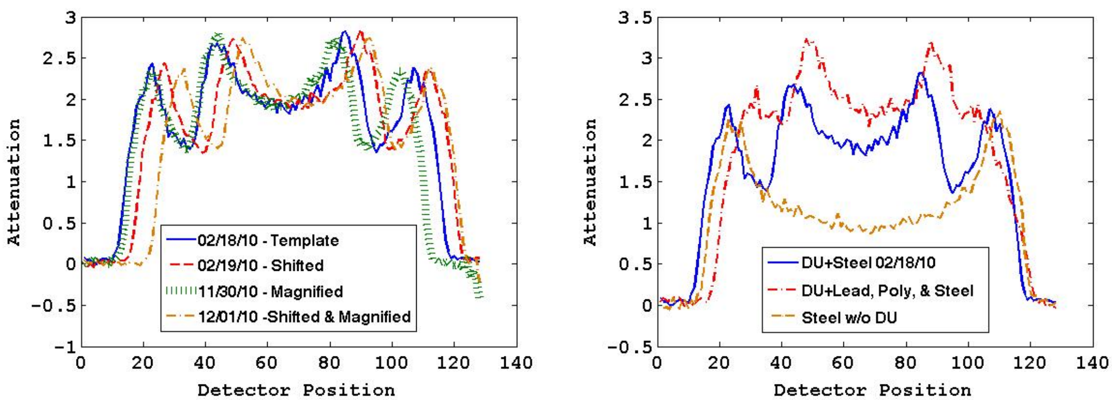

Figure 23. Example uncorrected attenuation profiles for (left) four sample measurements of DU with steel shielding and (right) sample measurements of DU with steel shielding, DU with lead, poly and steel shielding and steel shielding without DU.

Although magnification and shifting are both produced by the same cause, they are distinguished by the effect created on the attenuation profile. Magnification occurs when an object is moved closer or farther away from the neutron source than the original object, which will cause the attenuation profile to appear wider or narrower than the original object's attenuation profile. Shifting occurs when an object is located in a different lateral position with respect to the transmission detector positions compared to the template object, causing the attenuation profile to be laterally shifted compared with the original attenuation profile. It is also possible for an object that is moved either closer or farther away from the source and is translated laterally to have an attenuation profile that is both magnified and shifted from that of the original.

For the template analysis testing of shifting and magnification effects, the measurement of DU and steel performed on 02/18/10 was designated as the template measurement, and the remaining three measurements of DU and steel were designated as true test objects. The four full measurements of DU and steel were divided into samples of 30 s per subsample resulting in a total of 2 min of data acquisition for each measurement sample. False test measurements of DU with lead, poly and steel shielding and steel shielding without DU present were used as checks on the tests' alpha value, or threshold. Although the purpose of this template analysis testing was to determine if true test objects would be rejected due to normal measurement variation, the false test objects serve the purpose of verifying that the alpha value is not set so low that any amount of variation between template and test objects would be accepted as matching. The DU, lead, poly and steel measurement was subdivided into samples of 15 s per subsample for a total measurement length of 1 min. The steel shielding without DU measurement was subdivided into samples of 30 s per subsample for a total measurement length of 2 min An example of the measurement samples used in this testing can be seen in Figure 23. The increased statistical uncertainty associated with the shorter measurement times is demonstrated in the attenuation profiles seen in Figure 23 as compare to Figure 20-Figure

22. The effect of statistical uncertainty is therefore being testing in addition to the shifting and magnification of attenuation profiles.

Table 5. Results of template analysis for 2 min measurement of DU with steel shielding set as template and baseline correction applied.

Measurement	*True or False Test Object*	*Number of Trials*	*Alpha value*	*Percent Correctly Identified*
DU + Steel, 02/18/10	True	841	0.05 / 0.01	100 / 100
DU + Steel, 02/19/10	True	841	0.05 / 0.01	99.4 / 100
DU + Steel, 11/30/10	True	841	0.05 / 0.01	100 / 100
DU + Steel, 12/01/10	True	841	0.05 / 0.01	99.9 / 100
DU + Lead, Poly, & Steel	False	1740	0.05 / 0.01	100 / 100
Steel Shielding Only	False	841	0.05 / 0.01	100 / 100

Results of the template analysis testing of magnification and shifting with the DU and steel measurements are shown in Table 5. The baseline correction described in Section 4.2.1 was applied to the measurement samples prior to testing. The template analysis was unaffected by the magnification or shifting of the attenuation profiles, as evidenced by a total false positive rate of only 0.2% out of 3,364 trials with an alpha value of 0.05. No true test objects were misidentified out of 3,364 trials with an alpha value of 0.01. Additionally, 2,581 false test trials were conducted with each alpha value and no misidentification occurred. These results indicate that shifting and magnification of the attenuation profiles due to misplacement of the measured objects will not affect the outcome of the template analysis. The results also show that it would be possible to use different subsampling from template measurement to test object measurement, which would cause attenuation profiles to be associated with different detector positions, or image pixels, without affecting the template analysis.

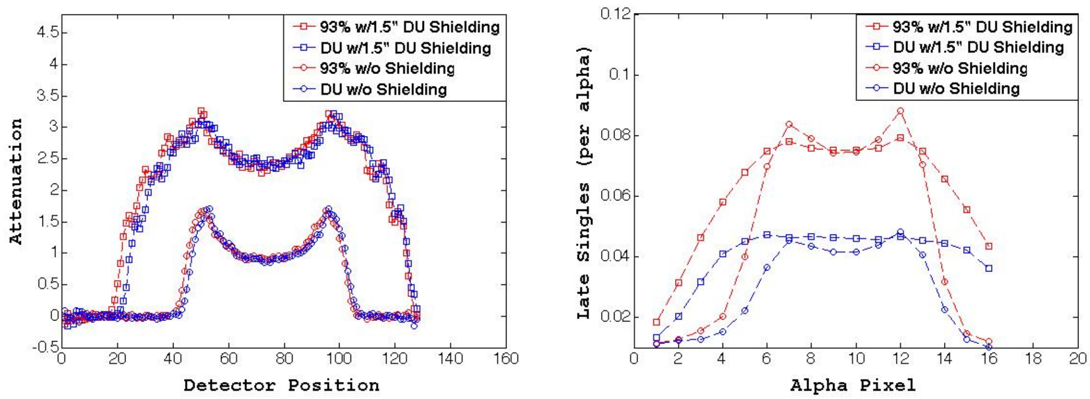

Figure 24. (left) Attenuation as a function of detector position and (right) late singles as a function of alpha pixel for measurements of 93 wt.% ^{235}U with and without 1.5 in of DU shielding, and DU with and without 1.5 in of DU shielding.

4.2.3 Fissile Detection. Since the template analysis relies on the K-S test in comparing attenuation profiles, one concern was that material with the same attenuation could be substituted for fissile material without being detected by the template analysis. An example of this would be if an object made of DU were substituted for an object of the same size and shape consisting of ^{235}U without being rejected due to both materials having the same attenuation. To study this, measurements of a 93.186 wt. % ^{235}U casting and a DU casting with various amounts of DU shielding (described in Section 4.1.1) were utilized in the template analysis testing. The plot on the left side of Figure 24 shows the attenuation profiles for the DU and ^{235}U castings without any shielding and with 1.5 in. of

DU shielding. Both the measurements of the bare castings and the castings with 1.5 in. of shielding appear indistinguishable in attenuation. To assist the template analysis in distinguishing between the materials, late fission singles recorded by the fission detectors were obtained from the list mode data collected for this measurement. The distribution of late singles as a function of alpha pixel can be seen on the right side of Figure 24. The late singles profile for the measurements of DU and ^{235}U can be clearly differentiated for measurements both with and without shielding. The late singles profile was therefore chosen as the metric to verify that the fissile nature of the test object matched the template in the template analysis. This additional metric means that the late singles profile of the test object as well as the attenuation profile must be accepted as matching the template for the test object and template to be confirmed as matching.

For the testing of the template analysis with the fissile material confirmation component, measurements with the ^{235}U casting were designated as templates while the measurements made with the DU casting were designated as false test objects. All of the full measurements were divided into samples of 15 s per subsample for a total of 1 min of data acquisition for each measurement sample. Results of the testing can be seen in Table 6 where the geometry identifiers None, I, M, and O refer to the DU shields used in the measurements, representing cases of no shielding, inner shield, middle shield, and outer shield, respectively, as shown in Figure 11. All K-S tests were performed with an alpha value of 0.05. The results demonstrate that if only attenuation profiles are used, the template analysis misidentifies the template as matching the test object when the DU casting is switched for the 235U casting in all 3,600 trials regardless of the amount of DU

Table 6. Results of template analysis testing the substitution of 93 wt.% ^{235}U casting with DU casting surrounded by various amounts of DU shielding, for a 1 min measurement. Alpha value of 0.05 used for all tests.

Geometry	*Thickness of DU Shielding*	*Number of Trials*	*Percent Correctly Identified w/o Late Singles*	*Percent Correctly Identified w/ Late Singles*
IMO	3.8 cm	900	0	100
IM	2.5 cm	900	0	100
I	1.3 cm	900	0	100
None	0 cm	900	0	100

shielding surrounding the castings. Alternatively, when the template analysis utilized both attenuation profiles and late singles profiles, the template and test object are correctly rejected as matching in all 3,600 trials regardless of thickness of DU shielding. Theses results illustrate the need to confirm late singles profiles in addition to attenuation profiles and also demonstrate the effectiveness in utilizing late singles as a metric to confirm the consistency of materials' fissile nature, even with short measurement times.

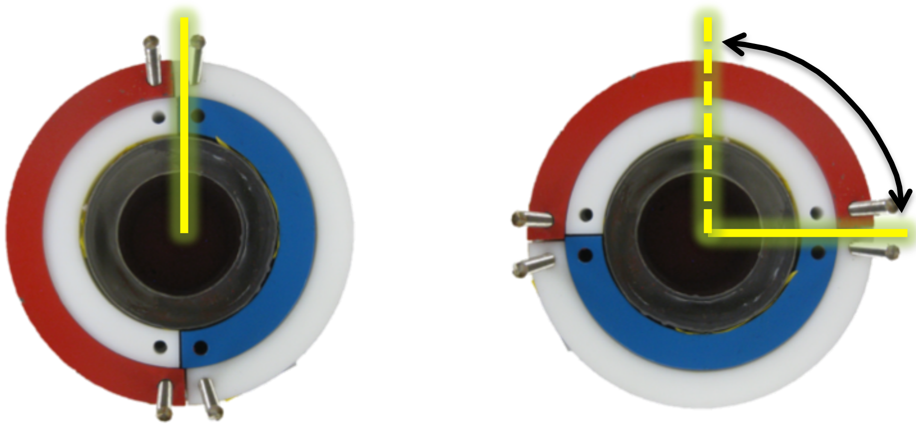

Figure 25. Top down view of object without rotational symmetry (right) at original position and (left) with 90°rotational offset.

4.3 Complex Configuration

4.3.1 Rotational Offset. Rotational offset is a situation that occurs when an object that is not rotationally symmetric is turned about its center axis so that it is shifted from the original position by a certain degree of offset. A pictorial example of rotational offset can be seen in Figure 25. If a template measurement is taken of an object that is not rotationally symmetric, there is a possibility that subsequent measurements of the same type of object will be rotationally offset from the original template measurement. This may lead to a rejection of an object as matching the template even though they are the same type of object because the rotational offset will cause the objects to appear to have differing geometries.

The INL inspection objects were utilized in the template analysis testing of rotational offset due the large degree of rotational asymmetry of the measured IOs. This requires more imaging measurements to be made to characterize the asymmetry. In this testing, attenuation profiles of the IOs were compared. The structure of templates and test objects obtained from full measurements was detailed in Section 4.1.2. In the template analysis testing, test objects were rotationally offset from templates in increments of 6° for IOs 3, 7, and 9 and in increments of 12° for IO 10, up to some maximum rotational variation. Maximum rotational variations of 24, 36 and 48° were tested for each of the IOs in comparison to all four measured objects. An example of how test trials are constructed for a maximum rotational offset can be seen in Figure 26. In this example, 3 templates and 12 test objects are used form 36 total test trials with a maximum rotational offset of 12° from the test object to the template.

For testing with the IO measurements, templates consisted of 6 projections with four subsamples for a total measurement time of 10 min while test objects contained 6 projections with one subsample for a total measurement time of 2.5 min. Prior to testing the effect of rotational offset on the template analysis, each IO was compared to the true test objects without rotational offset, and all were correctly identified as matching with an alpha value of 0.05. The results of the comparison of each IO including rotational offset

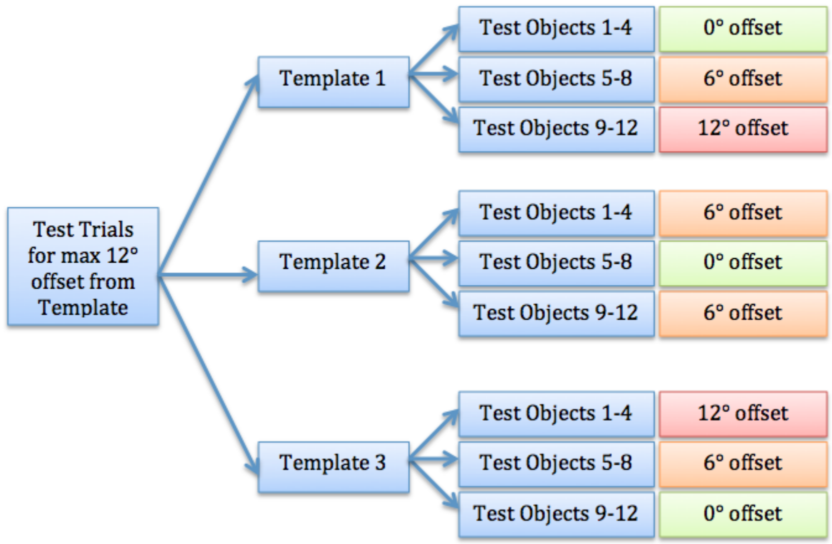

Figure 26. Diagram of test trial construction using an example consisting of 3 templates and 12 test objects to test a maximum rotational offset of 12°.

are shown in Table 7-Table 11. In general, the results show that the larger the rotational offset of the true test object from the template, the more likely it is to be rejected as matching the template. The degree of rotation that led to true test objects being rejected as matching the template depended on the IO, the amount of its internal variation, and the alpha value used in the analysis.

Template analysis results for IO 3 are shown in Table 7. When compared to IO 7 and IO 10, perfect classification is possible with even as high as a maximum 48° rotational variation present. Although perfect classification is still possible at the higher rotational variations for these IO comparisons, the range of alpha values which lead to perfect classification decreases as the maximum rotational offset increases from 24 to 36°. IO 9 has more similarity to IO 3, and perfect classification is not possible with a maximum rotational variation of 24° or higher. The alpha range chosen for IO 9 corresponds to values that maximize the true positive rate while minimizing the false positive rate. This range assumes that correctly identifying matching objects and rejecting non-matching objects is of equal importance. If a greater importance was placed on rejecting non-matching objects, a range of alpha values which insured a false positive rate of 0 could easily be identified for that objective. This would also increase the chance of incorrectly rejecting a matching object, however, as the alpha value would require a degree of accuracy to the template which would exceed the differences caused by measurement variation. Conversely, a range of alpha values with a true positive rate of 1 is also possible if insuring that all matching objects are correctly accepted is of greater importance. The trade off is that there is a greater chance of incorrectly identifying a non-

Table 7. Results of template analysis testing with IO 3 as template

Comparison IO	***Max Rotation Variation (Degrees)***	***Total Projections Utilized***	***True Test Object Trials***	***False Test Object Trials***	***Best True Positive Rate***	***Best False Negative Rate***	***Corresponding Low Alpha***	***Corresponding High Alpha***
7	24	60	100	100	1	0	0.012	0.054
7	36	60	196	196	1	0	0.012	0.02
7	48	60	324	324	1	0	0.012	0.02
9	24	60	100	100	0.87-0.94	0.02-0.13	0.084	0.15
9	36	60	196	196	0.821-0.852	0.051-0.133	0.084	0.124
9	48	60	324	324	0.793-0.846	0.031-0.093	0.084	0.124
10 (Height 1&2)	24	30	36	72	1	0	0.001*	0.053
10 (Height 1&2)	36	30	64	128	1	0	0.001*	0.021
10 (Height 1&2)	48	30	100	200	1	0	0.001*	0.021

*Indicates lowest alpha value tested in analysis

Table 8. Results of template analysis testing with IO 7 as template

Comparison IO	***Max Rotation Variation (Degrees)***	***Total Projections Utilized***	***True Test Object Trials***	***False Test Object Trails***	***Best True Positive Rate***	***Best False Negative Rate***	***Corresponding Low Alpha***	***Corresponding High Alpha***
3	24	60	100	100	1	0	0.012	0.066
3	36	60	196	196	1	0	0.012	0.026
3	48	60	324	324	0.9012-0.9198	0-0.1728	0.008	0.016
9	24	60	100	100	1	0	0.014	0.066
9	36	60	196	196	1	0	0.014	0.026
9	48	60	324	324	0.9012-0.9136	0-0.1173	0.012	0.016
10 (Height 1&2)	24	30	36	72	1	0	0.017	0.149
10 (Height 1&2)	36	30	64	128	1	0	0.017	0.034

Table 9. Results of template analysis testing with IO 9 as template

Comparison IO	Max Rotation Variation (Degrees)	Total Projections Utilized	True Test Object Trials	False Test Object Trials	Best True Positive Rate	Best False Negative Rate	Corresponding Low Alpha	Corresponding High Alpha
3	24	60	100	100	0.98-0.99	0.01-0.05	0.126	0.178
3	36	60	196	196	0.975-0.989	0.005-0.031	0.126	0.178
3	48	60	324	324	0.923-0.978	0.022-0.083	0.084	0.15
7	24	60	100	100	1	0	0.012	0.124
7	36	60	196	196	1	0	0.012	0.124
7	48	60	324	324	1	0	0.012	0.034
10 (Height 1&2)	24	30	36	72	1	0	0.001*	0.253
10 (Height 1&2)	36	30	64	128	1	0	0.001*	0.179
10 (Height 1&2)	48	30	100	200	1	0	0.001*	0.067

*Indicates lowest alpha value tested in analysis

Table 10. Results of template analysis testing with IO 10 [H1] as template

Comparison IO	Max Rotation Variation (Degrees)	Total Projections Utilized	True Test Object Trials	False Test Object Trials	Best True Positive Rate	Best False Negative Rate	Corresponding Low Alpha	Corresponding High Alpha
3	24	30	36	36	1	0	0.001 *	0.345
3	36	30	64	64	1	0	0.001 *	0.213
3	48	30	100	100	1	0	0.001 *	0.123
7	24	30	36	36	1	0	0.015	0.345
7	36	30	64	64	1	0	0.017	0.213
7	48	30	100	100	1	0	0.023	0.123
9	24	30	36	36	1	0	0.001 *	0.345
9	36	30	64	64	1	0	0.001 *	0.213
9	48	30	100	100	1	0	0.001 *	0.123

*Indicates lowest alpha value tested in analysis

Table 11. Results of template analysis testing with IO 10 [H2] as template

Comparison IO	***Max Rotation Variation (Degrees)***	***Total Projections Utilized***	***True Test Object Trials***	***False Test Object Trials***	***Best True Positive Rate***	***Best False Negative Rate***	***Corresponding Low Alpha***	***Corresponding High Alpha***
3	24	30	36	36	1	0	0.001 *	0.179
3	36	30	64	64	1	0	0.001 *	0.179
3	48	30	100	100	1	0	0.001 *	0.179
7	24	30	36	36	1	0	0.017	0.179
7	36	30	64	64	1	0	0.023	0.179
7	48	30	100	100	1	0	0.035	0.179
9	24	30	36	36	1	0	0.001 *	0.179
9	36	30	64	64	1	0	0.001 *	0.179
9	48	30	100	100	1	0	0.001 *	0.179

*Indicates lowest alpha value tested in analysis matching object as matching the template with an alpha value that is more forgiving of variations from the template.

Results from the template analysis testing are shown in Figure 27 and Figure 28. In Figure 27, the ROC curves for the comparison of IO 3 with IO 9 are shown for three maximum rotational variations: 12, 24 and 36°. The tests with a maximum rotation of 36° have 196 trials for both true and false test object sinograms for each of the 200 alpha values tested; the tests with maximum rotation of 24° have 100 trials for both true and false test object sinograms for each alpha tested; the tests with maximum rotation of 12° have 36 trials for each alpha tested. The line plotted indicates the location of the optimal identification, minimizing the false positive rate and maximizing the true positive rate, corresponding to the chosen optimal alpha test statistic range. As the offset between the true test object and the template increases, the accuracy of identification decreases causing lower true positive rates. The same trend is illustrated in Figure 28 where IO 7 is compared to IO 9. The template analysis testing with a maximum rotation of 36° used 196 trials of both true and false test object sinograms to investigate each of the 200 alpha values tested, and the tests with maximum rotation of 48° have 324 trials of both true and false test object sinograms for each alpha tested. In the template analysis comparing IO 7 and IO 9, the optimal alpha value varied from 0.014-0.26 for the 36° maximum rotation variation and 0.012-0.016 for the 48° maximum rotation variation demonstrating slight overlap from 0.14-0.16. Overall, no alpha values were found that provided optimal identification in all comparisons. Additional analysis on alpha values and optimized measurement settings is presented in Chapter 5.

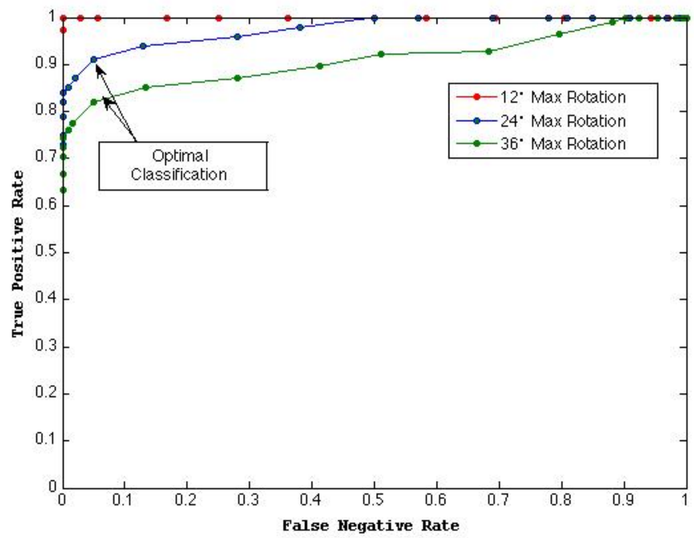

Figure 27. ROC curves of template analysis results with IO 3 as template and IO 9 as false test object with varying alpha value.

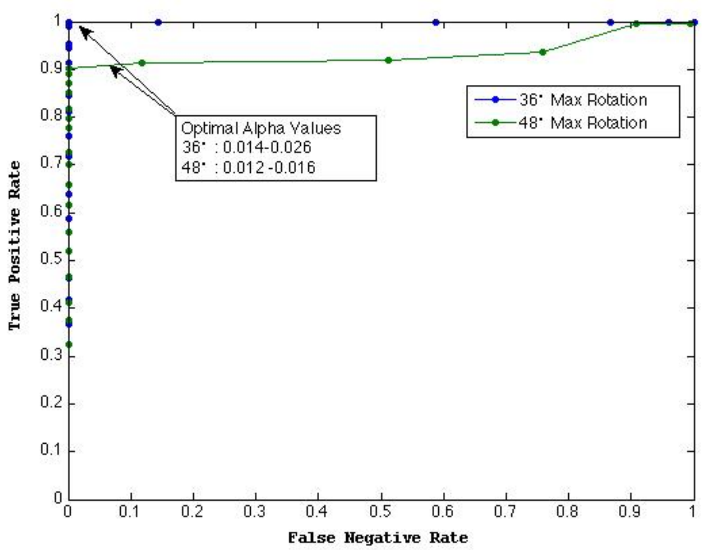

Figure 28. ROC curves of template analysis results with IO 7 as template and IO 9 as false test object with varying alpha value.

Chapter 5

Simulation Data Analysis

In the process of testing the template analysis, it was necessary to look at certain situations that were not covered in the existing measurement data. These situations included small changes in object dimensions and attenuation. Due to the need to test these situations, measurements were simulated for template analysis testing to supplement the existing measurement data. The template analysis testing required not only the modeling of each object to be studied but also the uncertainty associated with the length of measurement. For instance, it was desirable to determine how the template analysis performed using data obtained for 30 s, 60 s, 90 s and 120 s per subsample for each of the modeled objects. Also, for each simulated measurement time multiple attenuation profiles were needed to run multiple trials of the same set of variable combinations ensuring the statistical certainty of the template analysis results. This means that 200 or more simulations were needed for each modeled object.

Due to the large number of simulations needed and the time consuming nature of Monte Carlo type simulations, a simulation program was developed to quickly obtain attenuation profiles. This ray trace simulation program allowed for object simulations to be obtained in minutes rather than days, as would be needed with MCNP simulations. The ray trace program coupled with an error analysis of existing measurement data was used in the simulation of both simple and complex object configurations for studying the effects of changes in object dimensions and material substitution.

It is important to note that the results of the measurement simulations are not intended for exact predictions of template analysis abilities but rather guidelines for possible future use of this method. For instance, the results that indicate the amount of time needed to identify a certain change in object dimensions are given as estimations for a particular set of parameters as each unique measurement situation will affect the results of the template analysis. On the other hand, the general conclusions obtained such as the effect of user-defined parameters on the true positive and false negative rates should provide the most useful information for possible future applications of the template analysis.

5.1 Simulation Description

5.1.1 Ray Trace Program. The ray trace program is a relatively straightforward and concise C program that returns the attenuation profile given an input geometry and composition[1]. Since this program was specifically designed to simulate the attenuation profiles of NMIS measurements, it exclusively calculates the neutron attenuation along a path from the source, through the simulated object, to the defined transmission detector array. The limited scope of the program equates to quick results, providing simulated attenuation profiles in a fraction of the time of MCNP.

---

[1] Ray trace program was developed by Seth McConchie at the Oak Ridge National Laboratory in 2014

For a desired object configuration, the user defines each object's shape and dimensions as well as the material's attenuation coefficient for 14 MeV neutrons. The user also defines the numbers of rays, or paths, used in calculating the attenuation profile. Since the rays explicitly calculate the attenuation along a path, the number of rays does not relate to the statistical accuracy the way the number of source particles does in Monte Carlo calculations, but rather samples the physical space within an angle corresponding to the transmission detector array. The number of rays used in the presented simulations was 514, as this was more than adequate to sample the space, and increasing the number of rays did not affect the results.

To calculate the attenuation of a ray, the path starts at the source and traverses through the object towards the transmission detector array. The simulated object is modeled as a set of pixels with an attenuation value assigned to each pixel depending on the defined material's attenuation coefficient. As the ray encounters a pixel, the attenuation of the pixel is added to the ray's total attenuation. Thus, the attenuation for each pixel that the ray encounters along its path is summed to obtain the total ray attenuation. The ray's path and ultimate detector position are used to form the final attenuation profile. In addition to allowing the user to define the number of rays used in the simulation, the ray trace program also allows the user to control the source-to-detector distance, source-to-center distance, number of detectors, number of projections and number of subsamples.

To benchmark the ray trace program's performance against frequently used Monte Carlo simulations, an attenuation profile obtained with the ray trace program was compared to the same profile acquired from an MCNP6 simulation. In both programs, an annular DU casting with 3.5 in. inner diameter, 5 in. outer diameter and 6 in. height was modeled, surrounded by a 1 in. thick iron shield. In the ray trace program, a source-to-detector distance of 115 cm was used, and 32 detectors with 8 subsamples each provided a total of 256 detector pixels. In the MCNP6 calculation, the source was placed at the origin with a spherical mesh tally at 115 cm with azimuthal binning equal to the angular binning in the ray trace program for 256 pixels and an opening angle of 50.6 degrees. The azimuthal bin simulates the size of an actual detector and then the mesh is rotated relative to the annulus to simulate 8 subsamples. A total of 2 $x10^9$ histories were run with approximately 300 counts recorded per bin. The resulting attenuation profiles from the ray trace program and MCNP6 simulations can be seen in Figure 29. The comparison of the two attenuation profiles shows good agreement between the two programs with small discrepancies seen only in the highest attenuations of the DU casting.

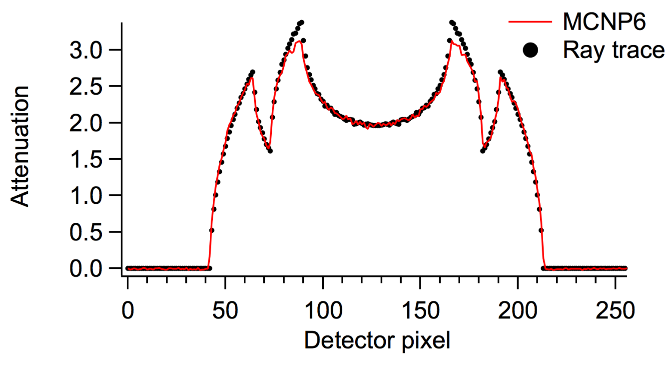

Figure 29. Comparison of attenuation profiles from simulated DU casting with iron shield using ray trace program and MCNP6.

The ray trace program was additionally benchmarked against measurements of five annular castings consisting of aluminum, DU, iron, lead, and tungsten. Each measured casting had an inner diameter of 3.5 in., an outer diameter of 5 in. and 6 in. height. The measurements, as well as their model representations, all had a source-to-detector distance of 115 cm and 32 detectors with 4 subsamples for a total of 128 detector positions. Attenuation coefficients of 0.105, 0.28, 0.22, 0.176 and 0.349 cm^{-1} were used in modeling the aluminum, DU, iron, lead and tungsten castings, respectively. The attenuation profile results of the measurements and ray trace simulation are shown in Figure 30. Again, the ray trace program shows good agreement with the various materials measured with only small discrepancies seen in the highest attenuations of the DU, iron and tungsten castings.

The small discrepancies seen between the ray trace program and measured castings do not greatly impact the template analysis testing presented in this chapter since the simulations are only compared to other simulations rather than being compared to measurements. In other words, the testing with simulations only looks at the differences between two simulated attenuation profiles to determine if the two are a match and any discrepancies will be present in both simulated profiles. Therefore, the discrepancies seen between measured attenuation and simulated attenuation will not affect that decision process.

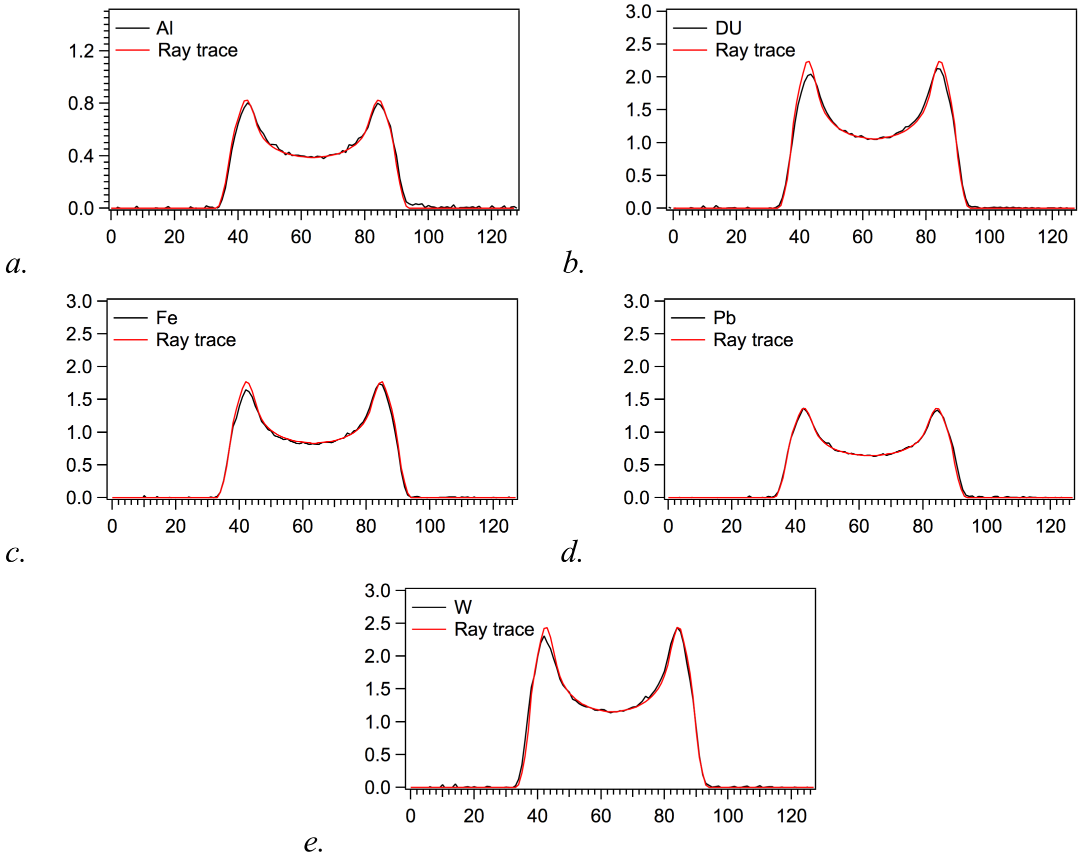

Figure 30. Comparison of attenuation profiles from measured casting of (a) aluminum, (b) DU, (c) iron, (d) lead, and (e) tungsten to those same casting simulated with the ray trace program. Attenuation is shown on the vertical axis with detector position on the horizontal axis.

5.1.2 Error Analysis. Since the ray trace program explicitly calculates the attenuation profiles of simulated objects, the profiles represent the expected attenuation without error. In order for the template analysis testing to compare the differences in various simulated measurement times it was necessary to add error to the attenuation profiles obtained from the ray trace program. To determine what error would be associated with a given attenuation and measurement duration, two measurements of the same object performed on different days were utilized. These measurements of a DU casting with steel shield performed on 2/19/10 and 11/30/10 were described in Section 4.1.1 and listed as the first measurement in Table 3.

The use of empirical data was chosen for the error analysis over the calculation of statistical uncertainty seen in all radiation measurements due to the inclusion of any systematic error that may be present in the measurement data. While the use of this measurement data is limited in its range of attenuation values and materials, it provides an understanding of the relationships between attenuation values, length of measurements and error required for the template analysis testing described in latter sections of this chapter.

For the error analysis, the two measurements were subdivided into smaller segments equivalent to 30, 60, 90 and 120 s per subsample measurement samples as described in Section 4.1.2. For each measurement of DU and steel, there were 29 sample measurements with 30 s per subsample pulled from the full measurement. For samples with 60, 90 and 120 s per subsample, 14, 9 and 7 sample measurements were subdivided respectively from the full measurement.

To determine the true attenuation of the measurement, the attenuation at each detector position for a measurement length of 1000 s per subsample was used as the true attenuation for that detector position. At 1000 s, or approximately 16.7 min, per subsample the statistical uncertainty was low enough that the error in the attenuation at a given detector position was considered negligible. The attenuation of the shorter measurement samples were then compared to the attenuation of the same detector position at 1000 s to obtain the error associated with the attenuations of the shorter measurement times.

For example, if the attenuation at detector position 30 was 2.1 in the 1000 s measurement sample but 2.06 in the 30 s measurement sample then an difference of 0.04 was recorded for a 30 s measurement and an attenuation of 2.1. The error of all sample measurement files were averaged for each detector position such that for each full measurement the error from 29 sample measurements representing 30 s measurement samples were averaged to provide the error in attenuation at 128 detector positions, the error from 14 sample measurements representing 60 s measurement samples were averaged to provide the error in attenuation at 128 detector positions, etc. A plot depicting the average error as a function of the attenuation at 1000 s is shown in Figure 31.

The average error obtained from the two measurements performed on 2/19/10 and 11/30/10 were combined and fit with two exponential functions for each measurement length as seen in Figure 32. The coefficients associated with the fitted functions as well as the adjusted R^2 values of the fits are listed in Table 12. Both measurements were

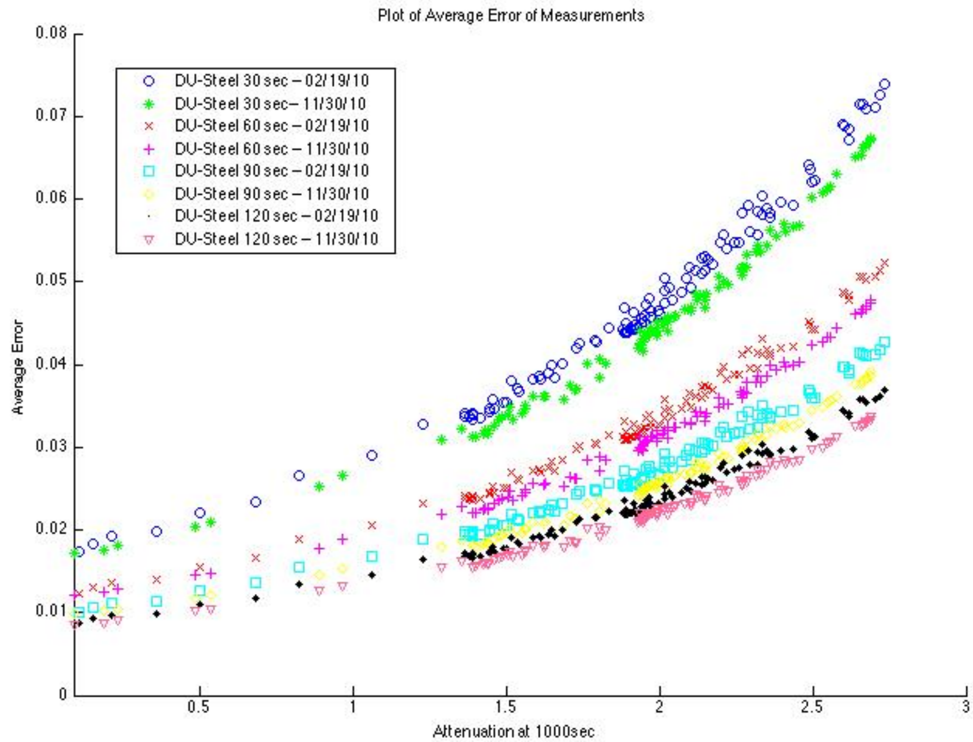

Figure 31. Average attenuation error as a function of attenuation at 1000 s for two measurements of DU and steel divided into measurement samples of various lengths.

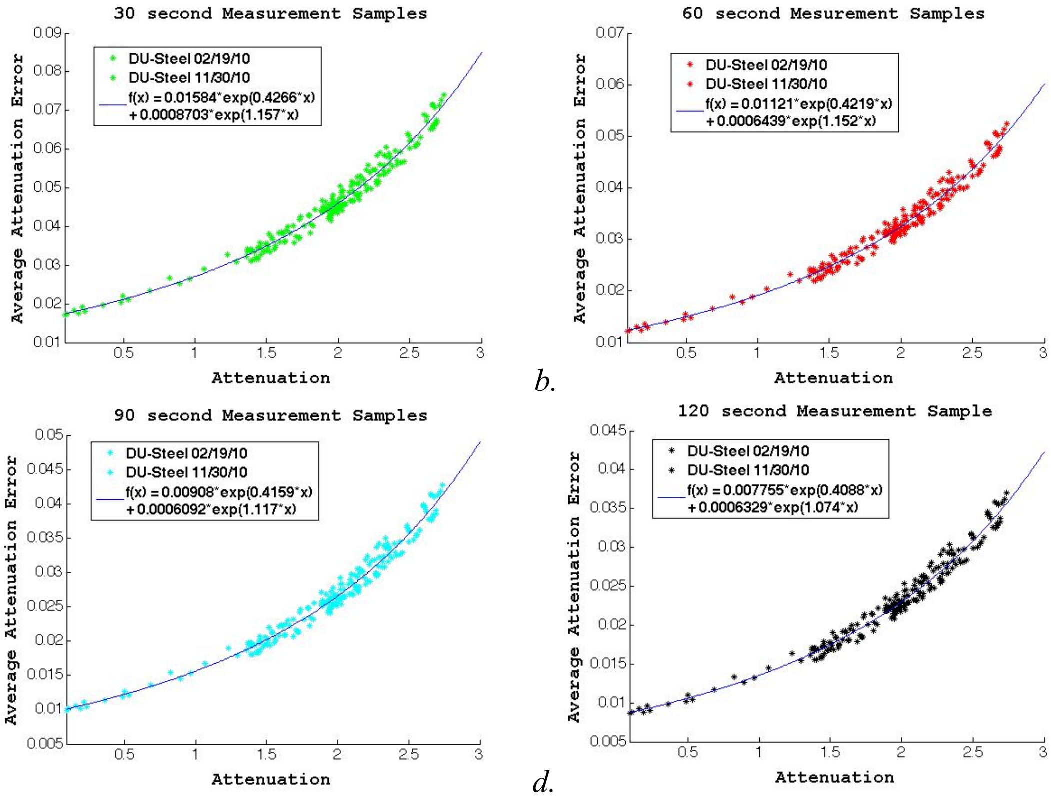

a. *b.* *c.* *d.*

Figure 32. Average attenuation error as a function of attenuation from measurements of DU and steel fit with two exponential functions for (a) 30 s, (b) 60 s, (c) 90 s, and (d) 120 s measurement samples.

Table 12. Coefficient values for f(x)=A•exp(B•x)+C•exp(D•x) fit to attenuation error for measurement samples of 30, 60, 90 and 120 seconds.

Measurement Sample Length	*Coefficient A*	*Coefficient B*	*Coefficient C*	*Coefficient D*	*Adjusted R^2*
30 sec	0.01584 (0.00958,0.02211)	0.4266 (0.0718,0.7814)	0.0008703 (-0.006,0.008)	1.157 (-0.641,2.956)	0.9766
60 sec	0.01121 (0.00656,0.01586)	0.4219 (0.0439,0.7999)	0.0006439 (-0.005,0.006)	1.152 (-0.664,2.968)	0.9752
90 sec	0.00908 (0.00451,0.01365)	0.4159 (0.0007,0.831)	0.0006092 (-0.005,0.006)	1.117 (-0.689,2.923)	0.9749
120 sec	0.007755 (0.00275,0.01276)	0.4088 (-0.063,0.8807)	0.0006329 (-0.005,0.006)	1.074 (-0.735,2.883)	0.9744

performed with the DT generator operating on high power. The measurement conducted on 2/19/10 recorded an average of approximately 7500 alphas per second per alpha pixel, and the measurement on 11/30/10 recorded an average of approximately 7360 alphas per second per alpha pixel. Therefore, the displayed fits and subsequent time approximations used in the template analysis testing are for an alpha rate of 7430 alphas per second per alpha pixel.

In the template analysis testing, the measurement length was simulated by taking the calculated attenuation profile obtained from the ray trace program and adding the error associated with the given attenuation and measurement time from the error analysis. To determine the amount of error added to the ray trace attenuation profile, the fit functions provided a value of error associated with the attenuation for a desired measurement length and this value was multiplied by a random number from a normal distribution with mean of zero and standard deviation of 1. Therefore, the errors added to the ray trace program were normally distributed about zero with a standard deviation equal to the amount of error determined by the fit functions for the attenuation of the detector position and measurement length.

5.1.3 Tested Configurations. Two types of object configurations were modeled for study in the template analysis testing: simple and complex. For each type of configuration, a template was modeled as well as two false objects representing material substitution and two false objects representing a change in object dimensions.

The simple configuration template was modeled as an annular DU casting with 3.5 in. inner diameter and 5 in. outer diameter. No shielding was used in the model. For the false objects representing material substitution, castings with the same 3.5 in. inner diameter and 5 in. outer diameter dimensions as the DU casting were modeled but with either iron or tungsten substituted for DU. Iron and tungsten were chosen due to having attenuation coefficients close to the 0.28 cm^{-1} attenuation coefficient of DU; iron is below DU at 0.22 cm^{-1} and tungsten is above it at 0.349 cm^{-1}. For the false objects representing dimension change, annular castings of DU were modeled with the same inner diameter as the template but with an increase in the outer diameter of $^1/_4$ in. for False Test Object 1 and an increase of ½ in. in the outer diameter of False Test Object 2. A pictorial representation of the simple configuration template and the false objects used in detecting dimension changes are shown in Figure 33.

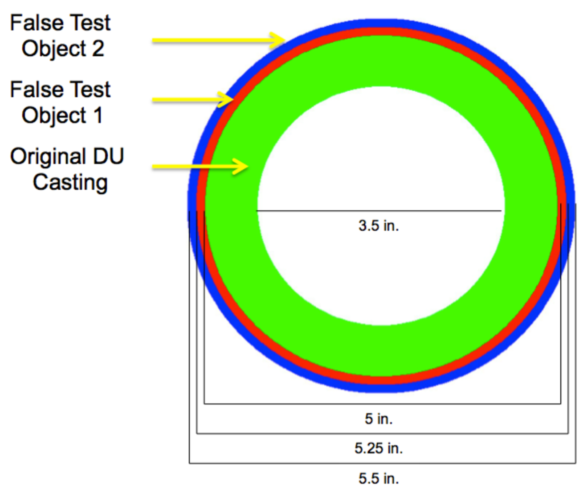

Figure 33. Top down representation of simple configurations simulated for testing of altered dimension identification. The increase in casting thickness between the template and false test object 1 is $^1/_8$ in., or ¼ in for false test object 2.

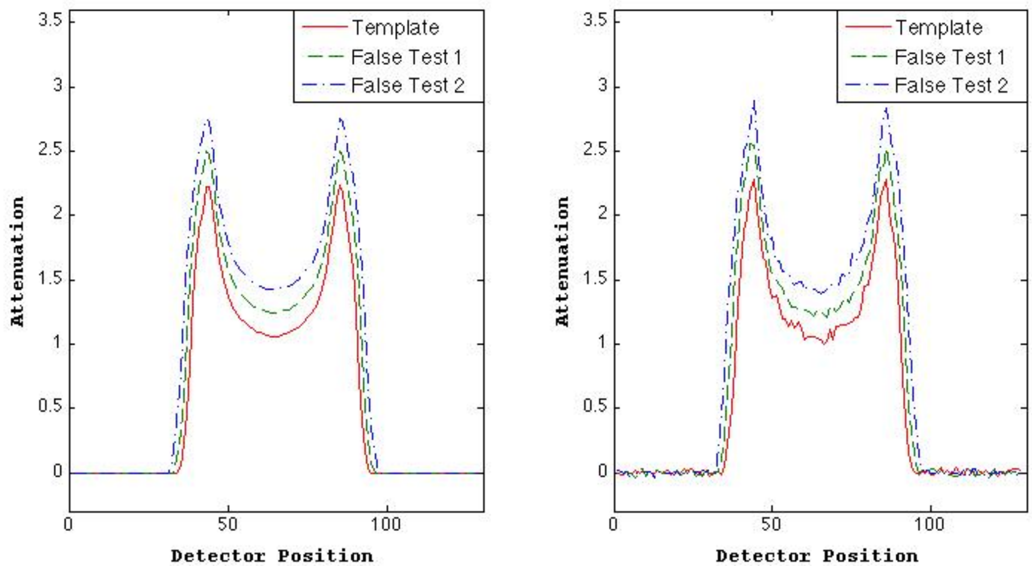

Figure 34. Attenuation profiles for simulated simple configuration of template DU casting, false test object 1 with ¹/₈ in. increase in thickness and false test object 2 with ¼ in. increase (left) without error added and (right) with error equivalent to 30 s subsamples.

In order to illustrate the effect of the error addition to the ray trace program attenuation profiles, attenuation profiles of the simple configuration template and the false objects used in detecting dimension changes are shown in Figure 34. The left side of the figure shows the attenuation profiles of the ray trace program without any error added, and the right side shows an example of the projections with error added equivalent to 30 s per subsample. The simple configuration template and false objects were all modeled with a 110 cm source-to-detector distance, 34 cm source-to-center of the object distance, 32 detectors and 4 subsamples.

The complex configuration template used in testing is pictorially represented in Figure 35. This complex configuration started with the same 3.5 in. inner diameter and 5 in. outer diameter DU casting that was used as the template in the simple configuration but then added ½ in. of lead shielding around the casting and placed the annuli into a 0.8 in. thick aluminum box along with a 4.3 in. x 6.3 in. iron block and a 4.3 in. x 6.3 in. tungsten block. The idea behind constructing the complex configuration was to create an object where detecting changes in the DU casting was more difficult due to the variety of materials present and the increased overall attenuation due to additional shielding.

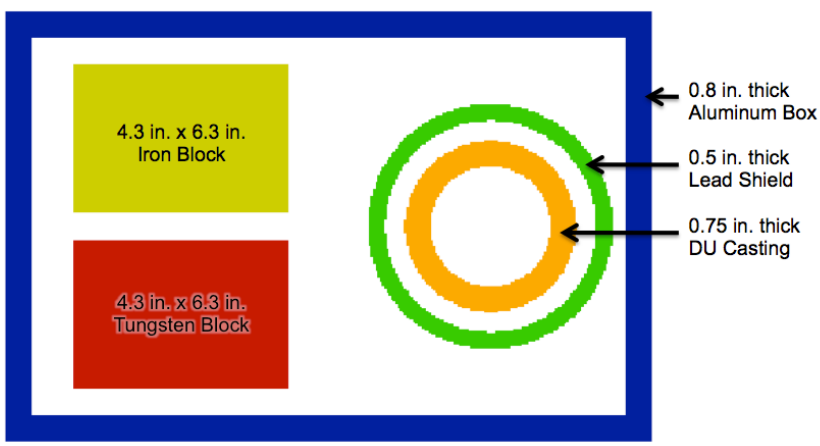

Figure 35. Top down representation of complex configuration template simulated for template analysis testing.

For the complex configuration, false objects representing material substitution, the orientation and dimensions remained the same as the template but either an iron or tungsten casting is substituted for the DU casting. The only changes to the template for the false objects representing dimension change were a ¼ in. increase in the outer diameter of the DU casting for False Test Object 1 and a ½ in. increase in the outer diameter for False Test Object 2. Figure 36 shows a sample attenuation profile for the complex configuration template along with the false objects with iron or tungsten substituted for DU. A detailed view of the region where the castings are located is shown without error added and with error associated with 30 s per subsample and 120 s per subsample. The complex configuration template and false objects were all modeled with a 115 cm source-to-detector distance, a 80 cm source-to-center of the object distance, 32 detectors and 8 subsamples. The attenuation coefficients used in the simulations for DU, iron, lead, aluminum and tungsten were 0.2831, 0.2203, 0.1757, 0.1051 and 0.3379 cm^{-1}, respectively.

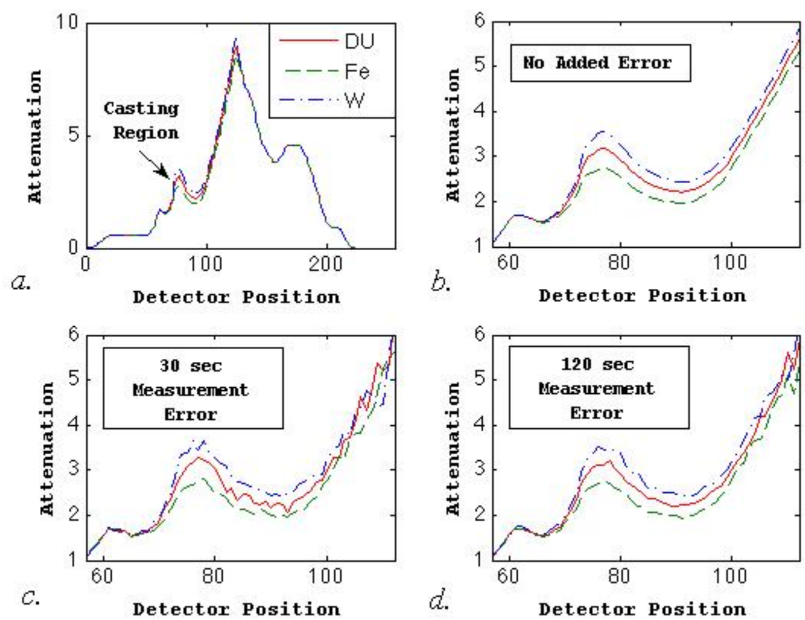

Figure 36. Attenuation profiles of complex configuration with iron and tungsten castings substituted for DU for (a) full attenuation profile from ray trace program and details of casting region of profile (b) without error added, (c) 30 s measurement error, and (d) 120 s measurement error.

5.1.4 Analysis Testing Setup. The template analysis testing was used to study the effects of user-defined variables on the performance of the template analysis in addition to the detection of material substitution and changes in object dimensions. Each time the template analysis is performed, the user must set certain variables within the measurement and K-S test, all of which affect the outcome and performance of the template analysis. These variables include the alpha value of the K-S test, the measurement time per subsample, the number of projections, and the number of subsamples. The rotation of the object is another variable of concern, but the assumption is that the user will attempt to minimize or eliminate a rotational offset in all cases.

For the testing of the simple configuration, alpha values were varied from 0.01 to 0.05 by increments of 0.01 and then from 0.05 to 0.25 by increments of 0.05 for a total of nine different alpha values. Measurement times per subsample were studied at the 30, 60, 90 and 120 s lengths and the use of 1, 2 and 4 subsamples were also studied. Only one projection was used due to the rotational symmetry of the configuration. In a measurement application of the template analysis more than one projection of the object would be necessary to confirm a test object match even for rotationally symmetric objects but eliminating one variable simplified testing in this case. For variables of alpha value, time per subsample and number of subsamples, 108 unique combinations of user-defined variables were tested with the template analysis for each combination of template and test object comparison. Using the error analysis addition of random error to the attenuation profiles allowed for the creation of multiple distinctive profiles for each measurement length. This permitted for 2500 trials for each of the 108 variable combinations and ensured statistical accuracy of reported results.

For the testing with complex configuration, alpha values were varied from 0.05 to 0.25 by increments of 0.05 for a total of 5 alpha values. Measurement times per subsample of 30, 60, 90 and 120 s were used as well as 1, 2, 4 and 8 subsamples. Furthermore, the use of 2, 3, 4, 5, 6, 10, 12, 15, 20 and 30 projections was added to the combination of variables. In all, 800 unique combinations of variables were studied for each comparison of the complex configuration template to one of the test objects, and 2500 trials were utilized for each combination of variables.

For each comparison of a template and test object with a unique combination of variables, either a true positive rate or false negative rate is reported. True positive rates are reported for the comparison of a template and true test object and a value of 1, or 2500/2500, indicates that all the test objects were correctly identified as matching the template. False negative rates are reported for the comparison of a template and false test object and a value of 0, or 0/2500, indicates that all the test objects were correctly rejected as matching the template.

5.2 Simple Configuration

Testing of the simple configuration started with comparing the template to true test objects. The left side of Figure 37 shows the true positive rate for the simple configuration as a function of alpha using 4 subsamples. A negative correlation between true positive rate and increasing alpha value is shown while a positive correlation

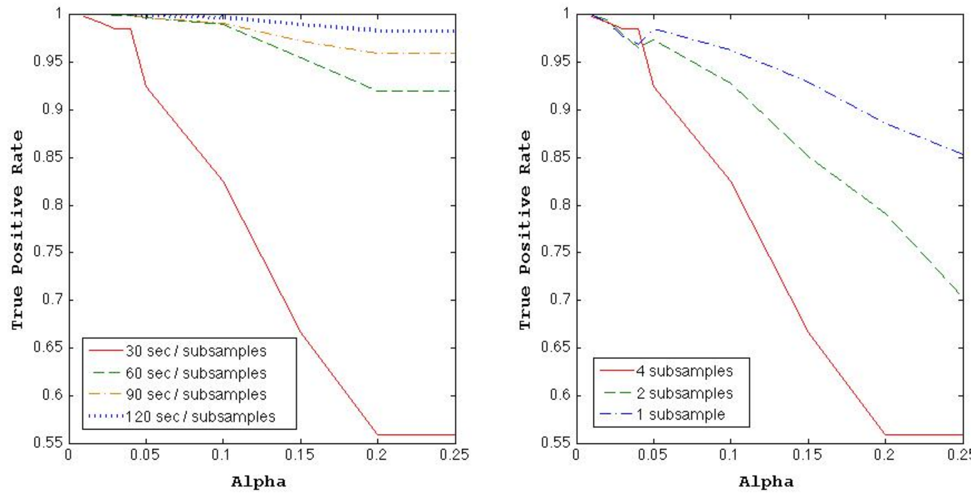

Figure 37. True positive rate as a function of alpha value using (left) 4 subsamples and (right) 30 seconds per subsample for template analysis comparisons of simple configuration template and true test objects.

between true positive rate and increasing subsample time is shown. The plot also shows, however, that the greatest effect of alpha value on the true positive rate occurs for the 30 s per subsample and that the true positive rate appears to plateau at an alpha value of 0.2. The right plot in Figure 37 shows the true positive rate as a function of alpha for differing number of subsamples and 30 s per subsample. This plot indicates a negative correlation between the true positive rate and the number of subsamples.

Using the information gained from the template analysis performance with the simple configuration template and true test object, the true positive rate would be maximized by using a low alpha value, as great a time per subsample as possible and only one subsample. In a measurement application of this method, however, the true positive rate would be the only known result of the template analysis, and any combination of variables that produced the desired true positive rate would work equally as well. For instance, if 4 subsamples with 30 s per subsample and an alpha value of 0.05 produce the desired true positive rate of 0.98 then this combination of variables will be as effective as using 1 subsample with 120 s per subsample and an alpha of 0.01 for the true positive rate. Since the true positive rate will be known, and it is controllable, the most effort should be on minimizing the unknown false negative rate. Not knowing the non-matching object means that it could display any combination of non-matching features with the template, and the false negative rate cannot be known. Therefore, choosing a set of variables that minimizes the false negative rate while maintaining a desired true positive rate would optimize the template analysis in a measurement application.

5.2.1 Material Substitution. The next step in testing with the simple configuration was to compare the simulated attenuation profiles of the template with the false objects representing material substitution. The left side of Figure 38 shows the false negative rate of the tungsten false test object as a function of alpha for various times per subsample and 4 subsamples. The plot shows a strong negative correlation between false negative rate and alpha as well as a negative correlation between false negative rate and increasing time per subsample. The negative correlation between false negative rate and alpha is much greater than the correlation between true positive rate and alpha, indicating that using the highest allowable alpha value may optimize performance of the template analysis by minimizing the false negative rate. The left side of Figure 38 also shows a strong negative correlation between false negative rate and increasing number of subsamples. This indicates that using a greater number of subsamples would also minimize the false negative rate.

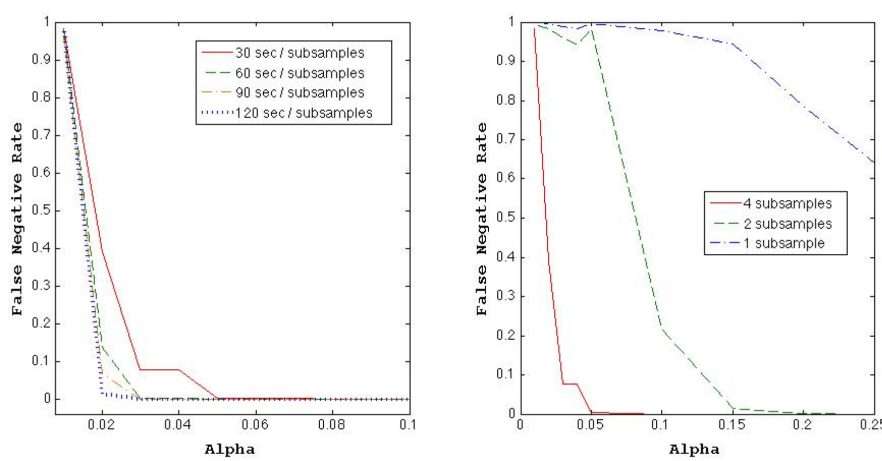

Figure 38. False negative rate as a function of alpha value using (left) 4 subsamples and (right) 30 seconds per subsample for template analysis comparisons of simple configuration template and tungsten false test object.

Table 13. Results of material change detection of simple configuration with template analysis using simulated attenuation profiles.

Time per Subsample	*Number of Subsamples*	*Max Alpha for TP ≥ 98%*	*FN Rate for Fe*	*FN Rate for W*	*Total Time (min)*
30	1	0.05	0.9952	0.9964	0.5
60	1	0.15	0.9292	0.9648	1
30	2	0.02	0.578	0.982	1
90	1	0.15	0.9792	0.9948	1.5
120	1	0.25	0	0.5768	2
60	2	0.10	0	0.12	2
30	4	0.04	0	0.0768	2
90	2	0.15	0	0.0008	3
120	2	0.25	0	0	4
60	4	0.10	0	0	4
90	4	0.10	0	0	6
120	4	0.25	0	0	8

The results listed in Table 13 display the false negative rates for the material substitution of iron and tungsten when using the maximum possible alpha value that produced a true positive rate of 0.98 or greater for a combination of time per subsample and number of subsamples. In other words, 0.98 was chosen as the minimum true positive rate, and the maximum alpha value producing the desired true positive rate was chosen to minimize the false negative rate. This represents the method that could be used in a measurement application where the true positive rate is controllable and the false negative needs to be minimized.

The results indicate that the substitution of iron has greater probability of being correctly rejected as matching the template than the substitution of tungsten, even though the difference in attenuation coefficients between iron and DU (0.0628) was greater than the difference between tungsten and DU (0.0548). The higher attenuation of the tungsten leading to greater uncertainty in the attenuation profiles likely causes the increased false negative rate. The results also show that for the same measurement time, the combination of lower time per subsample and more subsamples leads to a lower false negative rate than the combination of higher time per subsample and less subsamples. For instance, for a total measurement time of 2 min the false negative rate of tungsten decreases from 0.5768 for 1 subsample with 120 s per subsample, to 0.12 for 2 subsamples with 60 s per subsample, and again to 0.0768 for 4 subsamples with 30 s per subsample.

5.2.2 Changes in Object Dimensions. The final step in testing the simple configuration involved comparing the simulated template to the false objects representing a change in object dimensions. False Object 1 was modeled with a $^1/_8$ in. increase in casting thickness and False Object 2 was modeled with a ¼ in. increase in casting thickness. The left plot of Figure 39 shows the false negative rate of False Object 1 as a function of alpha. The plot shows the same strong negative correlation between the false negative rate and alpha and negative correlation between false negative rate and time per subsample that was seen in the material substitution. The plot on the right side of Figure 39 again shows a strong negative correlation between the false negative rate and increasing number of subsamples.

Results of the detection of dimension change with the simple configuration are shown in Table 14. Again, the minimum true positive rate was set to 0.98, and the maximum alpha rate that produced the required true positive rate was chosen for a set of

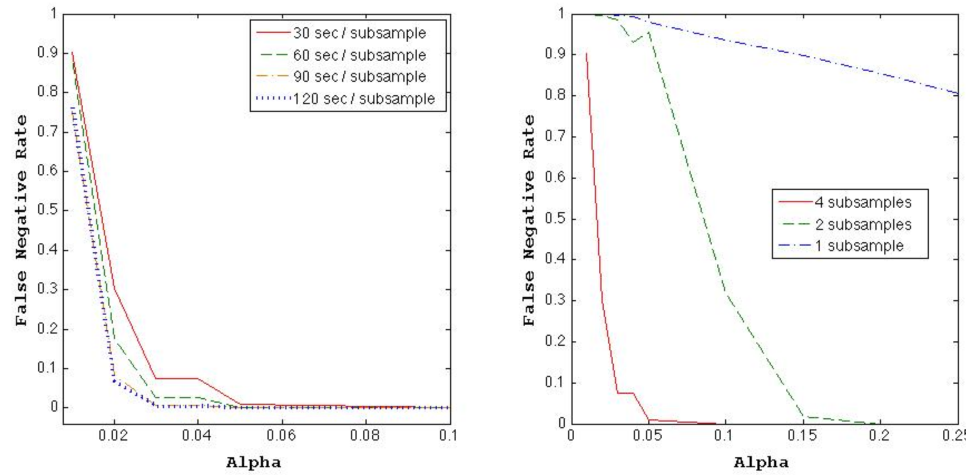

Figure 39. False negative rate as a function of alpha value using (left) 4 subsamples and (right) 30 seconds per subsample for template analysis comparisons of simple configuration template and false test object with $^{1}/_{8}$ in. increase in casting thickness.

Table 14. Results of dimension change detection of simple configuration with template analysis using simulated attenuation profiles.

Time per Subsample	***Number of Subsamples***	***Max Alpha for TP ≥ 98%***	***FN Rate for $^{1}/_{8}$ in. Increase***	***FN Rate for ¼ in. Increase***	***Total Time (min)***
30	1	0.05	0.9804	0.0132	0.5
60	1	0.15	0.968	0	1
30	2	0.02	0.9956	0	1
90	1	0.15	0.9792	0	1.5
120	1	0.25	0.8888	0	2
60	2	0.10	0.1488	0	2
30	4	0.04	0.0736	0	2
90	2	0.15	0.0004	0	3
120	2	0.25	0	0	4
60	4	0.10	0	0	4
90	4	0.10	0	0	6
120	4	0.25	0	0	8

variables. These results show, as expected, that the smaller increase of $^{1}/_{8}$ in. in casting thickness was more difficult to correctly reject as matching the template than the larger ¼ in. increase, requiring a total measurement time approximately six times a long to achieve the same false negative rate. The results also indicate, as the material substitution results did, that for a set total measurement time using more subsamples and less time per subsample minimizes the false negative rate. This can be seen in the case of the false negative rate of False Object 1 with a 2 min total measurement time which decreases from 0.8888 for 1 subsample with 120 s per subsample, to 0.1488 for 2 subsamples with 60 s per subsample, to 0.0736 for 4 subsamples with 30 s per subsample.

5.3 Complex Configuration

Due to the strong negative correlation between the false negative rate and the number of subsamples, it was of interest to determine if the minimum false negative rate was obtained simply by the test objects using the same number of subsamples as the template, or if increasing the number of subsamples in both the template and test objects decreased the false negative rate farther. Table 15 shows the results of comparing templates and test objects using 4 subsamples and 8 subsamples for the simple configuration case of material detection. For this study, the alpha value was held constant at 0.01. The results indicate that for the same amount of measurement time, increasing the number of subsamples in the template and test objects and measuring for less time per subsample lead to a decrease in both the true positive and false negative rates. Due to the increased attenuation present in the complex configuration objects requiring further

Table 15. Comparison of results of material change detection of simple configuration with template analysis using simulated attenuation profiles for templates with 4 subsamples and templates with 8 subsamples

Time per Subsample	Number of Subsamples	Number of Template Subsamples	Alpha	TP Rate	FN Rate for Fe	FN Rate for W	Total Time (min)
60	4	4	0.01	1	0	0.98160	4
30	8	8	0.01	0.9088	0	0	4
120	4	4	0.01	1	0	0.9732	8
60	8	8	0.01	0.9992	0	0	8

reduction in false negative rates and the ability to control the true positive rate, the complex configuration objects were all simulated with 8 subsamples.

The study of the complex configuration continued by looking at the comparison of the template and true test objects. The right plot of Figure 40 shows the true positive rate as a function of the number of projections used for various alpha values. The number of subsamples was held constant at 8 with 30 s per subsample. The plot shows the true positive rate decreasing as the number of projections increases and also decreasing with increasing alpha value. The left plot of Figure 40 shows the true positive rate as a function of subsamples for various times per subsample. For this example the alpha value was help constant at 0.25 as was the number of projections at 30. This plot indicates a negative correlation between the true positive rate and number of subsamples for the 30 s per subsample case but no definite correlation for the increased times per subsample. It also shows positive correlation between increased time per subsample and true positive rate although this correlation appears to weaken with longer time lengths per subsample.

5.3.1 Material Substitution. Material substitution was the first false test object case studied for the complex configuration. In these objects, an iron or tungsten casting was substituted for the DU casting in the template. The plot on the left of Figure 41 shows the false negative rate as a function of projection for various alpha values for the comparison of the template with the tungsten false test object. The number of subsamples was held constant at 4 with 60 s per subsample. The plot suggests a strong negative correlation between the false negative rate and increasing alpha value. It also appears to indicate a negative correlation between the false negative rate and number of projections that

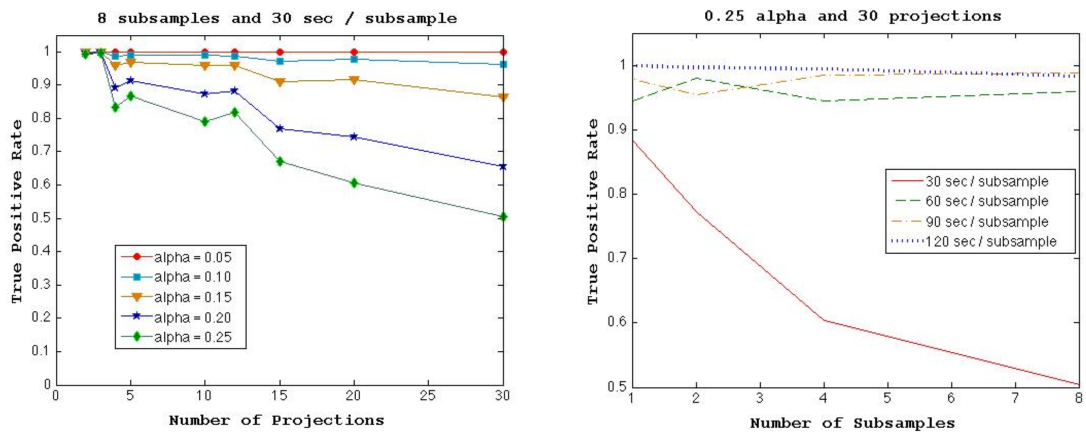

Figure 40. True positive rate as a function of (left) number of projections using 8 subsamples with 30 seconds per subsample and (right) number of subsamples using 30 projections and an alpha of 0.25 for template analysis comparisons of simulated complex configuration template and true test objects.

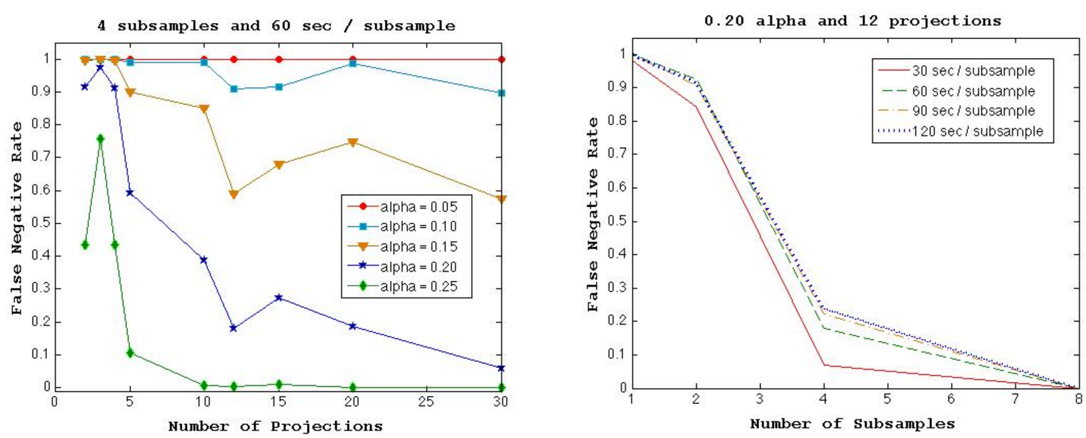

Figure 41. True positive rate as a function of (left) number of projections using 4 subsamples with 60 seconds per subsample and (right) number of subsamples using 12 projections and an alpha of 0.20 for template analysis comparisons of simulated complex configuration template and tungsten false test objects.

increases with increasing alpha value. The right plot of Figure 41 shows the relationship between the false negative rate, number of subsamples and time per subsample. The data indicates a strong negative correlation between false negative rate and the number of subsamples and slight positive correlation between false negative rate and the time per subsample. These results suggest that the number of subsamples and alpha value have a greater influence on the false negative rate for the complex configuration than the number of projections or time per subsample.

The results of the template analysis with material change for the complex configuration and total measurement time of 8 min are shown in Table 16 while the results for a total measurement time of 16 min are shown in Table 17. A minimum true positive rate of 0.98 was again used in this study and a maximum alpha value that produces the required true positive rate was employed. The results indicate that for a set measurement time using the greatest number of subsamples possible produces the lowest false negative rates. Table 18 displays the results of total measurement times of 24, 32 and 80 min using the maximum number of subsamples 8. These results suggest that once the maximum number of subsamples is chosen, the rejection of non-matching objects improves by selecting a higher measurement time per subsample and fewer projections for a set measurement time. For example, the false negative rate of tungsten substitution decreases from 0.2700 using 10 projections with 8 subsamples and 60 s per subsample to 0.0644 using 5 projections with 8 subsamples and 120 s per subsample for a set measurement time of 80 min.

Table 16. Results of material change detection of complex configuration with template analysis using simulated attenuation profiles and 8 min total measurement time.

Time per Subsample	Number of Subsamples	Number of Projections	Max Alpha for TP ≥ 98%	FN Rate for Fe	FN Rate for W	Total Time (min)
120	1	4	0.25	1	1	8
120	2	2	0.25	1	1	8
60	2	4	0.25	0.9924	0.9788	8
60	4	2	0.25	0.436	1	8
30	8	2	0.25	0	0.894	8

Table 17. Results of material change detection of complex configuration with template analysis using simulated attenuation profiles and 16 min total measurement time.

Time per Subsample	Number of Subsamples	Number of Projections	Max Alpha for TP ≥ 98%	FN Rate for Fe	FN Rate for W	Total Time (min)
120	2	4	0.25	0.9988	0.9992	16
120	4	2	0.25	0.5076	1	16
60	4	4	0.25	0.4348	0.9816	16
60	8	2	0.25	0	0.6496	16

Table 18. Results of material change detection of complex configuration with template analysis using simulated attenuation profiles with 8 subsamples and 24, 32 or 80 min total measurement time.

Time per Subsample	Number of Subsamples	Number of Projections	Max Alpha for TP ≥ 98%	FN Rate for Fe	FN Rate for W	Total Time (min)
60	8	3	0.25	0	0.8252	24
90	8	2	0.25	0	0.5664	24
60	8	4	0.25	0	0.6376	32
120	8	2	0.25	0	0.522	32
60	8	10	0.25	0	0.2700	80
120	8	5	0.25	0	0.0644	80

5.3.2 Changes in Object Dimensions. The results of the template analysis testing using a change in the dimension of the DU casting of the complex configuration are shown in Table 19. A minimum true positive rate of 0.98 was used with a maximum alpha value that produced that true positive rate. As with the change in material, these results suggest that for a set measurement time the variable that has the greatest impact on the false negative rate is the number of subsamples, followed by the time per subsample, and then the number of projections. Thus, in choosing parameters in a measurement application the longest permissible total measurement time would be used with the largest number of subsamples possible, then the greatest time per subsample and the most projections, with the knowledge that at least 2 projections are necessary, to produce the total measurement time.

Table 19. Results of dimension change detection of complex configuration with template analysis of simulated attenuation profiles for total measurement time of 4, 8, and 16 min.

Time per Subsample	*Number of Subsamples*	*Number of Projections*	*Max Alpha for TP ≥ 98%*	*FN Rate for $^1/_8$ in. Increase*	*FN Rate for ¼ in. Increase*	*Total Time (min)*
120	1	2	0.25	1	1	4
60	1	4	0.25	0.9960	1	4
60	2	2	0.25	1	0.8364	4
30	4	2	0.25	0.9840	0	4
120	1	4	0.25	1	1	8
120	2	2	0.25	1	0.8700	8
60	4	2	0.25	0.9964	0	8
30	8	2	0.25	0.2944	0	8
120	2	4	0.25	0.9968	0.8700	16
120	4	2	0.25	1	0	16
60	4	4	0.25	0.9904	0	16
60	8	2	0.25	0.0396	0	16

The false negative rate as a function of the change in the thickness of the DU casting in the complex configuration is shown for a total measurement time of 8 min in Figure 42, and a total measurement time of 4 min in Figure 43. These results show that it is possible to correctly reject a smaller change in the casting thickness by using the greatest number of subsamples and also by choosing fewer projections and greater measurement time per subsample for a set total measurement time. The plot also indicates that for a set measurement time there is a certain amount of change in the casting dimensions, which would be undetectable even with the optimization of user-defined variables. As the measurement time is decreased, the amount of change from the false test object to the template that the template analysis is not able to distinguish increases. Therefore, the optimization of variables can produce the best rejection of non-matching objects for a set total measurement time but ultimately the total measurement time determines the limit of possible detectable change.

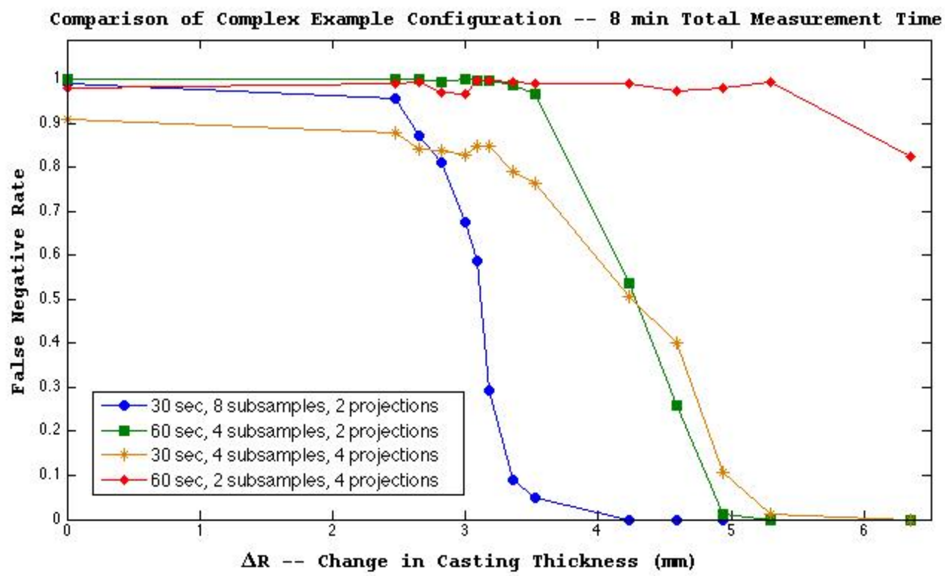

Figure 42. False negative rate as a function of the change in the casting thickness of the simulated complex configuration. Each combination of measurement time per subsample, number of subsamples and number of projections produces a total measurement time of 8 min.

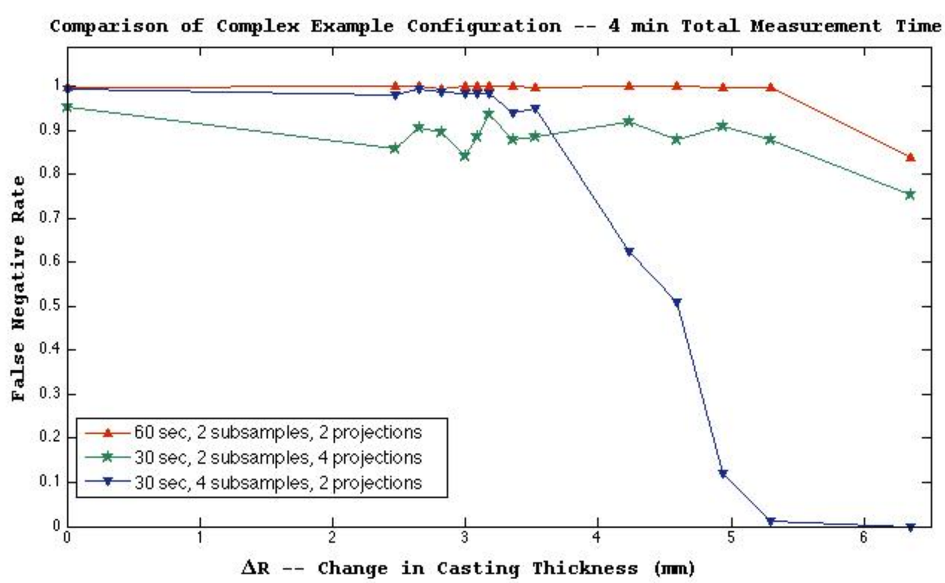

Figure 43. False negative rate as a function of the change in the casting thickness of the simulated complex configuration. Each combination of measurement time per subsample, number of subsamples and number of projections produces a total measurement time of 4 min.

Chapter 6

Conclusions and Future Work

The presented method demonstrates a unique, robust way to confirm the materials and dimensions of highly attenuating objects — without visually investigating the objects — by utilizing a template matching analysis for a tagged neutron interrogation system. By coupling the highly penetrating 14.1 MeV neutrons of a NMIS-type measurement system with the flexibility of the K-S test in comparing profiles of attenuation and late singles to those of a template object, verification of an object materials, dimensions, and fissile nature is possible in reasonable amounts of time.

Due to this method's intended use in measurement applications, its ability to perform well despite multiple sources of possible variation (unrelated to the objects themselves) is a necessity for the reliability of the results. Through the utilization of existing measurement data, it was possible to confirm that most measurement variation due to the equipment and electronics was removed in the construction of attenuation profiles. Since part of the calculation of attenuation involves taking the ratio of two measurements performed on the same day, the variation that is present in both measurements cancels out in the resulting attenuation profile.

The placement of the object relative to the measurement system also produces variability in the measurement's attenuation profiles that is unrelated to the object itself. Magnification of the attenuation profile occurs when the test object has a source-to-center distance different from the template measurement, causing the test object's attenuation profile to appear wider or narrower than the attenuation profile of the template. The source-to-center difference can also cause a baseline shift whereby the detector positions, or image pixels, outside the view of the object register counts due to small angle scatters resulting in a non-zero baseline. Shifting in the attenuation profile occurs when the test object is translated latterly with respect to the transmission detector array from the original position of the template resulting in an attenuation profile that is translated to the left or right with respect to detector position, or image pixel, from the attenuation profile of the template.

To address the issue of the baseline shift, a baseline correction consisting of averaging the attenuations for the first five image pixels, or detector positions, where the object is not in view and subtracting the value from the entire attenuation profile was used to correct the offset. In a measurement application, it would be possible to determine if the outermost detector of the transmission detector array is out of view of the object's container, or to position the container such that it is. This would ensure that the detector positions, or image pixels, corresponding to that detector would be outside the view of the object and could be used for the baseline correction. The baseline correction of attenuation profiles produced a significant improvement to the template analysis performance as two out of three measurements performed on the same object on different days were rejected as matching without the baseline correction, but all three were confirmed as matching when the correction was applied.

Testing of the effects of magnification and shifting was possible with the use of four measurements of the same configuration of DU and steel performed on different days. The template analysis looked at attenuation profiles using 4 subsamples with 30 s per subsample and used a single projection to confirm or reject the test objects as matching the template. The results of testing indicate that the template analysis was unaffected by the magnification or shifting of the attenuation profiles with a total false positive rate of only 0.2% out of 3,364 trials with an alpha value of 0.05, and no true test objects were misidentified out of 3,364 trials with an alpha value of 0.01. The results also show that it would be possible to use different subsampling from template measurement to test object measurement, which would cause attenuation profiles to be associated with different detector positions, or image pixels, without affecting the template analysis.

While the invariance of the K-S test to shifting and magnification is an obvious benefit to the template analysis overcoming measurement variation, it is possible that this characteristic could be utilized in spoofing the method. Even though a smaller or larger object of the same material would be rejected as matching due to the decrease or increase in attenuation, it may be possible to devise a smaller or larger object of a different material such that the attenuation matches the template, which would be accepted as matching. Therefore, a useful addition to the template matching would be a simple check to verify that not all projections of the test object have attenuation profiles that are wider or narrower than the template profiles. An additional check of this nature would ensure that this type of spoofing could not occur.

Measurement data was also used to determine if a change in the fissile nature of material could be identified with the template analysis. In this case, measurements of a ^{235}U casting with various amounts of DU shielding and a DU casting with various amounts of DU shielding were compared. Template analysis testing compared measurement samples of 4 subsamples with 15 s per subsample for a total of 1 min of data acquisition and an alpha value of 0.05. When just attenuation profiles were used to identify the objects as matching or not, the DU and ^{235}U was misidentified as matching in all 3,600 trials. By adding an additional K-S test comparing the late singles profiles of the two objects, the objects were correctly identified as not matching in all 3,600 trials. These results illustrate the need to confirm late singles profiles in addition to attenuation profiles and also demonstrate the effectiveness in utilizing late singles as a metric to confirm the consistency of materials' fissile nature even with short measurement times.

Measurements data obtained during the 2010 INL measurement campaign were also studied in the testing of rotational offset due to the increased complexity and high degree of rotational asymmetry of these measured objects. Rotational offset occurs when a test object without rotational symmetry is rotated about its vertical axis such that there is an offset with respect to the template measured. Test objects were offset from templates in increments of 6° for IOs 3, 7, and 9 and in increments of 12° for IO 10 up to a maximum rotational variation. Maximum rotational variations of 24, 36 and 48° were tested for each of the IOs in comparison to all four measured objects. Templates consisted of 6 projections with four subsamples for a total measurement time of 10 min while test objects contained 6 projections with one subsample for a total measurement time of 2.5 min. The alpha value of the tests was varied to determine the optimal identification rates possible.

In general, the results show that the larger the rotational offset of the true test object from the template, the more likely it is to be rejected as matching the template. The degree of rotation that led to true test objects being rejected as matching the template depended on the inspection object (IO), and the amount of its internal variation, and the alpha value used in the analysis. For example, in the template analysis comparing IO 7 and IO 9, the optimal alpha value varied from 0.014-0.26 for the 36° maximum rotation variation and 0.012-0.016 for the 48° maximum rotation variation demonstrating slight overlap from 0.14-0.16. Overall, no alpha values were found that provided optimal identification in all comparisons.

Due to the decrease in true positive rate as a result of increasing rotational offset, measurement application of this method would greatly benefit from ensuring the elimination or at least minimization of rotational offset with the template. It is possible this could be accomplished with some identifying feature on the outside of the container, such as a tag or sticker, that could be used to align objects in the same rotational position as the template. Future work could also include the implementation of an algorithm to identify some key feature of the template to align with the test object to reduce the rotational offset. This work would be complicated by the requirement that the algorithm be operational without a priori knowledge of the measured object and could be performed in a timely manner with data collected in the measurement exclusive of user input. Additionally, any algorithm that removed rotational offset after the object was measured would likely cause an increase in false negative rates as well as true positive rates, as both false test items and true test items would both be more closely aligned with the template.

Simulated attenuation profiles were created for the template analysis testing by the ray trace program coupled with an error analysis. Both simple and complex configurations were used in studying the template analysis performance with material substitution and changes in object dimensions. Additionally, the effect of user-defined variables on the template analysis performance was determined by looking at different combinations of alpha value, number of subsamples, time per subsample, and number of projections. The simulation testing results indicate that for a template consisting of a single DU casting, it may be possible to detect the substitution of iron or tungsten, or a $^{1}/_{8}$ in. increase in the casting thickness 92% of the time with a 4 min measurement, or 100% or the time with an 8 min measurement. These results are specific to the template object, however, and are highly dependent on the choice of user-defined variables.

The results of the study of user-defined variables with simulated attenuation profiles indicate that the choice of variables, as well as the measurement time, strongly affects the true positive and false negative rates in the template analysis. In a measurement application, the true positive rate could be predetermined for a specific scenario and set with the template analysis while the false negative rate would remain unknown, since it would not be possible to know how a non-matching object differed from the template. For this reason, the variables that affected the false negative rate the most were determined. The variable aside from alpha value that had the greatest impact on the false negative rate was the number of subsamples measured for the test objects' attenuation profiles. This was followed by the measurement time per subsample and the number of projections.

For a measurement application, the best method to reduce the false negative rate is to first determine the minimum allowable true positive rate and the maximum allowable measurement time of test objects. For example, setting a true positive rate of 98% would allow 2 out of 100 test objects to be rejected as matching the template when, in fact, they do match. These objects would likely need to be measured again, requiring additional time. Using the set measurement time, the highest number of subsamples would first be selected, followed by the highest possible measurement time per subsample and then the greatest number of projections, with the caveat that a minimum of 2 projections would be needed. For example, if a set measurement time of 16 min was determined for test objects and the template was measured with 4 subsamples and 60 s per subsample then the combination of 4 subsamples with 60 s per subsample and 4 projections would lead to the lowest possible false negative rates for the 16 min measurement time.

In a measurement application, the alpha value of the test should be determined by taking the determined set of parameters and choosing the highest possible alpha value that still produced the desired true positive rate. Future work could include automating a process that took the template measurement and either subdivided the measurement into smaller sections corresponding to the set of parameters of test objects or took the full measurement and added random error corresponding to the duration of measurement of the subsamples of the test objects. This could then be used as true test objects to determine the highest possible alpha value producing the desired true positive rate. Likewise, an algorithm could also be included that determined the number of subsamples, time per subsample, and number of projections for the test objects so that the only information that would be required from the user would be the number of subsamples and time per subsample of the template, the required true positive rate and the allowable measurement time per test object.

By choosing the template analysis variables in this way, the true positive rate, corresponding to the type I error, is set to an allowable level and the false negative rate, or type II error, is minimized. While prior knowledge of the template object could provide the opportunity to model scenarios to gain an understanding of the limitations of detecting non-matching objects with the template analysis, without a known template the choice of variables that minimize the false negative rate is key to rejecting non-matching items.

List of References

1 *IAEA safeguards glossary - 2001 ed.* International Verification Series No. 3, Vienna: International Atomic Energy Agency, 2002.

2 Nelson, G., and D. Reilly. "Ch 2 Gamma-Ray Interations with Matter ." In *Passive Nondestructive Assay Manual*, 27-42. Los Alamos National Laboratory, 1991.

3 Marleau, Peter, and Aaron Nowack. *Gamma/Neutron Time-Correlation for Special Nuclear Material Detection - Active Stimulation of Highly Enriched Uranium.* Sandia Report, Albuquerque: Sandia National Laboratories, 2013.

4 MacArthur, Duncan W. "Warhead Confirmation: A Follow-on to New START." *LA-UR-14-21945.* Presentation to Official LANL Visitors, 03 24, 2014.

5 *United States Nuclear Regulatory Commission - Material Control and Accounting.* January 13, 2015. http://www.nrc.gov/security/domestic/mca.html (accessed March 20, 2015).

6 DOE Standard. *Nuclear Materials Control and Accountability.* DOE-STD-1194-2011, Washington, D.C.: U.S. Department of Energy, 2012.

7 Decman, D. J., J. Glaser, J. M. Hernandez, and S. J. Luke. "Portable NDA equipment for enrichment measurements for the HEU transparency program." *INMM Annual Meeting Proceedings.* 1999.

8 Blessinger, C, Chris Pickett, John H. Leckey, and Amy DeMint. "Design of HEU test objects." *INMM Annual Meeting Proceedings.* 2009.

9 J. T. Mihalczo et al., "Fast Neutron Imaging with API DT Neutron Generators," *Portable Neutron Generators and Generator-Based Technologies International Conference,* Moscow, Russia, October 22-27, 2012.

10 Turner, James E. *Atoms, Radiation and Radiation Protection.* Weinheim: WILEY-VCH, 2007.

11 McConchie, Seth, and Kirsten Peña. *FY12 Annual Report for Minimum Data Requirements for a Fast Neutron Image-based Template Analysis.* WMS 24.3.2.30, Oak Ridge National Laboratory, 2013.

12 Grogan, B. R. *The Developement of a Parameterized Scatter Removal Algorithm for Nuclear Materials Identification System Imaging.* PhD Thesis, Knoxville: The University of Tennessee, 2010.

13 Duda, Richard O., Peter E. Hart, and David G. Stork. *Pattern Classification.* New York: John Wiley & Sons, Inc, 2001.

14 Olofsson, Peter. *Probability, Statistics and Stochastic Processes.* Hoboken: John Wiley & Sons, Inc., 2005. p337.

15 M. Whitney, Assistant Depurty Administrator. "February 2011 Highlights." Office of Nonproliferation and International Security (NIS), 2011.

16 K.D. Seager, D.J. Mitchell, T.W. Laub, K.M. Tolk, et al. "Trusted Radiation Identificaiton System." *Proceedings of the 42nd INMM Annual Meeting.* Northbrook, IL: Institute of Nuclear Material Management, 2001.

17 K.D. Jarman, W.K. Pitts, S.M. Robinson, T.A. White, et al. "Low-Intrusion Techniques and Sensitive Information Management for Warhead Counting and Verificatoin: FY2011 Annual Report." *PNNL-20840.* Pacific Northwest National Laboratory, 2011.

18 K.D. Jarman, B.S. McDondald, S.M. Robinson, et al. "Low-Intrusion Techniques and Sensitive Information Management for Warhead Counting and Verification: FY2012 Annual Report." *PNNL-21972.* Pacific Northwest National Laboratory, 2012.

19 L. Chichester, T. Johnson, and H. Seabury. "High-Resolution Fast-Neutron Spectrometry for Arms Control and Treaty Verification." *INL/CON-12-24554.* Idaho National Laboratory, 2012.

20 Stewart, J.E. "Passive Nondestructive Assay Manual - PANDA Ch 14 Principles of Total Neutron Counting." Los Alamos National Laboratory, March 1991.

21 Valentine, T.E., J. T. Mihalczo, J. K. Mattingly, and J. A. Mullens. "NWIS signatures for identification of weapons somponents at the Oak Ridge Y-12 Plant." *INMM Annual Meeting Proceedings.* 1997.

22 Mattingly, J.K., T.E. Valentine, and J.T. Mihalczo. *NWIS Measurements for Uranium Metal Annular Castings.* Y/LB-15,971, Oak Ridge Y12 Plant, Oak Ridge: Oak Ridge Y-12 Plant, 1998.

23 Mihalczo, J.T. “Use of Cf-252 as a randomly pulsed neutron source for prompt neutron decay measurements.” *Nuclear Science and Engineering* 2, no. 41 (1970): 296.

24 Mullens, J.A., B. Grogan, D. Archer, and J.T. Mihalczo. "Shipping Anomaly from NMIS Inmaging." *INMM Annual Meeting Proceedings.* 2008.

25 Mullens, James, Seth McConchie, and Paul Hausladen. "Neutron radiography and fission mapping measurements of nuclear materials with varying composition and shielding." *INMM Annual Meeting Proceedings.* 2011.

26 Grogan, B.R., J.T. Mihalczo, S. M. McConchie, and J. A. Mullens. "Identification of Shielding Material Configurations Using NMIS Imaging." *INMM Annual Meeting Proceedings.* 2011.

27 Mullens, J.A., T. E. Valentine, and J. T. Mihalczo. "Pattern Recognition Algorithms for Comparing NWIS Signatures for Weapons Components." *INMM Annual Meeting Proceedings.* 1997.

28 Mihalczo, J.T., T.E. Valentine, J.K. Mattingly, J.A. Mullens, and S.S. Hughes. *Active Neutron Interrogation for Verification of Storage of Weapons Components at the Oak Ridge Y-12 Plant.* YLB-15, 964, Oak Ridge: Oak Ridge Y1-2 Plant, 1998.

29 Crye, Jason. *Enrichment Determination of Uranium Metal in Shielded Configurations without Calibration Standards.* PhD Thesis, Knoxville: University of Tennessee, 2013.

30 Massey, F. "The Kolmogorov-Smirnov Test for Goodness of Fit." *Journal of the American Statistical Association* 46, no. 253 (Mar 1951): 68-78.

31 Darling, D. A. "The Kolmogorov-Smirnov, Cramer-von Mises Tests." *The Annals of Mathematical Statistics* 28, no. 4 (Dec 1957): 823-838.

32 R. Neibert, et al., "Passive and Active Radiation Measurements Capability at the INL Zero Power Physics Reactor (ZPPR) Facility", INL/EXT-11-20876, 2010.

33 McConchie, Seth, and Kirsten Peña. *FY13 Annual Report for Minimum Data Requirements for a Fast Neutron Image-based Template Analysis.* WBS 24.3.1.2.30, Oak Ridge National Laboratory, 2013.

34 McConchie, Seth (private conversation, 2015.)

Vita

Kirsten Peña received her Bachelors of Science in Nuclear Engineering from the University of Tennessee in 2009. She also received her Masters of Science in Nuclear Engineering from the University of Tennessee in 2011. She has worked as a student assistant with the Nuclear Materials Detection and Characterization Group at the Oak Ridge National Laboratory since 2008. Most of her research has concentrated on the modeling and testing of detector systems and applications to aid in nuclear nonproliferation and treaty verification.